ANALYTICAL STUDIES OF BOUNDARY LAYER GENERATED AIRCRAFT INTERIOR NOISE

M. S. Howe and P. L. Shah
Boston University, College of Engineering
110 Cummington Street, Boston MA 02215
6 October, 1997

Report AM-97-027

Prepared under Grant NAG1-1688 for
Dr. Richard J. Silcox
Structural Acoustics Branch
MS 463, NASA Langley Research Center
Hampton VA 23681-0001

TABLE OF CONTENTS

TABLE OF CONTENTS continued

CHAPTER 3.

CHAPTER 4.

PREFACE

The work reported here was performed under Grant NAG1-1688 from NASA Langley Research Center administered by Dr. Richard J. Silcox. PLS acknowledges additional support under Contract NAS1-19480 while in residence at the *Institute for Computer Applications to Science and Engineering* at NASA Langley Research Center in 1995. The authors acknowledge with gratitude the help and advice of Dr. Jay C. Hardin of the Fluid Mechanics and Acoustics Division of NASA Langley Research Center.

Modified versions of each of the four Chapters comprising this report are being (or have been) published as independent articles as follows:

Chapter 1: *Journal of the Acoustical Society of America* **99**, 3401 - 3411, 1996.
Chapter 2: *Journal of Sound and Vibration* **197**, 103 - 115, 1996.
Chapter 3: *Journal of Sound and Vibration* 1997 (in press).
Chapter 4: *Journal of Fluids and Structures* 1997 (in press).

The material of Chapter 1 was presented at the 1995 Winter Annual meeting of the American Society of Mechanical Engineers.

CHAPTER 1

INFLUENCE OF MEAN FLOW ON BOUNDARY LAYER GENERATED INTERIOR NOISE

SUMMARY

An analysis is made of the "interior noise" produced by high, subsonic turbulent flow over a thin elastic plate partitioned into "panels" by straight edges transverse to the mean flow direction. This configuration models a section of an aircraft fuselage that may be regarded as locally flat. The analytical problem can be solved in closed form to represent the acoustic radiation in terms of prescribed turbulent boundary layer pressure fluctuations. Two cases are considered: (i) the production of sound at an isolated panel edge (i.e., in the approximation in which the correlation between sound and vibrations generated at neighboring edges is neglected), and (ii) the sound generated by a periodic arrangement of identical panels. The latter problem is amenable to exact analytical treatment provided the panel edge conditions are the same for all panels. Detailed predictions of the interior noise depend on a knowledge of the turbulent boundary layer wall pressure spectrum, and are given here in terms of an empirical spectrum proposed by Laganelli and Wolfe. It is expected that these analytical representations of the sound generated by simplified models of fluid-structure interactions can used to validate more general numerical schemes.

1. INTRODUCTION

Interior cabin noise of passenger aircraft is usually attributed to *airborne sources*, which include the direct incidence of engine generated sound on cabin sidewalls and the high speed turbulent air flow over the exterior fuselage, and *structure borne sound* (transmitted to the cabin via vibrational motions of the airframe) caused by engine vibration, and by vibrations induced by impingement of engine exhausts on wings and flow control surfaces. Flight tests [1] with engines "off" indicate that the boundary layer is responsible for a substantial component of the interior noise. It is significant for practically all types of aircraft, and is usually considered to be one of the most important sources of cabin noise for a jet powered passenger aircraft in steady flight. The spectral levels and the effective frequency range of boundary layer pressure fluctuations change with increasing subsonic flight speed [2], and boundary layer generated cabin noise can vary significantly with frequency, in contrast to the smoother variations of the exterior wall pressures [3]. This is because fuselage transmission characteristics and boundary layer scattering mechanisms are critically dependent on the geometry of structural changes in the cabin walls.

To control interior noise one must be able to predict both the amplitude and phase of the cabin sound pressure field. For the random noise sources in a turbulent boundary layer, the most that can normally be done is to determine the space-time correlation of the interior sound, and possibly also the correlation between vibrating structural elements and the sound. Turbulence generated sound enters the cabin both by direct transmission through the fuselage and via the excitation of structural vibrations that subsequently generate sound. A statistical analysis of structural excitation and noise transmission must include the influence of the space-time correlation of the boundary layer wall pressures. Most work so far conducted on this problem has taken little or no account of the details of the spatial characteristics of the wall pressures [4], although it is well known that the convection of strong "hydrodynamic" pressure fluctuations over the fuselage is important when "coincidence" occurs (when the convection velocity is equal to the phase speed of a resonant wall mode), causing a large increase in the interior noise and wall vibrations [5, 6].

Hitherto it has been usual to simplify the analysis of such problems by neglecting the coupling between the structural and acoustic equations of motion. Relatively little work has been done on the fully coupled equations [7] in aeronautical applications, although the validity of the decoupled approximation is suspect at higher subsonic Mach numbers, when dynamic boundary layer pressure fluctuations can be large, and it is known to fail in analogous underwater applications where the coupling is large because of the relatively high density of water [8].

In this chapter an analytical investigation is made of a simplified model of the generation of interior noise by subsonic, high speed turbulent flow, when the fuselage is assumed to be locally flat. The coupled, fluid-structure equations can be solved in closed form in two general cases. In the first of these we examine the sound produced by turbulent flow interacting with a single straight edge, transverse to the mean flow, that separates two large elastic panels. This is a situation in which the sound and vibration produced at neighboring edges can be regarded as uncorrelated; it is unreasonable in practice, because it neglects strong couplings between neighboring edges via flexural motions of the panels. Next, this problem is extended to the case of periodic, identical panels with transverse edges, whose interaction with the boundary layer can be solved in closed form provided the panel edge conditions are the same for all panels. This arrangement may be regarded as a local model of periodic fuselage ring stiffeners, which are usually the dominant restraints on panel motions. Longitudinal "stringers" between the stiffeners are important in controlling panel resonance frequencies, but, because they are parallel to the exterior mean boundary layer flow, their contributions to the *generation* of sound and vibration by fluid-structure interactions will tend to be of less significance. Similarly, recent acoustic-holographic measurements [9] indicate that the more visually obvious structural discontinuities associated with cabin windows are also unlikely to be important sources of noise and vibration.

The analytical model is formulated in §2, where the reverse flow reciprocal theorem (discussed briefly in the Appendix) is applied to determine a Green's function for treating the "scattering" of boundary layer wall

pressures at panel edges. This is used (in §3) to investigate scattering at an isolated straight edge, when the edge is regarded as either *clamped* or *simply supported*. The edge radiated sound is expressed in terms of the wavenumber-frequency spectrum of the boundary layer wall pressure fluctuations [10, 11], whose properties are specified independently. Here we make use of an empirical model proposed by Laganelli and Wolfe [12]. The principal characteristics of the sound produced for either edge condition are similar, being dominated by the requirement that the panel displacement ζ, say, must *vanish* at the edge, rather than conditions related to restrictions on higher derivatives of ζ. The more general problem of a periodic array of coupled panels is discussed in §4. As the frequency varies, the coupling between neighboring panels causes large fluctuations in sound levels about those predicted for the isolated edge. The analysis is expected to be valid when the Strouhal number $\omega\delta^*/U < 1$ (ω being the radian frequency, δ^* the boundary layer displacement thickness, and U the velocity of the main stream), and we shall actually conclude that, for subsonic mean stream velocities, it is only when this condition is satisfied that significant production of sound occurs by the fluid-structure interaction. The results should be of value in validating more general numerical schemes for interior noise prediction.

2. THE GOVERNING EQUATIONS

2.1 The aerodynamic sound problem

Consider high speed turbulent flow of fluid of mean density ρ_1 and sound speed c_1 over the surface of a thin elastic plate that occupies the plane $x_2 = 0$ of the rectangular coordinate system (x_1, x_2, x_3) (see Figure 1). The mean flow is in the positive x_1-direction in the "exterior" region $x_2 < 0$. The plate is partitioned into *panels* by rectilinear edges at $x_1 = X_1, X_2, X_3, \ldots$. It is required to determine the sound radiated into the "interior" region $x_2 > 0$ as a result of the fluid-structure interaction. The fluid in $x_2 > 0$ is at rest in the undisturbed state, and has mean density and sound speed respectively equal to ρ_0 and c_0.

Take the equations of aerodynamic sound in the form [13]

$$\left[\frac{1}{c_0^2}\frac{\partial^2}{\partial t^2} - \nabla^2\right]B = 0, \qquad x_2 > 0, \tag{2.1}$$

$$\left[\frac{1}{c_1^2}\left(\frac{\partial}{\partial t} + U\frac{\partial}{\partial x_1}\right)^2 - \nabla^2\right]B = S(x,t), \quad x_2 < 0. \tag{2.2}$$

In these equations $B = w + \frac{1}{2}v^2$ is the total enthalpy, w being the specific enthalpy of the fluid, v the velocity, U is the uniform main stream velocity in the exterior region, and t denotes time. The aeroacoustic source term $S(x,t)$ vanishes except in those regions where the vorticity and entropy gradients are non-zero, but its functional form will not be required in the following analysis. When B is known, the acoustic pressure p can be calculated from the formula

$$\frac{1}{\rho}\frac{\partial p}{\partial t} = \frac{DB}{Dt}, \tag{2.3}$$

where ρ is the local mean density and D/Dt is the material derivative. This equation is valid at high Reynolds number provided the motion may be regarded as *isentropic* (i.e., the entropy of each fluid particle is constant), which we shall assume to be the case. Equation (2.2) is applicable provided the

characteristic wavelength of the sound is large compared to the boundary layer displacement thickness δ^*, which should be the case at radian frequencies ω satisfying $\omega\delta^*/U < 1$.

The panel motions are assumed to be governed by the linear thin plate equation, such that if $\zeta(x_1, x_3, t)$ is the flexural displacement in the x_2-direction, then

$$\left(D\nabla_2^4 + m\frac{\partial^2}{\partial t^2}\right)\zeta + [p] = 0, \tag{2.4}$$

where $\nabla_2^4 = (\partial^2/\partial x_1^2 + \partial^2/\partial x_3^2)^2$, D is the bending stiffness of the plate, m the mass per unit area, and

$$[p] = p(x_1, +0, x_3, t) - p(x_1, -0, x_3, t) \tag{2.5}$$

is the pressure loading. The linearized approximation is expected to be adequate for aircraft panels, where displacement amplitudes do not usually exceed 5 μm. In practice panel motions are damped by interior "trimming" to reduce interior noise levels. We shall take approximate account of this by introducing a panel loss factor η, such that for vibrational motions of radian frequency ω (proportional to $e^{-i\omega t}$),

$$D = D_o[1 - i\eta(\omega)], \quad \eta(-\omega) = -\eta(\omega), \tag{2.6}$$

where $D_o > 0$, and $\eta > 0$ for $\omega > 0$ [14]. The panel and fluid motions are also coupled by the linear relations

$$\frac{\partial^2\zeta}{\partial t^2} = -\frac{1}{\rho_0}\frac{\partial p}{\partial x_2}, \quad x_2 = +0; \qquad \left(\frac{\partial}{\partial t} + U\frac{\partial}{\partial x_1}\right)^2\zeta = -\frac{1}{\rho_1}\frac{\partial p}{\partial x_2}, \quad x_2 = -0, \tag{2.7}$$

which follow from the linearized, normal components of the fluid momentum equation just above and below the plate.

2.2 Green's function

Let $G(\mathbf{x},\mathbf{y},t-\tau)$ denote the time domain Green's function defined by the solution of equations (2.1), (2.2) with outgoing wave behavior when the source term S in (2.2) is replaced by an impulsive point source $\delta(\mathbf{x}-\mathbf{y})\delta(t-\tau)$ at $\mathbf{y}$. The acoustic pressure $p(\mathbf{x},t)$ in the interior region (where $B = p/\rho_0$) is then given by

$$p(\mathbf{x},t) = \rho_0 \int G(\mathbf{x},\mathbf{y},t-\tau)S(\mathbf{y},\tau)d^3\mathbf{y}d\tau, \tag{2.8}$$

where the spatial integration is over the boundary layer sources and the time integration is over $-\infty < \tau < \infty$. Green's function can be partitioned in the following way:

$$G(\mathbf{x},\mathbf{y},t-\tau) = G_o(\mathbf{x},\mathbf{y},t-\tau) + G_s(\mathbf{x},\mathbf{y},t-\tau), \tag{2.9}$$

where G_o is Green's function for a uniform, homogeneous plate, and G_s is the additional component attributable to the panel edges.

In practice the acoustic pressure $p(\mathbf{x},t)$ is required in the interior domain at large distances from the source region, typically at distances $|\mathbf{x}-\mathbf{y}|$ from the sources that are large relative to the acoustic wavelength. This observation permits the derivation of a simplified form of the Green's function.

To do this set

$$G(\mathbf{x},\mathbf{y},t-\tau) = \frac{-1}{2\pi}\int_{-\infty}^{\infty} G(\mathbf{x},\mathbf{y},\omega)e^{-i\omega(t-\tau)}\, d\omega, \tag{2.10}$$

where $G(\mathbf{x},\mathbf{y},\omega)$ satisfies

$$\left.\begin{aligned} [\nabla^2 + \kappa_0^2]G(\mathbf{x},\mathbf{y},\omega) &= 0, \qquad x_2 > 0, \\ [\nabla^2 + (\kappa_1 + iM\partial/\partial x_1)^2]G(\mathbf{x},\mathbf{y},\omega) &= \delta(\mathbf{x}-\mathbf{y}), \quad x_2 < 0, \end{aligned}\right\} \tag{2.11}$$

and

$$\kappa_0 = \omega/c_0, \ \kappa_1 = \omega/c_1, \ M = U/c_1. \tag{2.12}$$

For observer positions $\mathbf{x}$ many acoustic wavelengths $2\pi/\kappa_0$ from the point source at $\mathbf{y}$, we invoke the *reverse flow* reciprocal theorem, according to which

$$G(\mathbf{x},\mathbf{y},\omega) \equiv \frac{\rho_1}{\rho_0} G^R(\mathbf{y},\mathbf{x},\omega), \tag{2.13}$$

where $G^R(\mathbf{y},\mathbf{x},\omega)$ is the solution of equations (2.11) when $\mathbf{x}$ and $\mathbf{y}$ are interchanged (so that the source is now regarded as being at $\mathbf{x}$, in the interior domain, and the observer at $\mathbf{y}$ in the exterior flow region) and M is replaced by -M (i.e., the mean flow velocity is reversed; see Figure 2). This result is a particular case of a more general reverse flow reciprocal theorem (see, e.g., [15, 16]) whose proof is outlined for the present problem in the

Appendix.

When $|\mathbf{x}| \to \infty$ the sound wave $G_I^R(\mathbf{y},\mathbf{x},\omega)$, say, generated by the reciprocal source at $\mathbf{x}$ may be regarded as a plane wave impinging on the elastic plate. Thus, to calculate the reciprocal Green's function G^R in this limit we have only to solve a plane wave diffraction problem, in contrast to the direct calculation of G, which involves the interaction of the near field of a point source at y with the inhomogeneous plate. The incident, reciprocal plane wave (regarded as a function of y) is evidently given by

$$G_I^R(\mathbf{y},\mathbf{x},\omega) = \frac{-e^{i\kappa_0|\mathbf{x}-\mathbf{y}|}}{4\pi|\mathbf{x}-\mathbf{y}|} \approx \frac{-1}{4\pi|\mathbf{x}|} e^{i\kappa_0\{|\mathbf{x}| - \mathbf{n}\cdot\mathbf{y}\}}, \quad |\mathbf{x}| \to \infty, \tag{2.14}$$

where $\mathbf{n}$ is the unit vector

$$\mathbf{n} = \mathbf{x}/|\mathbf{x}|. \tag{2.15}$$

The diffraction problem is solved in two stages. First we determine the motion on and near the plate produced by the incident wave when the panel edges are ignored, i.e., for a homogeneous plate. This defines the reciprocal Green's function $G_o^R(\mathbf{y},\mathbf{x},\omega)$, say, that determines $G_o(\mathbf{x},\mathbf{y},t-\tau)$ of (2.9). Recalling that $G_I^R(\mathbf{y},\mathbf{x},\omega)$ represents the perturbation total enthalpy, it is easy to show in the usual way (by making use of the homogeneous forms of equations (2.11) in the reciprocal problem and of equations (2.3), (2.4), (2.6) [17]) that the displacement ζ_o of the *homogeneous* plate produced by the reciprocal source can be expressed in the form

$$\zeta_o = \zeta_I e^{-i\kappa_0(n_1 y_1 + n_3 y_3)}, \tag{2.16}$$

where

$$\zeta_I = \frac{\mathfrak{I}(\mathbf{n},\omega)e^{i\kappa_0|\mathbf{x}|}}{2\pi i\omega c_0|\mathbf{x}|}, \tag{2.17}$$

$$\mathfrak{I}(\mathbf{n},\omega) = \frac{i\epsilon}{\left\{\left[(1-i\eta)\left(\frac{\omega}{\omega_c}\right)^2(n_1^2+n_3^2)^2 - 1\right]\frac{\omega}{\omega_c} - i\epsilon\left[\frac{1}{n_2} + \frac{(\rho_0 c_0^2/\rho_1 c_1^2)(c_0/c_1 - Mn_1)^2}{\sqrt{\{(c_0/c_1 - Mn_1)^2 - (n_1^2+n_3^2)\}}}\right]\right\}}. \tag{2.18}$$

In these expressions

$$\sqrt{\{(c_0/c_1 - Mn_1)^2 - (n_1^2+n_3^2)\}} = \mathrm{sgn}(c_0/c_1 - Mn_1)\,|(c_0/c_1 - Mn_1)^2 - (n_1^2+n_3^2)|^{1/2}$$
$$= i\,\mathrm{sgn}(\omega)\,|(c_0/c_1 - Mn_1)^2 - (n_1^2+n_3^2)|^{1/2}$$

according as the argument of the square root is $\gtrless 0$. The quantity ω_c (> 0) is the coincidence frequency $c_0^2(m/D_o)^{1/2}$, at which the *in vacuo* phase velocity of bending waves on the plate in the absence of damping is equal to the speed of sound in the interior region. Then ϵ is a fluid loading parameter defined by

$$\epsilon = \frac{\rho_0 c_0}{\omega_c m} . \tag{2.19}$$

For an aluminum plate in air, for example, $\epsilon \approx 0.0022$, and $\omega_c h/c_0 \approx 0.22$, where h is the plate thickness.

To complete the diffraction calculation it is necessary to examine the interaction between the panel edges and the incident flexural disturbance (2.16). This interaction produces scattered flexural motions on the panels, which we denote by $\zeta_s(y_1)e^{-in_3 y_3}$, and potential flow motions in the fluid which satisfy the reciprocal forms of equations (2.11) (with the source omitted). If the velocity potentials are denoted by $\varphi_0 e^{-in_3 y_3}$ and $\varphi_1 e^{-in_3 y_3}$ respectively for $y_2 \gtrless 0$, it follows from the reciprocal equations of motion that,

$$\left.\begin{aligned} \zeta_s(y_1) &= \int_{-\infty}^{\infty} \zeta_s(k) e^{iky_1}\, dk, \\ \varphi_0 &= -\int_{-\infty}^{\infty} \frac{\omega \zeta_s(k)}{\gamma(k)}\, e^{i(ky_1+\gamma y_2)}\, dk, \quad y_2 > 0, \\ \varphi_1 &= \int_{-\infty}^{\infty} \frac{(\omega+Uk)\zeta_s(k)}{\Gamma_+(k)}\, e^{i(ky_1-\Gamma_+ y_2)}\, dk, \quad y_2 < 0, \end{aligned}\right\} \tag{2.20}$$

where $\gamma \equiv \gamma(k) = [\kappa_0^2(1-n_3^2)-k^2]^{1/2}$ (branch cuts being chosen such that, for real k, $\mathrm{sgn}(\gamma) = \mathrm{sgn}(\omega)$ when γ is real and is otherwise positive imaginary). The function $\Gamma_+(k)$ and a related function $\Gamma_-(k)$, also needed below, are defined for real k by

$$\begin{aligned} \Gamma_\pm(k) &= \mathrm{sgn}(\kappa_1 \pm Mk)\,|(\kappa_1 \pm Mk)^2 - \kappa_0^2 n_3^2 - k^2|^{1/2}, \text{ for } (\kappa_1 \pm Mk)^2 - \kappa_0^2 n_3^2 - k^2 > 0, \\ &= i\,|(\kappa_1 \pm Mk)^2 - \kappa_0^2 n_3^2 - k^2|^{1/2}, \text{ for } (\kappa_1 \pm Mk)^2 - \kappa_0^2 n_3^2 - k^2 < 0. \end{aligned} \tag{2.21}$$

Using the representations (2.20) and (2.3) (noting that $B = i\omega\varphi_j$, $j = 0$, 1 in irrotational flow), we find in the reciprocal problem that the jump in the scattered pressure $p_s e^{-i\kappa_0 n_3 y_3}$ across the plate is given by

$$[p_s] = -i\int_{-\infty}^{\infty} \left[\frac{\rho_0\omega^2}{\gamma(k)} + \frac{\rho_1(\omega+Uk)^2}{\Gamma_+(k)}\right]\zeta_s(k)e^{iky_1}\,dk, \tag{2.22}$$

where $[p_s]$ is defined as in (2.5). The scattered pressure and displacement must satisfy the thin plate equation (2.4) *except* at the panel edges, i.e., substituting from (2.20) and (2.22) into (2.4), we must have

$$\int_{-\infty}^{\infty} \mathcal{L}_+(k,\omega)\zeta_s(k)e^{iky_1}\,dk = 0,\ y_1 \neq X_1,\ X_2,\ X_3,\ \ldots, \tag{2.23}$$

where

$$\mathcal{L}_\pm(k,\omega) \equiv D(\kappa_0^2 n_3^2 + k^2)^2 - m\omega^2 - i\left[\frac{\rho_0\omega^2}{\gamma(k)} + \frac{\rho_1(\omega\pm Uk)^2}{\Gamma_\pm(k)}\right]. \tag{2.24}$$

Now $\mathcal{L}_\pm(k,\omega) \approx O(k^4)$ as $|k| \to \infty$, which implies that if $\zeta_s(y_1)$ is to remain finite as $y_1 \to X_N \pm 0$ ($N = 1, 2, 3, \ldots$), the general solution of (2.23) must be taken in the form

$$\zeta_s(k) = \sum_N \zeta_I\left(A_{N0} + A_{N1}k + A_{N2}k^2 + A_{N3}k^3\right)\frac{e^{-ikX_N}}{\mathcal{L}_+(k,\omega)}, \tag{2.25}$$

where the coefficients $A_{Nj} \equiv A_{Nj}(\omega)$ are independent of k, and are to be determined from the panel edge conditions. Thus, if $\zeta = Z(y_1)e^{-i\kappa_0 n_3 y_3}$ is the net displacement of the plate in the reciprocal problem, including the component ζ_o of (2.15) for the homogeneous plate, we can write

$$\frac{Z(y_1)}{\zeta_I} = \sum_N \int_{-\infty}^{\infty} \left(A_{N0} + A_{N1}k + A_{N2}k^2 + A_{N3}k^3\right)\frac{e^{ik(y_1 - X_N)}}{\mathcal{L}_+(k,\omega)}\,dk + e^{-i\kappa_0 n_1 y_1}. \tag{2.26}$$

It remains to determine the values of the coefficients A_{Nj} from conditions specified at the panel edges $y_1 = X_1, X_2, X_3, \ldots$. The details of this calculation are outlined in §§3, 4 for two different panel configurations. The velocity potential φ_1 defined in (2.20) may then be evaluated by substituting for $\zeta_s(k)$ from (2.25). Then (2.10) and the

reciprocal formula (2.13) yield the following representation for the component G_s of the time domain Green's function

$$G_s(x,y,t-\tau) = -\frac{i\rho_1}{2\pi\rho_0}\int_{-\infty}^{\infty}\omega\varphi_1(y_1,\omega)e^{-i[\kappa_0 n_3 y_3+\omega(t-\tau)]}\,d\omega,$$
$$y_2 < 0,\ |x| \to \infty. \qquad (2.27)$$

Here the source point y ($y_2 < 0$) is located within the mean flow in the exterior domain, and the observer position x is in $x_2 > 0$ in the interior region. Substituting for φ_1 we find

$$G_s(x,y,t-\tau) = \frac{-\rho_1}{(2\pi)^2 c_0\rho_0|x|}\sum_N\int_{-\infty}^{\infty}\frac{\mathfrak{I}(n,\omega)(\omega+Uk)}{\Gamma_+(k)\mathcal{L}_+(k,\omega)}\left(A_{N0}+A_{N1}k+A_{N2}k^2+A_{N3}k^3\right)$$
$$\times e^{i\{k(y_1-X_N)-\Gamma_+ y_2-\kappa_0 n_3 y_3-\omega(t-\tau-|x|/c_0)\}}\,dk\,d\omega,$$
$$y_2 < 0,\ |x| \to \infty. \qquad (2.28)$$

The condition that G_s is a real valued quantity implies that

$$A_{Nj}(-\omega) = (-1)^j A^*_{Nj}(\omega), \qquad (2.29)$$

where the asterisk denotes the complex conjugate.

3. NOISE GENERATED AT AN ISOLATED PANEL EDGE

3.1 The acoustic pressure spectrum

To assess the importance of different edge conditions we first assume the infinite plate of Figure 1 consists of two semi-infinite panels connected by a single edge at $x_1 = X_1 \equiv 0$ (so that the summations of §2 reduce to one term, corresponding to $N = 1$, say). The acoustic pressure generated by the boundary layer is given by equation (2.8), where Green's function G is the sum (2.9) of the homogeneous plate Green's function G_o and the correction G_s due to the panel edges. The contribution from G_o is identical to the radiation produced by turbulent flow over a smooth plate, and will be ignored. In subsonic flows this is expected to be relatively weak compared to the sound generated by the interaction of the boundary layer pressures with the panel edges. The latter is determined by replacing G in (2.8) by G_s.

By making use of the representation (2.28) for a single edge we find

$$p(\mathbf{x},t) \approx \frac{-(2\pi)^2\rho_1}{c_0|\mathbf{x}|}\sum_j \int_{-\infty}^{\infty} \frac{\mathfrak{I}(n,\omega)(\omega-Uk)}{\Gamma_-(k)\mathcal{L}_-(k,\omega)}\,\bar{S}(k,\Gamma_-,\kappa_0 n_3,\omega)a_j(\omega)(-k)^j\, e^{-i\omega[t]}dkd\omega \qquad |\mathbf{x}| \to \infty, \quad (3.1)$$

where

$$\bar{S}(k_1,k_2,k_3,\omega) = \frac{1}{(2\pi)^4}\int_{-\infty}^{\infty} S(\mathbf{y},\tau)e^{-i\{k_1y_1+k_2y_2+k_3y_3-\omega\tau\}}\, d^3\mathbf{y}d\tau, \quad (3.2)$$

is the space-time Fourier transform of the aeroacoustic source term, and $[t] = t-|\mathbf{x}|/c_0$ is the retarded time. The summation is over $j = 0$ to 3, where the shorthand notation $a_j = A_{1j}$ has been introduced; the minus signs in $(-k)^j$ and in the subscripts of Γ_-, $\mathcal{L}_-$ have arisen because the integration variable k has been replaced by -k.

The acoustic pressure can be related to empirical representations of the wall pressure fluctuations $p_w(x_1,x_3,t)$ beneath the turbulent boundary layer by expressing $\bar{S}(k,\Gamma_-,\kappa_0 n_3,\omega)$ in terms of the Fourier transform

$$p_w(k,\kappa_0 n_3,\omega) = (1/2\pi)^3\int_{-\infty}^{\infty} p_w(x_1,x_3,t)\exp\{-i(kx_1+\kappa_0 n_3 x_3-\omega t)\}dx_1\,dx_3\,dt$$

of the pressure fluctuations that would be produced by the same turbulent

boundary layer flow over a smooth, rigid wall. The edge scattered pressure fluctuations (including sound and hydrodynamic pressures) then represent the correction of the wall pressure produced by the structural inhomogeneities.

When the wall is *rigid* equations (2.2) and (2.3) are easily solved to supply

$$p_w(k,\kappa_0 n_3,\omega) = \frac{2\pi i \rho_1(\omega-Uk)}{\omega\Gamma_-(k)}\,\bar{S}(k,\Gamma_-,\kappa_0 n_3,\omega). \tag{3.3}$$

This relation permits (3.1) to be cast in the form

$$p(x,t) \approx \frac{2\pi i}{c_0|x|}\sum_j \int_{-\infty}^{\infty} \frac{\omega\mathfrak{Z}(n,\omega)}{\mathcal{L}_-(k,\omega)}\, p_w(k,\kappa_0 n_3,\omega)a_j(\omega)(-k)^j e^{-i\omega[t]}\,dkd\omega$$

$$|x| \to \infty, \tag{3.4}$$

which determines the interior noise pressure fluctuations in terms of the wall pressure fluctuations that are generated by the same turbulent flow on a rigid wall (the so-called boundary layer *blocked pressure* [10, 11, 18, 19]).

The characteristic dimension of the boundary layer turbulence eddies is of the same order as the boundary layer *displacement thickness* δ^* [20, 21]. When this is much smaller than the extent of the boundary layer the wall pressure $p_w(x_1,x_3,t)$ may assumed to be statistically *stationary*, and to possess a wall pressure wavenumber-frequency spectrum $P_w(k_1,k_3,\omega)$, which varies slowly with streamwise location x_1. If a transverse section $-\frac{1}{2}L < x_3 < \frac{1}{2}L$ of the elastic plate is wetted by the turbulent flow, where $L \gg \delta^*$, $p_w(k_1,k_3,\omega)$ satisfies

$$\langle p_w(k_1,k_3,\omega)p_w^*(K_1,k_3,\omega')\rangle \approx \frac{L}{2\pi}\,\delta(\omega-\omega')\delta(k_1-K_1)P_w(k_1,k_3,\omega),\ \delta^* \ll L, \tag{3.5}$$

The mean square acoustic pressure $\langle p^2(x,t)\rangle$ in the interior may now be expressed in terms of a frequency spectrum density $\Phi(x,\omega)$ (> 0) according to

$$\langle p^2(x,t)\rangle = \int_0^{\infty} \Phi(x,\omega)\,d\omega, \tag{3.6}$$

and equations (3.4) and (3.5), with account taken of the relations (2.29),

then yield

$$\Phi(x,\omega) \approx \frac{4\pi L\omega^2 |\Im(n,\omega)|^2}{c_0^2|x|^2} \int_{-\infty}^{\infty} \frac{P_w(k,\kappa_0 n_3,\omega)}{|\mathcal{L}_-(k,\omega)|^2} \left|\sum_j a_j(\omega)(-k)^j\right|^2 dk, \quad |x| \to \infty. \tag{3.7}$$

3.2 Clamped edge

When the panel edges are *clamped* the displacement $Z(y_1)$ of (2.26) must satisfy $Z = \partial Z/\partial y_1 = 0$ as $y_1 \to \pm 0$. These conditions imply that Z and $\partial Z/\partial y_1$ are continuous at the edge, and therefore that $a_2 = a_3 \equiv 0$. Then a_0 and a_1 are determined by

$$a_0 I_0 + a_1 I_1 = -1, \quad a_0 I_1 + a_1 I_2 = \kappa_0 n_1, \quad \text{where } I_j = \int_{-\infty}^{\infty} k^j dk/\mathcal{L}_+(k,\omega). \tag{3.8}$$

The solutions of these equations are conveniently expressed in the following dimensionless forms:

$$\left.\begin{aligned} a_0 &= \frac{m\omega^2}{K_o}\alpha_0, \quad a_1 = \frac{m\omega^2}{K_o^2}\alpha_1, \\ \alpha_0 &= \frac{\Psi_2 + \Psi_1\mu n_1}{\Psi_1^2 - \Psi_0\Psi_2}, \qquad \alpha_1 = \frac{-[\Psi_1 + \Psi_0\mu n_1]}{\Psi_1^2 - \Psi_0\Psi_2}, \end{aligned}\right\} \tag{3.9}$$

where,

$$\Psi_j = \int_{-\infty}^{\infty} \frac{\lambda^j d\lambda}{(1-i\eta)\Lambda^4 - 1 - \frac{i\epsilon}{\mu}\left(\frac{1}{\sqrt{(\mu^2-\Lambda^2)}} + \frac{(\rho_0 c_0^2/\rho_1 c_1^2)(c_0/c_1 + M\lambda/\mu)^2}{\sqrt{\{(c_0\mu/c_1 + M\lambda)^2 - \Lambda^2\}}}\right)},$$

$$\Lambda^2 = \lambda^2 + \mu^2 n_3^2, \quad K_o = (m\omega^2/D_o)^{1/4} > 0, \quad \mu = \sqrt{\omega/\omega_c}. \tag{3.10}$$

In these expressions K_o is the *in vacuo* wavenumber of bending waves of radian frequency ω. The value of the integrand is made unique by taking branch cuts for $\sqrt{(\mu^2-\Lambda^2)}$ from $\lambda = \pm\mu(1-n_3^2)^{1/2}$ to $\pm i\infty$ in the complex λ-plane, and for $\sqrt{\{(c_0\mu/c_1 + M\lambda)^2 - \Lambda^2\}}$ (when $M < 1$) from

$$\lambda = \mu[c_0 M/c_1 \pm \{(c_0/c_1)^2 - (1-M^2)n_3^2\}^{1/2}]/(1-M^2) \text{ to } \pm i\infty;$$

it may be assumed that $\omega > 0$, and relations (2.29) can then be used to evaluate a_0 and a_1 for $\omega < 0$.

3.3 Simply supported edge

When the panel edges are simply supported the displacement satisfies $Z = \partial^2 Z/\partial y_1^2 = 0$ as $y_1 \to \pm 0$. In this case $a_1 = a_3 \equiv 0$, and

$$\left.\begin{aligned} a_0 &= \frac{m\omega^2}{K_o}\,\alpha_0, \quad a_2 = \frac{m\omega^2}{K_o^3}\,\alpha_2, \\ \alpha_0 &= \frac{\Psi_2' - \Psi_1'(\mu n_1)^2}{\Psi_1'^2 - \Psi_0'\Psi_2'}, \qquad \alpha_2 = \frac{-[\Psi_1' - \Psi_0'(\mu n_1)^2]}{\Psi_1'^2 - \Psi_0'\Psi_2'}, \end{aligned}\right\} \tag{3.11}$$

where,

$$\Psi_j' = \frac{\pi z^{2j+1}}{2}\,[i - (-1)^j]$$

$$+ \int_{-\infty}^{\infty} \frac{\dfrac{i\epsilon}{\mu}\left(\dfrac{1}{\sqrt{(\mu^2-\Lambda^2)}} + \dfrac{(\rho_1 c_1^2/\rho_0 c_0^2)(c_1/c_0 + M\lambda/\mu)^2}{\sqrt{\{(c_0\mu/c_1 + M\lambda)^2 - \Lambda^2\}}}\right)\lambda^{2j}\,d\lambda}{\left[(1-i\eta)\Lambda^4 - 1 - \dfrac{i\epsilon}{\mu}\left(\dfrac{1}{\sqrt{(\mu^2-\Lambda^2)}} + \dfrac{(\rho_1 c_1^2/\rho_0 c_0^2)(c_0/c_1 + M\lambda/\mu)^2}{\sqrt{\{(c_0\mu/c_1 + M\lambda)^2 - \Lambda^2\}}}\right)\right]\left[(1-i\eta)\Lambda^4 - 1\right]}, \tag{3.12}$$

and $z = 1/(1-i\eta)^{1/4}$.

3.4 Numerical results

To evaluate the integral in (3.7) for the acoustic pressure spectrum the functional form of the wall pressure wavenumber-frequency spectrum $P_w(k, \kappa_0 n_3, \omega)$ must be specified. The dominant wall pressure fluctuations are associated with wavenumbers k in the convective domain, which peaks in the neighborhood of $k = \omega/U_c$, where the mean convection velocity $U_c \approx 0.7U$. We shall present numerical predictions of $\Phi(\mathbf{x},\omega)$ only for $n_3 \equiv x_3/|\mathbf{x}| = 0$, i.e., for radiation directions in the plane of symmetry of the boundary layer flow. The crudest approximation for the dominant wall pressure fluctuations is then obtained by writing

$$P_w(k,0,\omega) \approx \frac{\ell_3}{\pi}\,\delta(k-\omega/U_c)\Phi_{pp}(\omega), \tag{3.13}$$

where ℓ_3 is a spanwise correlation length (in the x_3-direction) of wall pressure fluctuations of frequency ω, and $\Phi_{pp}(\omega)$ is the point frequency spectrum, which satisfies $\langle p_w^2 \rangle = \int_{-\infty}^{\infty} \Phi_{pp}(\omega) d\omega$.

To further simplify the discussion, we shall limit consideration to the case $\rho_0 = \rho_1$, $c_0 = c_1$. Then (3.7) becomes,

$$\Phi(\mathbf{x},\omega) \approx \frac{4L\ell_3}{|\mathbf{x}|^2} \frac{M_c^8 (\omega/\omega_c)^3 |\mathfrak{I}(\Theta,\omega)|^2 |\sum_j \alpha_j(\omega)(-\mu/M_c)^j|^2 \Phi_{pp}(\omega)}{\left| \left[(1-i\eta)\left(\frac{\omega}{\omega_c}\right)^2 - M_c^4 \right] \frac{\omega}{\omega_c} - \frac{\epsilon M_c^5}{\sqrt{(1-M_c^2)}} - \frac{\epsilon M_c^3 (M-M_c)^2}{\sqrt{[1-(M-M_c)^2]}} \right|^2}, \quad \omega > 0, \quad (3.14)$$

where $M_c = U_c/c_0$ is the convection Mach number, $\Theta \equiv \sin^{-1}(x_1/|\mathbf{x}|)$ is the observer direction indicated in Figure 3, in the plane of symmetry $x_3 = 0$, and

$$\mathfrak{I}(\Theta,\omega) = \frac{i\epsilon}{\left(\left[(1-i\eta)\left(\frac{\omega}{\omega_c}\right)^2 \sin^4\Theta - 1 \right] \frac{\omega}{\omega_c} - i\epsilon \left[\frac{1}{\cos\Theta} + \frac{(1-M\sin\Theta)^2}{\sqrt{\{(1-M\sin\Theta)^2 - \sin^2\Theta\}}} \right] \right)}. \quad (3.15)$$

Equation (3.14) expresses the acoustic pressure spectrum directly in terms of the turbulent wall pressure frequency spectrum $\Phi_{pp}(\omega)$. The ratio

$$\Delta(\omega) = \frac{[\Phi(\mathbf{x},\omega)/\Phi_{pp}(\omega)]}{[Lh/|\mathbf{x}|^2]}, \quad (3.16)$$

represents the efficiency of sound production by the interaction of the boundary layer with the panel edge. This is plotted as a function of ω/ω_c in Figure 3 for a *clamped* edge connecting aluminum panels in air for three different mean flow Mach numbers $M = U/c_0$ when $\Theta = 0$, $\eta = 0.2$ and the correlation length ℓ_3 is given by the Corcos approximation $\ell_3 \approx 1.4U_c/\omega$, $U_c = 0.7U$ [10, 11, 18, 19, 22]. The efficiency decreases with increasing frequency, except at the resonance peaks, which occur where the convection velocity is close to the phase speed of flexural waves on the undamped plate; the magnitudes of these peaks are determined by the loss factor η, whose influence is important only close to the resonance frequencies. The large value $\eta = 0.2$ used in these calculations is assumed to account for the relatively high damping of structural motions that would in practice be produced by the "trimming" of aircraft panels. The corresponding frequency

dependence of Δ for the simply supported edge is very similar to that shown in Figure 3.

To make quantitative predictions of the acoustic pressure spectrum $\Phi(\mathbf{x},\omega)$ we use the following approximation for the boundary layer point pressure spectrum $\Phi_{pp}(\omega)$ proposed by Laganelli and Wolfe [12] (extending earlier analyses reported in [23, 24]) for an *adiabatic* wall:

$$\frac{(U/\delta^*)\Phi_{pp}(\omega)}{(\rho_o v_*^2)^2} \approx \frac{\sigma^2 F^{-0.57}}{4\pi(v_*/U)^4[1 + F^{2.87}(\omega\delta^*/U)^2]}, \quad (3.17)$$

where ρ_o is the mean density and v_* is the *friction velocity* [20, 21]. The friction velocity varies with the boundary layer Reynolds number, but is typically of order 0.04U. Also, $F = 1+0.13M^2$, $\sigma = p_{rms}/\frac{1}{2}\rho_1 U^2$, where p_{rms} is the root mean square wall pressure fluctuation. Recent studies indicate that $\sigma \approx 0.01$ [25], and this value is used below. Figures 4 and 5 depict predictions of the nondimensional interior acoustic pressure spectrum

$$\frac{\Phi(\mathbf{x},\omega)}{\delta^*\rho_0^2 c_0^3[Lh/|\mathbf{x}|^2]} \equiv \frac{\Delta(\omega)\Phi_{pp}(\omega)}{\delta^*\rho_0^2 c_0^3}, \quad (3.18)$$

respectively for clamped and simply supported edge conditions. The calculations are for a one mm thick aluminum plate at three different mean flow Mach numbers for $\Theta = 0°$, $\eta = 0.2$, when the boundary layer displacement thickness δ^* is assumed to vary as $1/M^{1/5}$ [20, 21], with $\delta^* = 1$ cm at $M = 0.3$. Both figures exhibit increasing acoustic power at low frequencies and resonance contributions at higher frequencies (the resonance being relatively more important at low Mach numbers) where the convection velocity U_c coincides with the flexural wave speed. The overall levels are similar for either edge condition, especially at low frequencies where the coefficient α_0 of (3.11) turns out to be very large compared to the other scattering coefficients α_j, $j > 0$. The predicted large sound power at low frequencies occurs because the Laganelli and Wolfe model spectrum (3.17) is effectively constant for $\omega\delta^*/U < 1$, which is consistent with an alternative empirical representation proposed by Efimtsov [26] (see also [27, 28]). Note, in particular, that the generated sound is significant only for $\omega\delta^*/U < 1$, which is in accord with our assumption in §2.

4. PERIODIC PANELS WITH CLAMPED EDGES

Consider next a plate divided into a periodic array of parallel, infinitely long panels of width d, with edges at $x_1 = X_N \equiv Nd$ transverse to the mean flow direction (where N ranges over all integers in $-\infty < N < \infty$). When the edge conditions are the same for all panels, periodicity implies that the coefficients A_{Nj} in the representation (2.28) of the scattering Green's function can be written

$$A_{Nj} = a_j e^{-iN\kappa_0 n_1 d}, \quad j = 0, 1, 2, 3. \tag{4.1}$$

The equations determining the coefficients a_j are obtained by application of the edge conditions at any one of the edges. When the edges are clamped $Z = \partial Z/\partial y_1 = 0$ at $y_1 = Nd$, and we then find that $a_2 = a_3 = 0$, and that a_0, a_1 are given by (3.9) in terms of the following discrete analog of the definition (3.10)

$$\Psi_j = \frac{2\pi}{K_o d} \sum_{N=-\infty}^{\infty} \frac{\lambda_N^j}{(1-i\eta)\Lambda_N^4 - 1 - \frac{i\epsilon}{\mu}\left[\frac{1}{\sqrt{(\mu^2-\Lambda_N^2)}} + \frac{(\rho_1 c_1^2/\rho_0 c_0^2)(c_0/c_1+M\lambda_N/\mu)^2}{\sqrt{((c_0\mu/c_1+M\lambda_N)^2-\Lambda_N^2)}}\right]},$$

$$\lambda_N = 2N\pi/K_o d - \mu n_1, \quad \Lambda_N^2 = \lambda_N^2 + \mu^2 n_3^2. \tag{4.2}$$

By proceeding as in §3.1 we may express the far field acoustic pressure in the interior region in the form

$$p(x,t) \approx \frac{(2\pi)^2 i}{c_0 d|x|} \sum_{N=-\infty}^{\infty} \int_{-\infty}^{\infty} \sum_j \frac{\omega \mathfrak{I}(n,\omega)(-1)^j a_j(\omega)}{\mathcal{L}_-(\kappa_0 n_1 + 2N\pi/d, \omega)}$$

$$\times \{\kappa_0 n_1 + 2N\pi/d\}^j p_w(n_1 + 2N\pi/d, \kappa_0 n_3, \omega) e^{-i\omega[t]}\, d\omega, \qquad |x| \to \infty. \tag{4.3}$$

To use this result to calculate the acoustic frequency spectrum $\Phi(x,\omega)$ it is necessary to restrict the region of excitation of the panels by the boundary layer to a finite area A, since Φ must increase linearly with A. When $\sqrt{A} \gg d \gg \delta^*$, there are contributions from many edges, and

$$\langle p_w\left(k_1+\frac{2\pi N}{d},k_3,\omega\right)p_w^*\left(k_1+\frac{2\pi N'}{d},k_3,\omega'\right)\rangle \approx \frac{A}{(2\pi)^2}\delta_{NN'}\,\delta(\omega-\omega')P_w\left(k_1+\frac{2\pi N}{d},k_3,\omega\right), \qquad (4.4)$$

where $\delta_{NN'}$ is the Kronecker delta (equal to 1 for N = N', and 0 otherwise). The acoustic pressure frequency spectrum is then given by the following generalization of (3.7)

$$\Phi(x,\omega)$$

$$\approx \frac{8\pi^2 A\omega^2 |\Im(n,\omega)|^2}{c_0^2 d^2 |x|^2}\sum_{N=-\infty}^{\infty}\frac{P_w(\kappa_0 n_1+2N\pi/d,\kappa_0 n_3,\omega)}{|\mathcal{L}_-(\kappa_0 n_1+2N\pi/d,\omega)|^2}\,\left|\sum_j a_j(\omega)(-1)^j(\kappa_0 n_1+2N\pi/d)^j\right|^2 \qquad (4.5)$$

The value of the summation with respect to N depends on the functional form of the wall pressure wavenumber-frequency spectrum $P_w(k_1,k_3,\omega)$. In the absence of precise measurements at Mach numbers of interest in the present application, we shall fall back on the simple model (3.13). This can be used in (4.5) provided it is assumed that the length scale of the turbulent motions is small compared to the distance d between the edges. The summation can then be approximated by an integral with respect to k, say, where we set $k = \kappa_0 n_1+2N\pi/d$, and $dk = 2\pi/d$. This is equivalent to assuming that the direct turbulence excitations at different edges are statistically independent. In the simplified case considered in §3, in which $\rho_0 = \rho_1$, $c_0 = c_1$, and $n_3 = 0$, we then obtain

$$\Phi(x,\omega) \approx \frac{4A\ell_3}{d|x|^2}\,\frac{M_c^8(\omega/\omega_c)^3|\Im(\Theta,\omega)|^2\left|\sum_j \alpha_j(\omega)(-\mu/M_c)^j\right|^2\Phi_{pp}(\omega)}{\left|\left[(1-i\eta)\left(\frac{\omega}{\omega_c}\right)^2-M_c^4\right]\frac{\omega}{\omega_c}-\frac{\epsilon M_c^5}{\sqrt{(1-M_c^2)}}-\frac{\epsilon M_c^3(M-M_c)^2}{\sqrt{[1-(M-M_c)^2]}}\right|^2}, \quad \omega > 0, \qquad (4.6)$$

This is formally N_p times larger than the corresponding expression (3.14) for a single, isolated panel edge, where $N_p = A/dL$ is the number of panel edges within the area A of the boundary layer. However, the functions (3.10) and (4.2) used in the definitions of the coefficients α_0 and α_1 are equivalent only when $K_o d$ is large, i.e., when the characteristic bending wavelength of disturbances on a panel is small compared to the panel width, which occurs at high frequencies. At lower frequencies we might therefore expect predictions of (4.6) and (3.14) to differ substantially.

The efficiency Δ of sound generation can be defined by analogy with expression (3.16) for a single edge:

$$\Delta(\omega) = \frac{[\Phi(\mathbf{x},\omega)/\Phi_{pp}(\omega)]}{[Ah/d|\mathbf{x}|^2]} . \tag{4.7}$$

The variation of $\Delta(\omega)$ with ω/ω_c is depicted in Figure 6 for two mean flow Mach numbers $M = 0.3$ and 0.9 and $\Theta = 0°$, for the aluminum plate considered previously in §3 ($\eta = 0.2$) with panel edge separation of $d = 50$ cm. At very high frequencies, when flexural motions are rapidly damped, the efficiency of sound production at each edge would be expected to reduce to that shown in Figure 3 for an isolated edge. Interference between sound production by different edges causes the high frequency behavior to be oscillatory, and it is clear from the figures that, at these frequencies, it is only at the higher Mach number of $M = 0.9$ that the single and multiple edge radiation efficiencies are similar. The interference arises because flexural motions generated at a panel edge are subsequently scattered into sound at neighboring edges; alternatively, they may be interpreted in terms of resonance modes of the panels, since the peaks and troughs respectively occur where $\Psi_1^2 - \Psi_0\Psi_2$ is small and large, and where the coefficient α_0 in (4.6) is large and small ($\alpha_1\mu$ is uniformly small). In all cases, however, the radiation efficiencies decrease very rapidly above the *convective* resonance frequencies indicated in the figure. At low frequencies the density of structural modes is small for multiple edges, and the efficiency is then very much smaller than for a single edge.

The corresponding predictions of the interior acoustic pressure spectrum

$$\frac{\Phi(\mathbf{x},\omega)}{\delta^*\rho_0^2 c_0^3 [Ah/d|\mathbf{x}|^2]} \equiv \frac{\Delta(\omega)\Phi_{pp}(\omega)}{\delta^*\rho_0^2 c_0^3}, \tag{4.8}$$

are shown in Figure 7 for $M = 0.3$, 0.6, 0.9, when the wall pressure frequency spectrum $\Phi_{pp}(\omega)$ is given by the Laganelli and Wolfe formula (3.17) (as in §3 we assume the boundary layer displacement thickness δ^* varies like $1/M^{1/5}$, with $\delta^* = 1$ cm when $M = 0.3$). Comparison with the single edge case of Figure 4 reveals that interference between edges causes large fluctuations in the spectrum about the single edge case, especially at lower Mach numbers; at low

frequencies the radiation is significantly smaller than for the single edge. The number of these fluctuations increases with increasing Mach number, their amplitudes being governed by the value of the loss factor η, and are progressively larger as $\eta \to 0$. At very high frequencies the amplitude of the sound, although fluctuating rapidly, does not vary significantly with Mach number. As before, it should be noted that significant generation of sound is predicted only for $\omega\delta^*/U < 1$.

The directivity of the sound is illustrated in Figure 8 for $\omega\delta^*/U = 0.05$. These plots have been made by using the Laganelli and Wolfe spectrum (3.17) at a constant displacement thickness $\delta^* = 1$ cm. The directivity exhibits a uniform, monopole type of behavior in the plane of symmetry of the flow ($x_3 = 0$), except for a very narrow null at $\Theta = \sin^{-1}(1/(1+M))$. This angle corresponds to the angle of incidence in the reciprocal, reverse flow problem at which the pressure differential $[p^R]$, say, across the homogeneous plate vanishes identically, and the associated flexural response ζ_o of equation (2.16) is null. These results are, of course, strictly relevant only in the flat plate approximation.

5. CONCLUSION

An important component of mid-to-high frequency aircraft interior noise is produced by the scattering of intense boundary layer wall pressures by structural inhomogeneities of the fuselage. In this chapter an idealized configuration has been investigated in which the fuselage is plane, and formed by thin elastic panels of infinite length in the direction transverse to the mean flow. This may be regarded as a local model describing the influence of fuselage ring stiffeners, which usually constitute the most significant constraint on panel motions. The excitation of the panels by the high Reynolds number boundary layer flow was expressed in terms of a prescribed boundary layer wall pressure spectrum. The sound produced by the interaction of these wall pressures with the panels and their edges has been determined analytically for the case where all panels have equal width and are subject to the same edge conditions. The procedure is expected to be valid provided the principal acoustic wavelengths are larger than the boundary layer displacment thickness, which is the case at subsonic mean velocities provided $\omega\delta^*/U < 1$, and the detailed predictions indicate that sound generation at higher frequencies is negligible. The numerical results give explicit representations of the influence of the main stream Mach number on sound generation. Detailed results of this type can be used to validate more general numerical prediction schemes.

The material of this chpater is an expanded version of a presentation made at an *Interior Noise Workshop* organized by Dr. R. J. Silcox at NASA Langley Research Center (25 - 27 April, 1995).

APPENDIX: REVERSE FLOW RECIPROCITY

For given points $\mathbf{x}_A$ and $\mathbf{x}_B$ respectively in the interior ($x_2 > 0$) and exterior ($x_2 < 0$) domains of Figure 2, the reciprocal theorem (2.13) can be stated in the form

$$G(\mathbf{x}_A,\mathbf{x}_B,\omega) = \frac{\rho_1}{\rho_0}\, G^R(\mathbf{x}_B,\mathbf{x}_A,\omega), \tag{A.1}$$

where G and G^R represent perturbation *stagnation enthalpies* associated respectively with the direct problem

$$\left.\begin{aligned} [\nabla^2 + \kappa_0^2]G(\mathbf{x},\mathbf{x}_B,\omega) &= 0, && x_2 > 0, \\ [\nabla^2 + (\kappa_1 + iM\partial/\partial x_1)^2]G(\mathbf{x},\mathbf{x}_B,\omega) &= \delta(\mathbf{x}-\mathbf{x}_B), && x_2,\ x_{B2} < 0, \end{aligned}\right\} \tag{A.2}$$

and the reciprocal (or *adjoint*) problem

$$\left.\begin{aligned} [\nabla^2 + \kappa_0^2]G^R(\mathbf{x},\mathbf{x}_A,\omega) &= \delta(\mathbf{x}-\mathbf{x}_A), && x_2,\ x_{A2} > 0, \\ [\nabla^2 + (\kappa_1 - iM\partial/\partial x_1)^2]G^R(\mathbf{x},\mathbf{x}_A,\omega) &= 0, && x_2, < 0. \end{aligned}\right\} \tag{A.3}$$

Let ρ denote the local mean fluid density. In the usual way [29], multiply equations (A.2) by $\rho G^R(\mathbf{x},\mathbf{x}_A,\omega)$ and (A.3) by $\rho G(\mathbf{x},\mathbf{x}_B,\omega)$, subtract corresponding resulting equations in (A.2) and (A.3), and integrate with respect to $\mathbf{x}$ over their respective regions of validity. The divergence theorem is then applied to transform the volume integrals into integrals over the upper and lower surfaces of the plate (the radiation condition ensures that there are no contributions from surfaces at infinity).

If ζ and ζ^R denote the flexural displacements of the plate in the direct and reciprocal problems, then

$$\partial G/\partial x_2 = -\omega^2\zeta, \qquad \partial G^R/\partial x_2 = -\omega^2\zeta^R, \qquad x_2 \to +0,$$

$$\partial G/\partial x_2 = i\omega(-i\omega+U\partial/\partial x_1)\zeta, \qquad \partial G^R/\partial x_2 = i\omega(-i\omega-U\partial/\partial x_1)\zeta^R, \quad x_2 \to -0.$$

These relations are used to eliminate normal derivatives of G and G^R from the surface integral. By integrating by parts with respect to x_1 and making use

of the time-harmonic form of (2.3) we then find

$$-\omega^2\int_{-\infty}^{\infty}\Big(\zeta[p^R] - \zeta^R[p]\Big)dx_1\,dx_3 = \rho_1 G^R(x_B, x_A, \omega) - \rho_0 G(x_A, x_B, \omega), \qquad (A.4)$$

where the integration is over the undisturbed plane $x_2 = 0$ of the plate, and $[p]$, $[p^R]$ are defined as in (2.5). Equation (A.1) is now deduced by substituting for $[p]$ and $[p^R]$ from the corresponding time-harmonic bending wave equation (2.4), and observing that the resulting integral vanishes identically. In doing this, note that contributions to the integral in (A.4) from the immediate neighborhoods of the edges are null since the displacements and pressure discontinuities are finite.

REFERENCES

1. R. E. Hayden, B. M. Murrey and M. A. Theobald, "A study of interior noise levels, noise sources and transmission paths in light aircraft," NASA CR-172152 (1983).
2. W. V. Bhat, "Flight test measurement of exterior turbulent boundary layer pressure fluctuations on Boeing model 737 airplane," J. Sound Vib. 14, 439 - 457 (1971).
3. J. F. Wilby, C. D. McDaniel and E. G. Wilby, "In-flight acoustic measurements on a light twin-engined turboprop airplane," NASA CR-178004, (1985).
4. J. S. Mixson and J. F. Wilby, "Interior noise". Chapter 16 of *Aeroacoustics of Flight Vehicles: Theory and Practice (Vol. 2)*. NASA Ref. Pub. No. 1258, (1991).
5. J. F. Wilby and F. L. Gloyna, "Vibration measurements of an airplane fuselage structure:I. Turbulent boundary layer excitation," J. Sound Vib. 23, 443 - 466 (1972).
6. W. R. Graham, "Boundary layer noise and vibration," Doctoral Thesis, Cambridge University Engineering Department (1993).
7. E. H. Dowell, G. F. Gorman and D. A. Smith, "Acoustoelasticity: General Theory, acoustic natural modes and forced response to sinusoidal excitation, including comparisons with experiment," J. Sound Vib. 52, 519 - 542 (1977).
8. M. S. Howe, "Sound produced by an aerodynamic source adjacent to a partly coated, finite elastic plate," Proc. Roy. Soc. Lond. A436, 351 - 372 (1992).
9. B. H. Houston, E. G. Williams, P. C. Herdic and K. B. Washburn, "Surface velocity and interior pressure measurements associated with an aircraft fuselage section." Paper presented at the *Interior Noise Workshop*, NASA Langley Research Center, Hampton VA, 25 - 27 April, 1995.
10. D. M. Chase, "Modeling the wavevector-frequency spectrum of turbulent boundary layer wall pressure," J. Sound Vib. 70, 29 - 67 (1980).
11. D. M. Chase, "The character of the turbulent wall pressure spectrum at subconvective wavenumbers and a suggested comprehensive model," J. Sound Vib. 112, 125 - 147 (1987).

12. A. L. Laganelli and H. Wolfe "Prediction of fluctuating pressure in attached and separated turbulent boundary layer flow," *AIAA Paper 89 - 1064*, (1989).
13. M. S. Howe, "Contributions to the theory of aerodynamic sound, with application to excess jet noise and the theory of the flute," J. Fluid Mech. 71, 625 - 673 (1975).
14. L. L. Beranek and I. L. Vér, *Noise and Vibration Control Engineering* (John Wiley, New York, 1992).
15. M. S. Howe, "The generation of sound by aerodynamic sources in an inhomogeneous steady flow," J. Fluid Mech. 67, 579 - 610 (1975).
16. W. Möhring, "Modelling low Mach number noise," pp 85 - 96, *Proc. Symp. Mechanics of Sound Generation in Flows*, Göttingen, August 28 - 31 (editor E.-A. Müller: Springer, Berlin, 1979).
17. M. C. Junger and D. Feit, *Sound, Structures and their Interactions* (Acoustical Society of America, New York, 1993).
18. W. K. Blake, *Mechanics of flow-induced sound and vibration, Vol. 2: Complex flow-structure interactions* (Academic Press, New York, 1986).
19. M. S. Howe, "Surface pressures and sound produced by turbulent flow over smooth and rough walls," J. Acoust. Soc. Am. 90, 1041 - 1047 (1991).
20. J. O. Hinze, *Turbulence*, Second edition (McGraw-Hill, New York, 1975).
21. H. Schlichting, *Boundary Layer Theory*, Seventh edition (McGraw-Hill, New York, 1979).
22. G. M. Corcos, "The structure of the turbulent pressure field in boundary layer flows," J. Fluid Mech. 18, 353 - 378 (1964).
23. M. V. Lowson, "Pressure fluctuations in turbulent boundary layers," *NASA Tech. Note TN D-3156* (1965).
24. A. L. Laganelli, A. Martellucci and L. L. Shaw, "Wall pressure fluctuations in attached boundary layer flow," AIAA J. 21, 495 - 502 (1983).
25. G. Schewe, "On the structure and resolution of wall pressure fluctuations associated with turbulent boundary layer flow," J. Fluid Mech. 134, 311 - 328 (1983).

26. B. M. Efimtsov, "Characteristics of the field of turbulent wall pressure fluctuations at large Reynolds numbers," Sov. Phys. Acoust. 28, 289 - 292 (1982).

27. A. E. Landmann, "Spatial-Temporal boundary layer models for aircraft interior noise." Paper presented at the *NASA Langley Workshop on Interior Noise*, Hampton VA, 25 - 27 April (1995).

28. W. R. Graham, "A comparison of models for the wavenumber-frequency spectrum of turbulent boundary layer pressures," *AIAA Paper 95-097*, (1995).

29. P. M. Morse and H. Feshbach, *Methods of Theoretical Physics*, Vol. 1 (McGraw-Hill, New York, 1953).

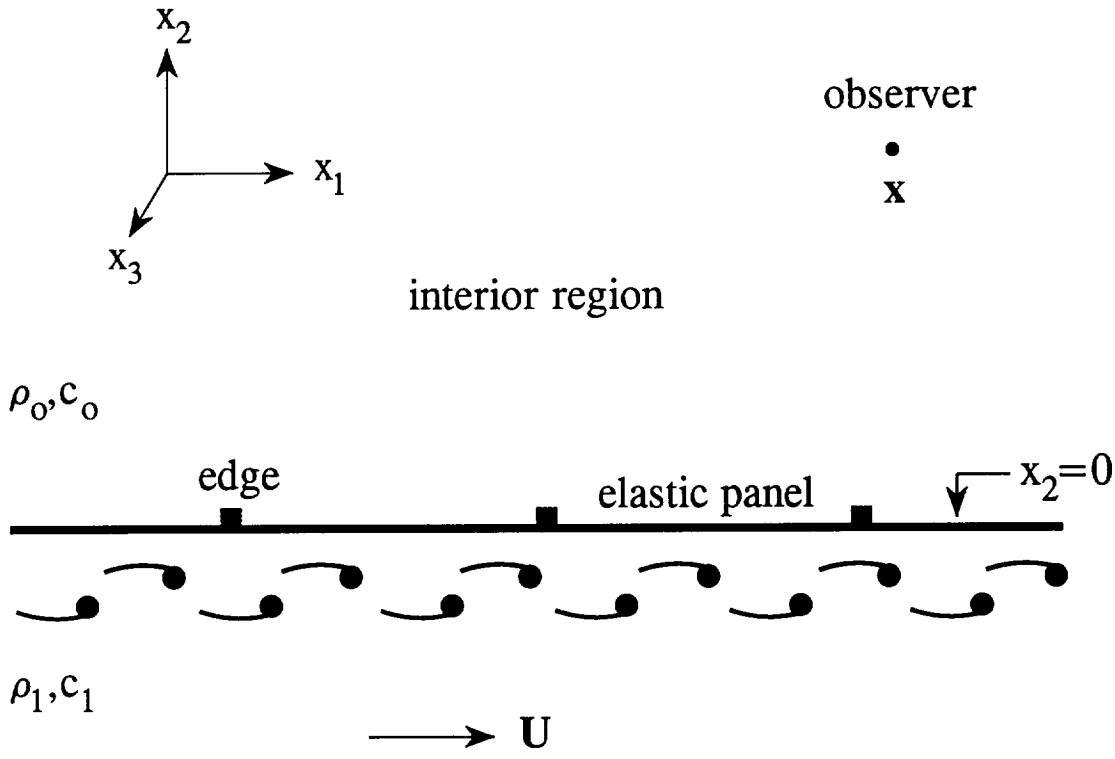

Figure 1. Configuration of the turbulent flow and inhomogeneous elastic plate.

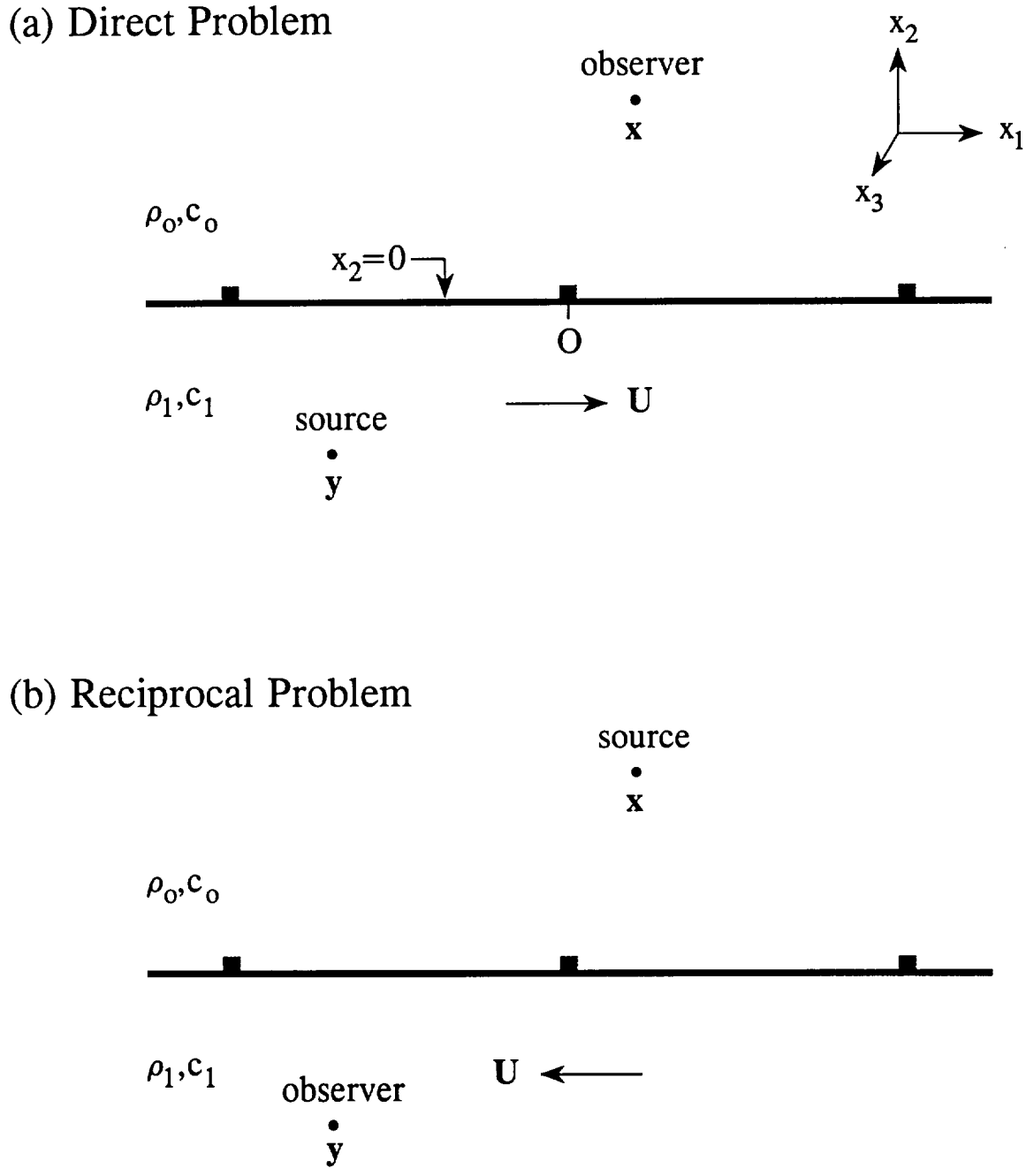

Figure 2. Reverse flow reciprocity.

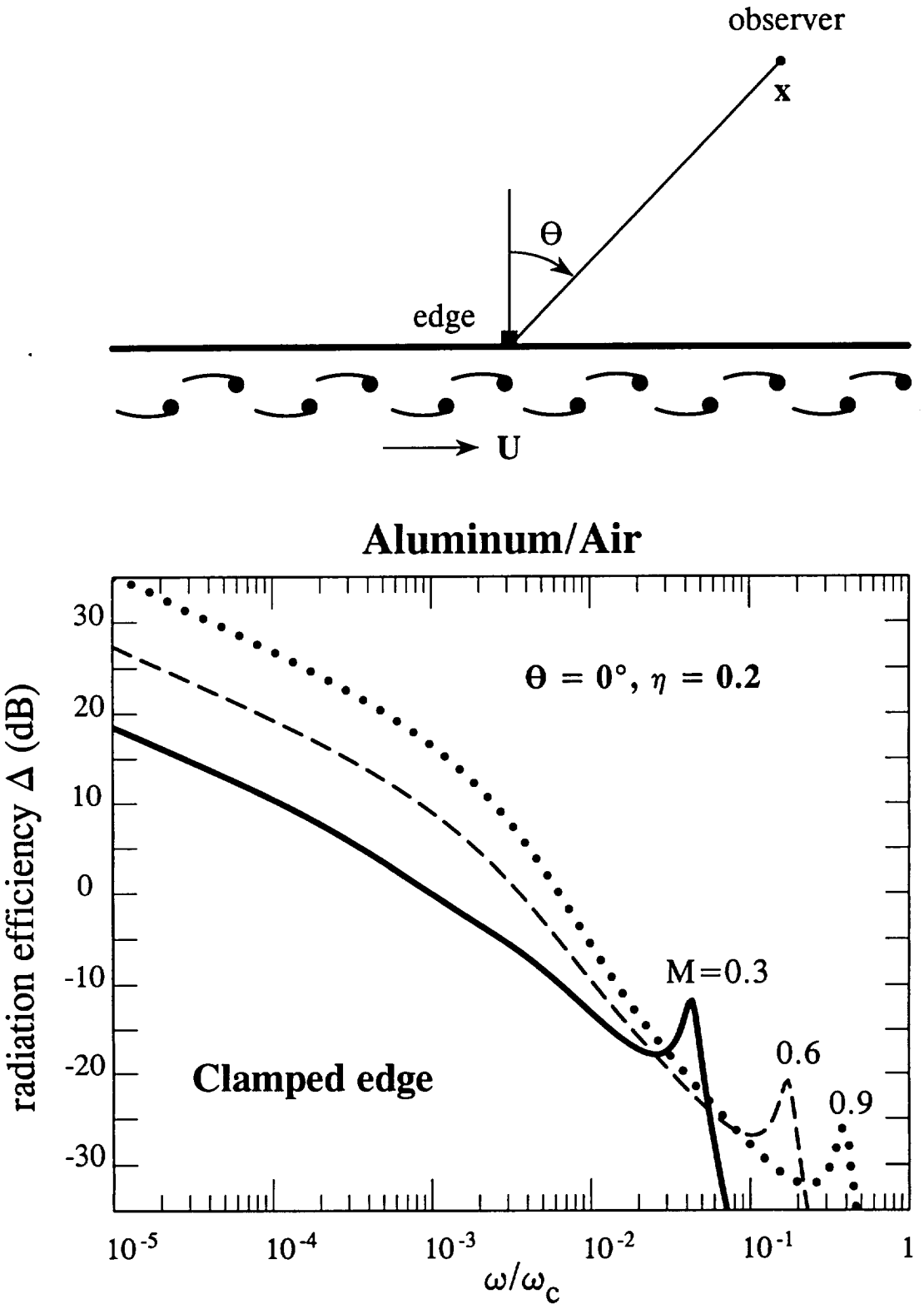

Figure 3. The efficiency (3.16) of sound production by turbulent flow over a clamped panel edge.

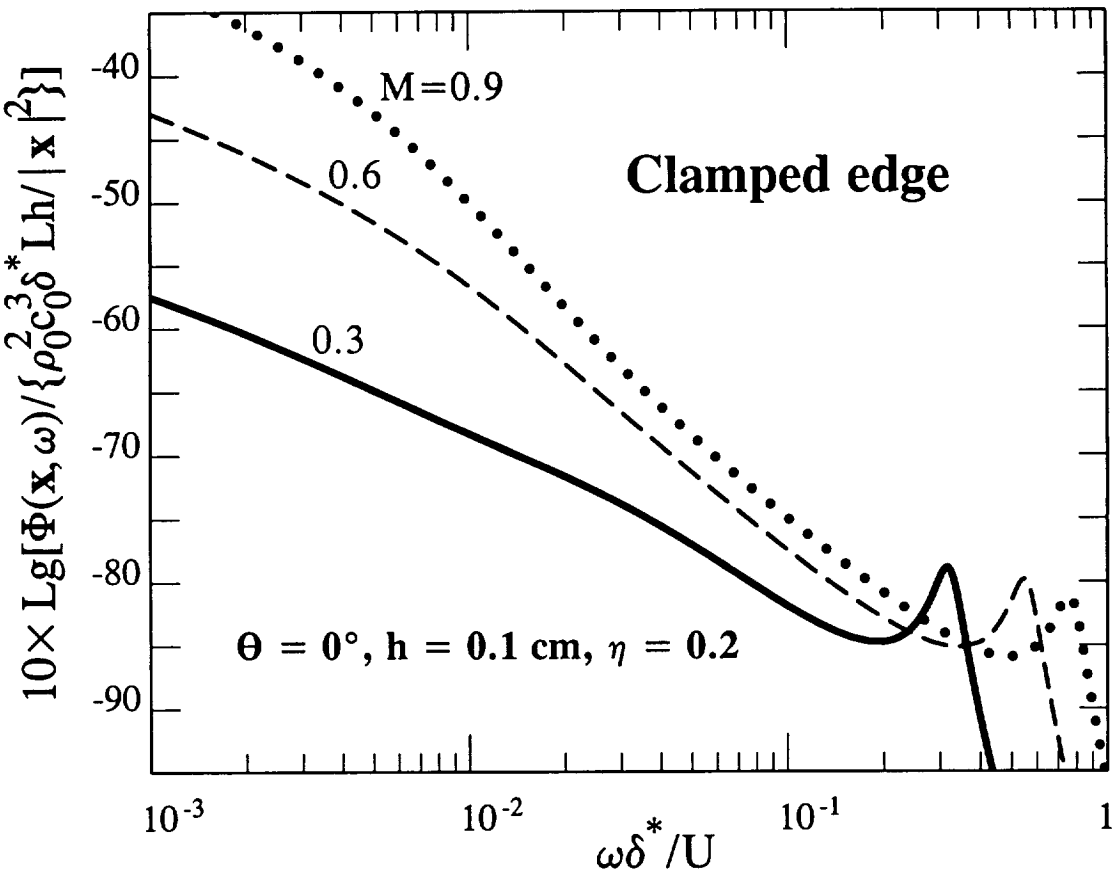

Figure 4. Predicted interior sound pressure spectrum level

$$10\times Lg[\Phi(\mathbf{x},\omega)/(\delta^* \rho_0^2 c_0^3 Lh/|\mathbf{x}|^2)]$$

for an isolated clamped aluminum panel edge in air when $\Theta = 0°$, $h = 0.1$ cm, $\eta = 0.2$. The displacement thickness δ^* is assumed to vary as $1/M^{1/5}$, with $\delta^* = 1$ cm when $M = 0.3$.

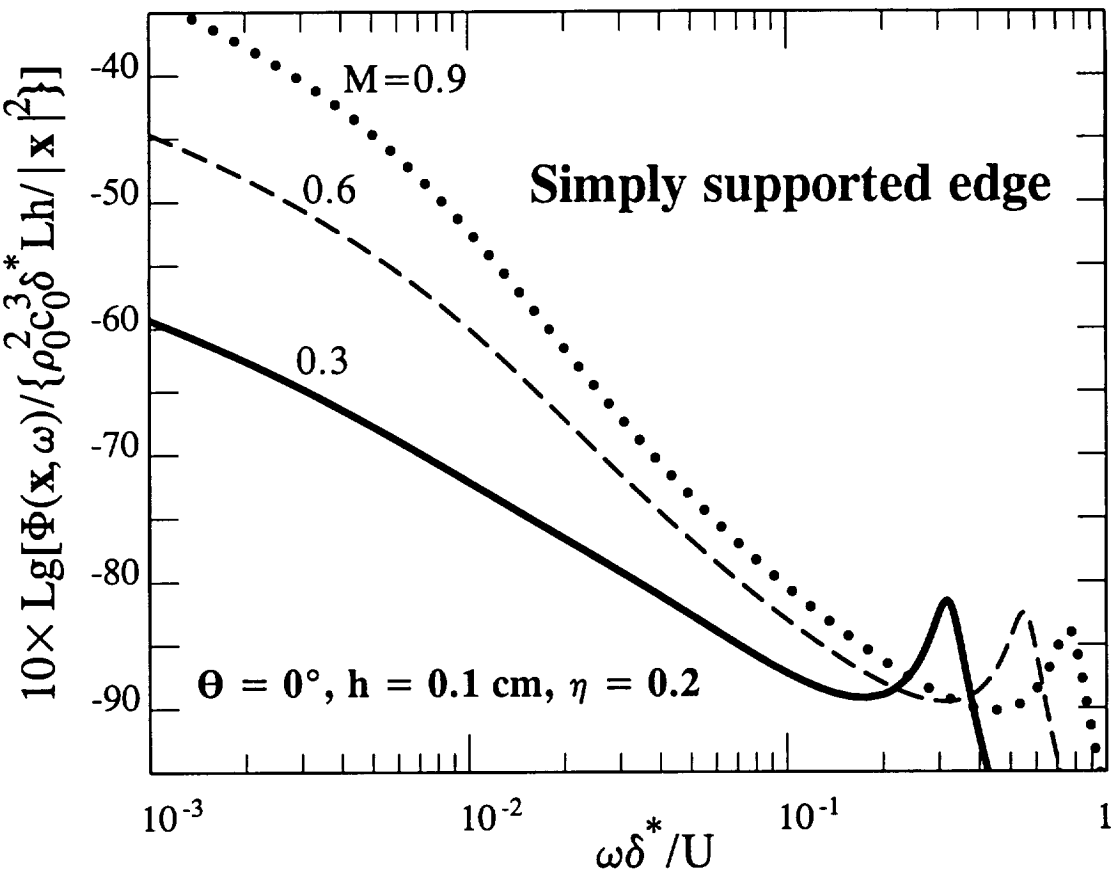

Figure 5. Predicted interior sound pressure spectrum level

$$10\times Lg[\Phi(\mathbf{x},\omega)/\{\delta^* \rho_0^2 c_0^3 Lh/|\mathbf{x}|^2\}]$$

for an isolated simply supported aluminum panel edge in air when $\Theta = 0°$, $h = 0.1$ cm, $\eta = 0.2$. The displacement thickness δ^* is assumed to vary as $1/M^{1/5}$, with $\delta^* = 1$ cm when $M = 0.3$.

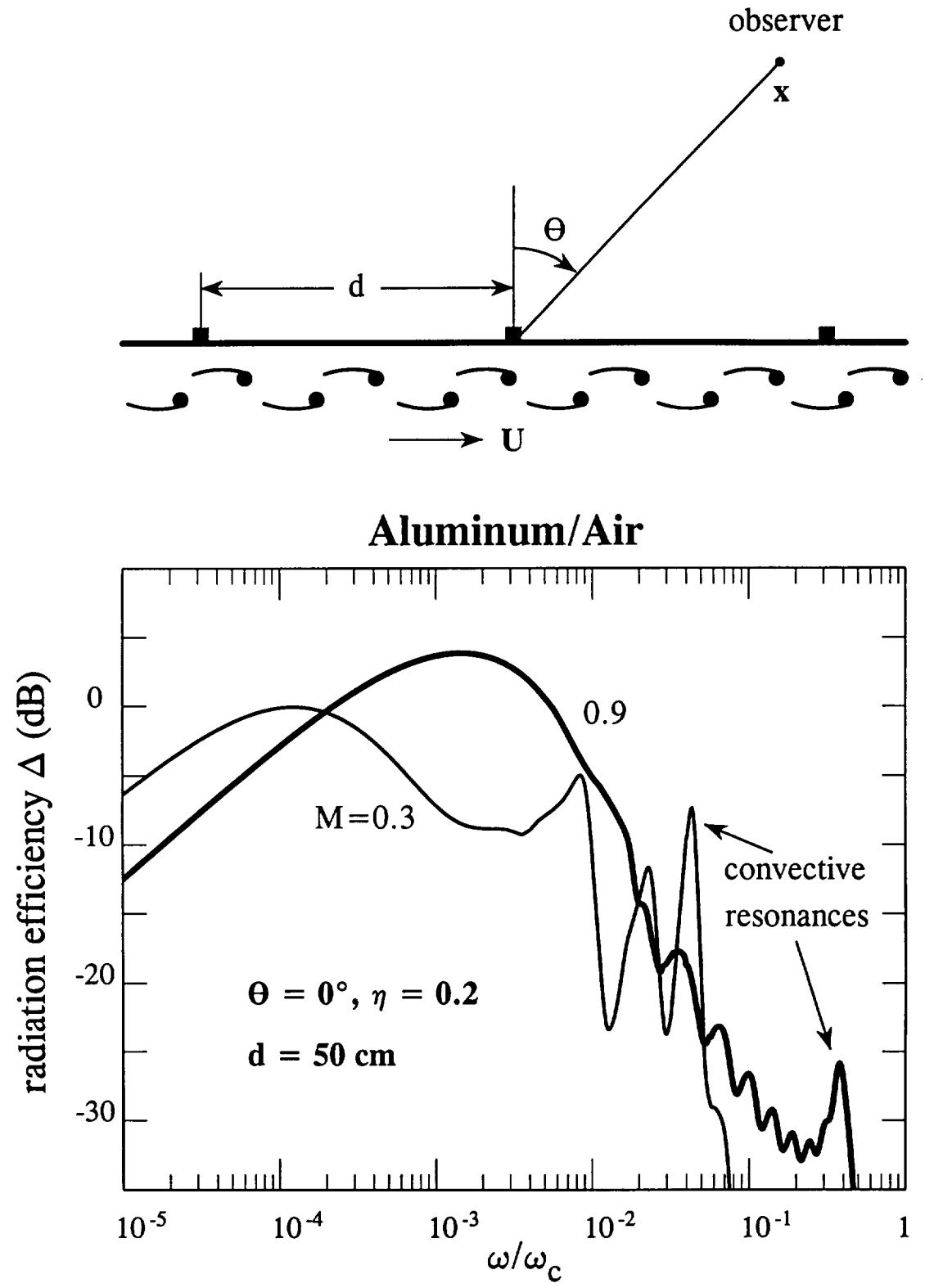

Figure 6. The efficiency (4.7) of sound production by turbulent flow over a periodically clamped plate.

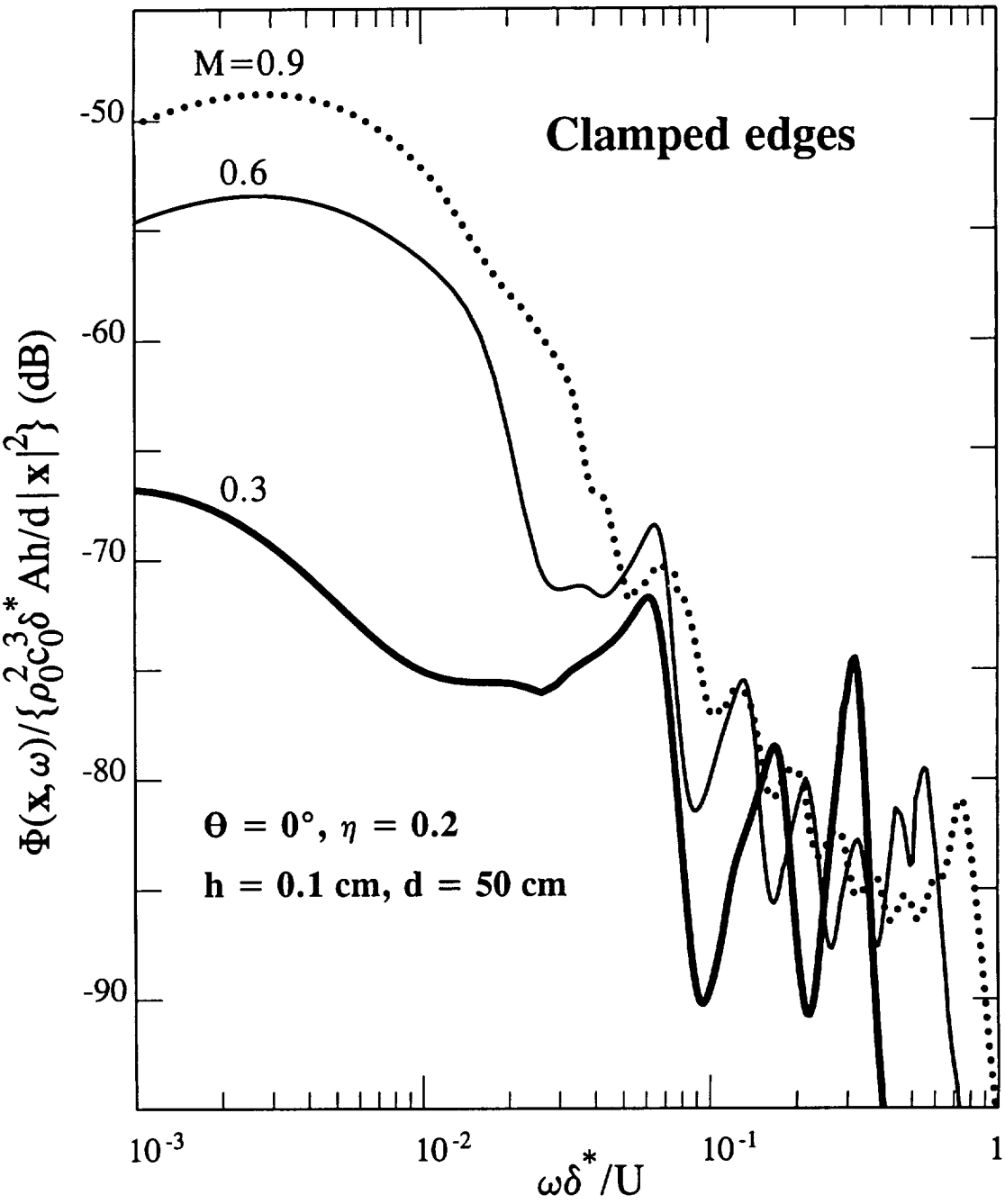

Figure 7. Predicted interior sound pressure spectrum level

$$10\times Lg[\Phi(x,\omega)/\{\delta^* \rho_0^2 c_0^3 Ah/d|x|^2\}]$$

for a periodically clamped aluminum plate in air when $\Theta = 0°$, $h = 0.1$ cm, $d = 50$ cm, $\eta = 0.2$, and when $\Phi_{pp}(\omega)$ is given by the Laganelli and Wolfe formula (3.17). The displacement thickness δ^* is assumed to vary as $1/M^{1/5}$, with $\delta^* = 1$ cm when $M = 0.3$.

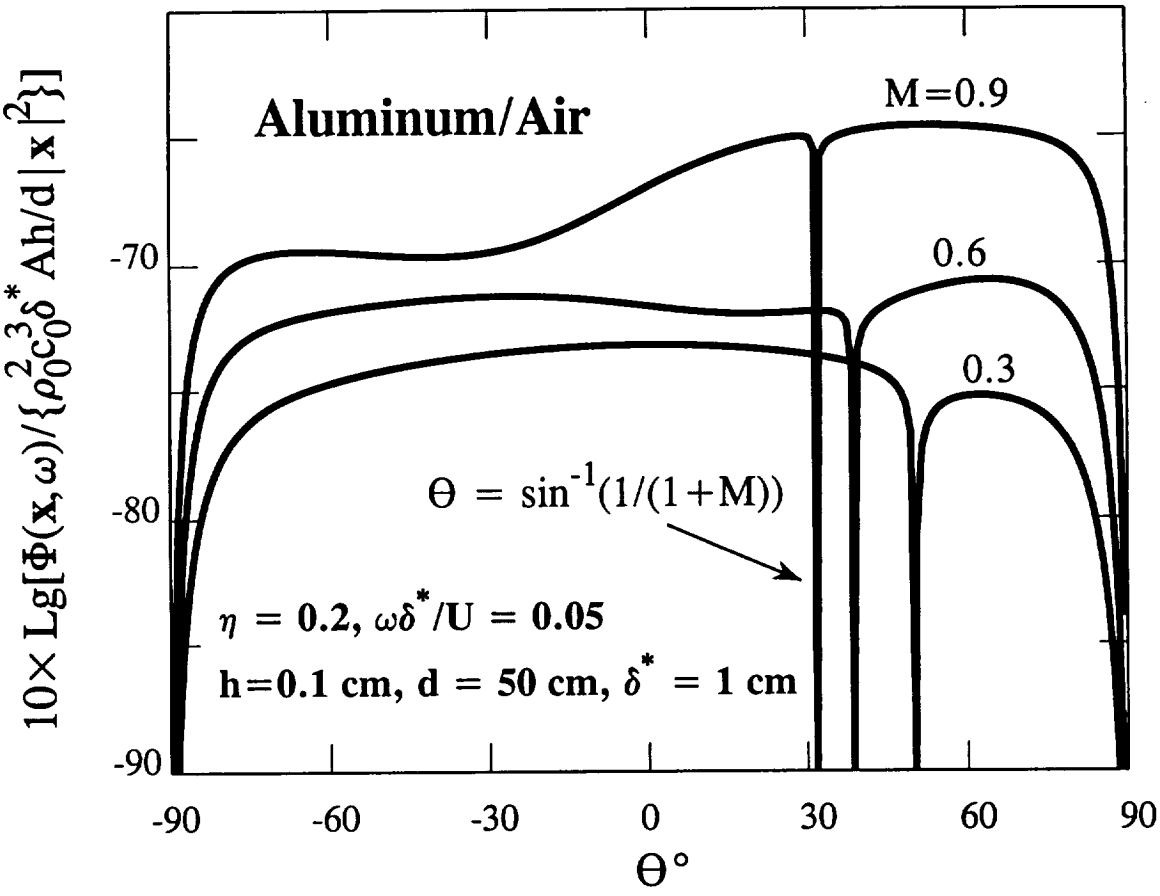

Figure 8. Predicted interior noise directivity (for $x_3 = 0$) for a periodically clamped aluminum plate in air when h = 0.1 cm, d = 50 cm, $\eta = 0.2$, $\delta^* = 1$ cm, and $\Phi_{pp}(\omega)$ is given by (3.17).

CHAPTER 2

SOUND GENERATED BY A VORTEX INTERACTING WITH A RIB-STIFFENED ELASTIC PLATE

SUMMARY

An analytical investigation is made of the sound produced when a line vortex translates over a parallel, nominally smooth rib-stiffener on a thin elastic plate. This is a canonical fluid-structure interaction that is believed to be an important source of boundary layer generated aircraft interior noise. To eliminate additional complications introduced by mean flow, the vortex motion is assumed to be controlled by its image in the plate. The arrival of the vortex at the rib is preceded by bending wave forerunners which are excited in the plate at that frequency Ω at which the flexural wave phase velocity is just equal to the vortex translational velocity v. These waves have group velocity equal to $2v$, and extend over a length of plate ahead of the vortex determined by the structural damping. The principal acoustic source is the interaction of this forerunner with the stiffener, and the sound is predominantly of frequency Ω. The amplitude of the radiation progressively increases to a maximum as the vortex approaches the rib, and subsequently decreases rapidly to zero with passage of the vortex over the rib. Numerical results for the efficiency of sound generation, its directivity, and the acoustic pressure signature, are given for clamped and simply supported conditions at the stiffener for aluminum plates in air.

1. INTRODUCTION

A variety of noise sources contribute to aircraft cabin noise, and are generally classified as airborne or structure-borne sources [1]. Structure-borne sound is caused by engine vibration and by vibrations induced by impingement of engine exhausts on wings and flow control surfaces, and is transmitted to the fuselage via vibrational motions of the airframe. Airborne sources include the direct incidence of engine generated sound on cabin walls and the high speed turbulent air flow over the exterior fuselage. A critical role is played by the frequency-dependent transmission characteristics of the fuselage which are manifested by irregular variations of sound levels with frequency and location within the cabin [2]. Fuselage ring-stiffeners, stringers, windows, etc, have a significant influence on the modal response of the cabin to outside forcing and incident sound, but they can also behave as sources of sound when they interact with the exterior turbulent flow and with structural vibrations induced by the flow. This *boundary layer* generated noise is believed to make a substantial contribution to the interior noise of a jet transport in steady cruise, and is currently the subject of intense experimental scrutiny and numerical modeling [3 - 7].

Numerical schemes for predicting boundary layer generated interior noise must take proper account not only of sound waves produced by the fluid-structure interaction, but also of structural vibrations generated by the flow that can subsequently generate sound by their interactions with structural inhomogeneities. Such predictions must ultimately be validated by comparison with experiment, but it is also useful to have available a collection of benchmark analytic solutions against which the numerical results can be compared.

In this chapter we investigate a canonical problem that includes all of the major aspects of the fluid-structure interactions involved in boundary layer generated interior noise, yet is simple enough to be treated analytically. This problem involves an idealized boundary layer disturbance in the form of a line vortex. The vortex is adjacent to a section of the fuselage which is taken to be a locally flat elastic plate, and is propelled

under the influence of its image in the plate towards a rib stiffener where the plate is either clamped or simply supported. The stiffener is assumed to be parallel to the vortex, which further simplifies the analysis of their interaction, which is then governed by two-dimensional equations of motion. In a first approximation the vortex translates at a constant speed v, say, over the plate and generates predominantly bending waves of a fixed frequency whose phase velocity is v. However, for an elastic plate in air the group velocity of these waves is about $2v$, so that the arrival of the vortex at the stiffener is preceded by flexural vibrations of fixed frequency and wavelength which generate sound by their interaction with the stiffener. We calculate the amplitude and waveform of the scattered sound, and determine the dependence of the efficiency of sound generation and the acoustic field shape on frequency.

The fluid-structure interaction problem is formulated and solved for an arbitrary two-dimensional flow inhomogeneity adjacent to a rib-stiffened infinite plate in §2. In §3 we discuss the frequency dependence of the radiated sound for clamped and simply supported conditions at the stiffener, and consider in §4 specific results related to a vortex convecting at subsonic velocity over the stiffener.

2. EQUATIONS OF MOTION

2.1 Formulation of the problem

Consider the generation of sound by aeroacoustic sources adjacent to a thin, elastic plate which coincides with the plane $x_2 = 0$ of the rectangular coordinate system (x_1, x_2, x_3). The fluid on both sides of the plate is at rest in the undisturbed state, with mean density and sound speed respectively equal to ρ_0 and c_0 (Figure 1). The plate is divided into two semi-infinite, homogeneous "panels" which are smoothly joined by a rib coinciding with the x_3-axis, where their abutting edges are assumed to be either clamped or simply supported. It is required to determine the influence of this joint on the production of sound.

To fix ideas, suppose the aeroacoustic sources are confined to the region $x_2 > 0$, and, with t denoting time, let $p_w(x_1, x_3, t)$ be the *blocked* pressure [8 - 12], i.e., the pressure that these sources would exert on the surface $x_2 = +0$ of the plate when the latter is assumed to be *rigid*. In principle this pressure distribution can always be calculated, both on the plate and within the fluid in $x_2 > 0$, when the sources are known, which we shall assume to be the case. Since the blocked pressure is the solution of the governing equations in the absence of surface motion, it may be taken as a prescribed surface driving stress in the actual problem involving the ribbed, elastic plate.

When the surface motion is only linearly disturbed from its planar form by the blocked pressure, the sound produced by the fluid-structure interaction can be determined at an arbitrary point **x** in the fluid by application of Rayleigh's reciprocal theorem [13, 14]. Write

$$p_w(x_1, x_3, t) = \int_{-\infty}^{\infty} p_w(x_1, x_3, \omega) e^{-i\omega t}\, d\omega, \tag{1}$$

and consider a reciprocal problem in which a time harmonic *volume* point source $q^R e^{-i\omega t}$ is placed at **x**. Then Rayleigh's theorem asserts that

$$p(\mathbf{x}, \omega) q^R = -i\omega \int_{-\infty}^{\infty} p_w(y_1, y_3, \omega) \zeta^R(y_1, y_3, \omega) dy_1 dy_3, \tag{2}$$

where $\zeta^R(y_1, y_3, \omega) e^{-i\omega t}$ is the displacement of the plate (in the x_2-direction)

at the point (y_1, y_3) produced by the source q^R, and $p(\mathbf{x},\omega)e^{-i\omega t}$ is the acoustic pressure generated by the harmonic component $p_w(x_1, x_3, \omega)e^{-i\omega t}$ of the blocked pressure.

2.2 The reciprocal problem in two dimensions

We now specialize the discussion to two-dimensional source distributions, which are independent of the coordinate x_3 parallel to the rib, so that here and henceforth $\mathbf{x} = (x_1, x_2)$, etc. The principal source of sound attributable to the fluid-structure interaction is confined to a neighborhood of the rib, near the coordinate origin, and equation (2) will be applied to determine the radiation at large distances. The propagation of sound of frequency ω is governed by the Helmholtz equation

$$(\nabla^2 + \kappa_0^2)p = 0, \qquad \kappa_0 = \omega/c_0, \tag{3}$$

where the acoustic wavenumber κ_0 may be assumed to have a small positive imaginary part. Small amplitude, time harmonic motion of the plate satisfies the thin plate bending wave equation [14, 15]

$$(B\partial^4/\partial x_1^4 + m\omega^2)\zeta + [p] = 0, \qquad x_1 \neq 0, \tag{4}$$

where B is the bending stiffness, m the mass per unit area of the plate, ζ the flexural displacement of the plate (in the x_2 direction), and

$$[p] = p(x_1, +0, \omega) - p(x_1, -0, \omega) \tag{5}$$

is the pressure loading. To account for damping in the plate we write

$$B = B_o(1 - i\eta(\omega)), \tag{6}$$

where B_o is real and $\eta(\omega)$ is a loss factor satisfying $\eta(-\omega) = -\eta(\omega)$ which will be assumed to be of constant absolute value.

In the reciprocal problem, q^R is taken to be a line source of unit strength located at $\mathbf{x}$. The velocity potential produced by this source at the point $\mathbf{y}$ in an *unbounded* medium is

$$\varphi_I^R(\mathbf{y},\omega) = -\tfrac{i}{4}H_0^{(1)}(\kappa_0|\mathbf{x}-\mathbf{y}|), \tag{7}$$

where $H_0^{(1)}$ is a Hankel function [16]. As the observer position $\mathbf{x}$ recedes to infinity, and for $\mathbf{y}$ near the plate,

$$\varphi_I^R(y,\omega) \approx \varphi_o e^{-i\kappa_0 n\cdot y} , \quad \varphi_o = \frac{-e^{i(\kappa_0|x|+\pi/4)}}{\sqrt{(8\pi\kappa_0|x|)}} , \qquad |x| \to \infty, \tag{8}$$

where $n = (\sin\Theta,\cos\Theta)$ and Θ is the observer angle shown in Figure 1. We shall assume that $x_2 > 0$; the case of an observer in the lower region $x_2 < 0$ is obtained by changing the sign of n_2. Scattered waves are produced when the *plane wave* (8) impinges on the plate. When the influence of the rib is ignored, the scattered waves are plane reflected and transmitted waves, and the reciprocal velocity potential near the plate would then be

$$\begin{aligned} \varphi_o^R &= \varphi_o\left(e^{-i\kappa_0 n_2 y_2} + Re^{i\kappa_0 n_2 y_2}\right)e^{-i\kappa_0 n_1 y_1}, \quad y_2 > 0, \\ &= \varphi_o T e^{-i\kappa_0(n_1 y_1 + n_2 y_2)} , \qquad\qquad y_2 < 0, \end{aligned} \tag{9}$$

where R and T are suitable reflection and transmission coefficients. These coefficients are found in the usual way [15], by making use of the bending wave equation (4), and the linear relations $p = i\rho_0\omega\varphi$, $-i\omega\zeta = \partial\varphi/\partial y_2$, between pressure, velocity potential and displacement at $y_2 = \pm 0$, leading to

$$T(\omega,\Theta) = 1 - R(\omega,\Theta) = \frac{-2i\epsilon}{\{(1-i\eta)(\omega/\omega_c)^2\sin^4\Theta - 1\}(\omega/\omega_c)\cos\Theta - 2i\epsilon}, \tag{10}$$

where $\omega_c = c_0^2(m/B_o)^{1/2}$ is the *coincidence frequency* of the undamped plate [15], above which the phase velocity of flexural waves on the plate *in vacuo* exceeds the speed of sound c_0, and $\epsilon = \rho_0 c_0/\omega_c m$ is a fluid loading parameter that depends only on the material properties of the fluid and plate [17]. By making use of the general relation $-i\omega\zeta = \partial\varphi/\partial y_2$ $(y_2 \to \pm 0)$, we find that the reciprocal displacement ζ_o^R of the plate when the rib is ignored is given by

$$\zeta_o^R = \zeta_I e^{-i\kappa_0 n_1 y_1} , \quad \zeta_I = \frac{-n_2 T(\omega,\Theta)e^{i(\kappa_0|x|+\pi/4)}}{c_0\sqrt{(8\pi\kappa_0|x|)}} . \tag{11}$$

Because of the rib, the net reciprocal displacement ζ^R, say, of the plate includes an additional contribution that may be interpreted as the flexural motions induced by the scattering of ζ_o^R at the rib. The general solution of scattering problems of this type is discussed in [18, 19], where it is shown that

$$\zeta^R/\zeta_I = \int_{-\infty}^{\infty} \sum_n \frac{a_n k^n e^{iky_1}\, dk}{D(k,\omega)} + e^{-i\kappa_0 n_1 y_1} , \tag{12}$$

where the summation is from n = 0 to 3. The four "scattering" coefficients a_n are determined by the mechanical conditions at the rib. They are independent of k and satisfy $a_n(-\omega) = (-1)^n a_n^*(\omega)$, where the asterisk denotes complex conjugate (see [6]). $D(k,\omega)$ is the dispersion function for flexural waves on a fluid loaded plate [15]:

$$D(k,\omega) \equiv Bk^4 - m\omega^2 - 2\rho_0\omega^2/(\kappa_0^2 - k^2)^{1/2}. \tag{13}$$

The sound received at x as a result of the fluid-structure interaction is now obtained by substituting from (12) into Rayleigh's formula (2). The total radiation received at x is found by adding to this prediction the radiation associated with the interaction of the aeroacoustic sources with a *rigid* wall, i.e, by adding the acoustic far field of the blocked pressure p_w. Thus, the resulting expression for the acoustic pressure consists of two distinct terms: the first involves p_w and the component of (2) due to the flexural displacement ζ_o^R (corresponding to the second term on the right of equation (12)). This is just the sound produced by the same aeroacoustic sources adjacent to a smooth, homogeneous plate with no rib. For this component of the radiation the plate behaves as a *passive* reflector of the sound that would be generated by the same sources if the plate were removed. This is because there is no "wavenumber conversion" mechanism at a plane boundary, i.e., the energy of an incident disturbance of given trace wavenumber remains in that wavenumber after interacting with the plate, and only incident energy that is *already* sound will be re-radiated from the plate as sound. In particular, this radiation is null when the source consists of a steady disturbance translating over the plate at a constant subsonic velocity. Our applications in §§3,4 will be to sources of this type, and we shall therefore discard this term.

The remaining contribution to the scattered sound is determined by the reciprocal flexural displacement generated at the rib, i.e., by the first term on the right of (12), and represents the interaction of the aeroacoustic sources with the rib. By substituting from (12) into (2), retaining only this

contribution, and integrating over all frequency ω, the fluid-structure interaction noise is accordingly found to be given by

$$p(x,t) = \frac{\pi i n_2}{\sqrt{(2\pi|x|)}} \int_{-\infty}^{\infty} \sum_n \frac{\sqrt{i\kappa_0}\, T(\omega,\Theta) a_n (-k)^n p_w(k,\omega) e^{-i\omega[t]}}{D(k,\omega)}\, dk d\omega, \quad |x| \to \infty, \tag{14}$$

where $[t] = t - |x|/c_0$ is the retarded time, and

$$p_w(k,\omega) = (1/2\pi)^2 \int_{-\infty}^{\infty} p_w(x_1,t) e^{-i(kx_1 - \omega t)}\, dx_1 dt, \tag{15}$$

is the space-time Fourier transform of the blocked pressure.

2.3 Scattering coefficients for clamped and simply supported rib conditions

The coefficients a_n are determined from the mechanical conditions at the rib. For *clamped* and *simply supported* conditions ζ^R satisfies respectively

$$\zeta^R = \partial\zeta^R/\partial y_1 = 0 \text{ and } \zeta^R = \partial^2\zeta^R/\partial y_1^2 = 0 \text{ as } y_1 \to \pm 0.$$

Introduce dimensionless coefficients α_n defined by

$$a_n = (m\omega^2/K_o^{n+1})\alpha_n, \tag{16}$$

where $K_o = (m\omega^2/B_o)^{1/4} > 0$ is the *in vacuo* wavenumber of bending waves of radian frequency ω. The evaluation of the α_n using the representation (12) can be accomplished by the method of reference [18], which supplies:

Clamped

$$\alpha_0 = -1/\Psi_0, \quad \alpha_1 = \mu n_1/\Psi_2, \quad \alpha_2 = \alpha_3 = 0, \tag{17}$$

where,

$$\Psi_n = 2\int_0^{\infty} \frac{\lambda^n d\lambda}{(1-i\eta)\lambda^4 - 1 - 2i\epsilon/\mu\sqrt{(\mu^2-\lambda^2)}}, \qquad \mu = \sqrt{\omega/\omega_c}. \tag{18}$$

It may be assumed that $\omega > 0$ in applying these formulae; the values of $a_n \equiv a_n(\omega)$ for $\omega < 0$ are obtained from the relation $a_n(-\omega) = (-1)^n a_n^*(\omega)$. The integration contour in (18) runs below all singularities of the integrand on the real axis; in particular, the branch of $\sqrt{(\mu^2-\lambda^2)}$ which is positive imaginary for $\lambda > \mu$ (> 0) is taken.

Simply supported

$$\alpha_0 = \frac{\Psi_2' - \Psi_1'(\mu n_1)^2}{\Psi_1'^2 - \Psi_0'\Psi_2'}, \quad \alpha_1 = 0, \quad \alpha_2 = \frac{-[\Psi_1' - \Psi_0'(\mu n_1)^2]}{\Psi_1'^2 - \Psi_0'\Psi_2'}, \quad \alpha_3 = 0, \tag{19}$$

where,

$$\Psi_n' = \frac{\pi z^{2n+1}}{2}[i - (-1)^n] + 4i\epsilon\int_0^\infty \frac{\lambda^{2n}\, d\lambda}{\{[(1-i\eta)\lambda^4 - 1]\mu\sqrt{(\mu^2-\lambda^2)} - 2i\epsilon\}\{(1-i\eta)\lambda^4 - 1\}}, \tag{20}$$

and $z = 1/(1-i\eta)^{1/4}$.

3. SOUND GENERATED BY A TIME HARMONIC GUST

The blocked pressure generated by an arbitrary, uniformly convecting aerodynamic source, which is independent of x_3, is equivalent to a superposition of elementary time harmonic "gusts" of the form

$$p_w = p_o(\omega)e^{-i\omega(t-x_1/v)} , \tag{21}$$

where v = constant is the convection velocity, which is assumed to be subsonic ($< c_0$). In §4 we shall use such a decomposition for a source consisting of a line vortex. Here we shall investigate the sound produced by the individual Fourier components (21) and their dependence on v.

It follows immediately from equation (14) that the far field sound produced by the gust (21) is given by

$$\frac{p(\mathbf{x},t)}{p_o\sqrt{(h/|\mathbf{x}|)}} = \frac{-\sqrt{(\pi/2)}\cos\Theta T(\omega,\Theta)M^4 \sum_n \mu^2(-\mu/M)^n\alpha_n e^{-i\{\omega[t] + \pi/4\}}}{\sqrt{(\omega_c h/c_0)}\{[(1-i\eta)\mu^4 - M^4]\mu^2 - 2\epsilon M^5/\sqrt{(1-M^2)}\}} , \quad \mu = \sqrt{\omega/\omega_c}, \tag{22}$$

where h is the thickness of the plate, and $M = v/c_0$ is the convection Mach number.

The dependence of $p(\mathbf{x},t)$ on the radiation direction Θ is governed by the transmission coefficient $T(\omega,\Theta)$ (defined in (10)) and the Θ-dependence of the scattering coefficients α_n. The influence of the latter turns out to be small, and equations (10) and (22) therefore imply that the radiation will tend to have a dipole character, with $p \propto \cos\Theta$, when $\mu^2 \equiv \omega/\omega_c < \epsilon$, whereas at higher frequencies (but less than ω_c) the field shape resembles that of a monopole source. These conclusions are illustrated in Figure 2 for an aluminum plate in air, for which

$$\omega_c h/c_0 \approx 0.22, \ \epsilon \approx 0.0021. \tag{23}$$

Thus, dipole behavior is expected for $\omega/\omega_c < 10^{-3}$. In Figure 2 the plate is assumed to be clamped at the rib, and $|p(\mathbf{x},t)|^2$ is plotted as a function of Θ

for a convection Mach number M = 0.5, although the actual dependence on Mach number is small. The plots are scaled to the same level in the normal direction $\Theta = 0°$. The directivities for simply supported conditions at the rib differ imperceptibly from those shown in Figure 2. At very high frequencies (not shown), when $\omega > \omega_c$, the directivity is ultimately dominated by the radiation from "leaky" flexural waves generated at the rib. These waves have supersonic phase velocities and decay by radiating their energy into the fluid as sound. They correspond to complex roots of the denominator of expression (10) for $T(\omega,\Theta)$ that occur near the real angles $\Theta = \pm\sin^{-1}\{\sqrt{(\omega_c/\omega)}\}$ when $\omega_c/\omega < 1$, so that the radiation pattern is consists of two lobes centered on $\Theta \approx \pm\sin^{-1}\{\sqrt{(\omega_c/\omega)}\}$. However, the efficiency with which sound is generated at these frequencies is very small, since when $\omega \geq \omega_c$ flexural motions of the plate induced by the gust become negligible.

The efficiency of sound production at different frequencies is illustrated in Figures 3 and 4, where $10\times\log\{|p(x,t)/p_o|^2/(h/|x|)\}$ (dB) is plotted against ω/ω_c for $\Theta = 0°$, and for three different convection Mach numbers, respectively for clamped and simply supported conditions. The "resonance" peaks occur near $\omega/\omega_c \approx M^2$, where the real part of the denominator on the right of (22) vanishes; at this frequency the gust convection velocity v coincides with the bending wave phase speed. The magnitudes of the peaks depend on the loss factor η which has been assigned a nominal value of 0.01. At higher frequencies the efficiency of sound production by scattering decreases precipitously.

4. VORTEX SOUND

Turn attention now to the special case in which the gust of Figure 1 is a line vortex of circulation Γ. The vortex is assumed to translate over the plate with velocity induced by images in the plate. If the plate were rigid the translational velocity would be $v = \Gamma/4\pi d$, where d is the distance of the vortex from the plate, which would then be constant. The order of magnitude of the displacement of the plate beneath the vortex can be estimated from the bending wave equation (4) to be given by

$$\zeta/d \approx (d/h)\rho_0 v^2/[\rho_s c^2 (h/d)^2 + \rho_s v^2] \tag{24}$$

where ρ_s is the density of the plate material, and c is the velocity of longitudinal plate waves. In aircraft applications the distance d may be identified with a boundary layer displacement thickness, and the ratio d/h is then typically of order 10. For an aluminum plate in air and a vortex velocity $v < c_0$, equation (24) then implies that $\zeta/d \ll 1$. In a first approximation it is therefore reasonable to neglect the compliance of the plate in calculating the self-induced motion of the vortex, at least during the interval of time in which the vortex interacts significantly with the rib.

In these circumstances the vortex may be imagined to exert a steady blocked pressure distribution on the plate that translates uniformly at speed $v = \Gamma/4\pi d$. We shall assume that the vortex translates in the positive x_1-direction, and passes over the rib at time t = 0. The blocked pressure field of the vortex will be approximated by that for a vortex in *incompressible* flow; any differences due to the effects of finite Mach number will modify the overall level of the acoustic radiation, but should not affect its general characteristics. Thus [20]

$$p_w(x_1,t) = \rho_0 v^2 \frac{4d^2\{(x_1-vt)^2-d^2\}}{\{(x_1-vt)^2+d^2\}^2},$$

and

$$p_w(k,\omega) = -2\rho_0 d^2 |\omega| e^{-|\omega d/v|}\delta(k-\omega/v). \tag{25}$$

Before proceeding to the evaluation of the radiation integral (14), further insight into the expected form of the interaction radiation can be obtained by considering the flexural wave motions produced by vortex. These waves generate sound by their subsequent impingement on the rib. To do this, replace [p] by [p] + p_w in the bending wave equation (4), where p is a solution of equation (3) with "outgoing" wave behavior. When the presence of the rib is ignored, the flexural displacement ζ_w produced by the vortex is then found to be

$$\zeta_w = -2\rho_0 d^2 \int_{-\infty}^{\infty} \frac{|\omega| e^{-|\omega d/v| - i\omega(t-x_1/v)}\, d\omega}{D(\omega/v,\omega)}. \tag{26}$$

At large distances from the vortex the value of this integral is dominated by residue contributions from poles of the integrand near the real ω-axis. These poles are located *above* the real axis at $\omega = \pm v^2\{m/[B_o(1\mp i\eta)]\}^{1/2}$, provided the small influence on their locations of fluid loading is neglected. It follows that

$$\zeta_w \approx \zeta_w^o \sin\{\Omega(t-x_1/v)\}\exp\{-\tfrac{1}{2}\eta\Omega(x_1/v-t)\}, \quad x_1 - vt \to +\infty$$

$$\approx 0, \quad x_1 - vt \to -\infty, \tag{27}$$

where $\Omega = v^2(m/B_o)^{1/2} \equiv M^2\omega_c$ $(M = v/c_0)$, and ζ_w^o is a constant determined by the residues at the poles.

The frequency Ω is that of the flexural wave resonantly excited by the vortex, whose phase velocity is the same as the vortex translation velocity v. However, the *group velocity* [21, 22]

$$\partial\omega/\partial k = -(\partial D(k,\omega)/\partial k)/(\partial D(k,\omega)/\partial\omega) \approx 2k(B_o/m)^{1/2}$$

of this wave is $2v$, so that energy imparted to the surface by the vortex runs ahead of the vortex. In the absence of damping ($\eta \to 0$) this flexural wave "forerunner" would extend infinitely far ahead of the current location $x_1 = vt$ of the vortex, and its interaction with the rib would generate time harmonic radiation of constant strength and frequency Ω for all times prior to the arrival of the vortex at the rib. According to (27), the flexural wave energy in the wake of the vortex is negligible, so that the acoustic radiation should decay rapidly after the passage of the vortex over the rib. It should be

noted that this conclusion is in no way an artifact of the present idealized model; energy supplied to a plate by boundary layer excitation at hydrodynamic coincidence [11] will also tend to propagate ahead of the convecting forcing region, although this is not usually evident when the interaction is analyzed solely in the wavenumber-frequency domain.

These qualitative predictions are borne out by numerical evaluation of the radiation integral (14), with $p_w(k,\omega)$ given by (25). The integral can be expressed in the following form

$$\frac{p(x,t)}{\rho_0 c_0^2 \sqrt{(h/|x|)}} = \int_0^\infty \mathrm{Re}\left[f(\Theta,M,z) e^{-iz\upsilon[t]/d} \right] dz, \tag{28}$$

where $M = \upsilon/c_0$,

$$f(\Theta,M,z) = \frac{2\sqrt{(2\pi)} M^6 \cos\Theta T(\omega,\Theta) z\mu^2 \sum_n (-\mu/M)^n \alpha_n e^{-(z+i\pi/4)}}{\sqrt{(\omega_c h/c_0)}[(1-i\eta)\mu^6 - M^4\mu^2 - 2\epsilon M^5/(1-M^2)^{1/2}]}, \tag{29}$$

and $\mu = \sqrt{\omega/\omega_c}$, $\omega/\omega_c = zM(h/d)/(\omega_c h/c_0)$. Observe that $f(\Theta,M,z)$ has a pole close to the real axis near $\omega/\omega_c = M^2$ when $\epsilon \ll 1$, i.e., at the resonance frequency Ω.

Figures 5 and 6 depict calculated acoustic pressure signatures (28) for clamped and simply supported rib conditions at several subsonic Mach numbers $M = \upsilon/c_0$. The calculations have been performed for an aluminum plate in air for

$$h/d = 0.1, \ \eta = 0.05 \text{ and } \Theta = 0°,$$

and the curves are plotted as a function of the retarded position of the vortex scaled on the stand-off distance d. The acoustic pressure is dominated by the resonant mode of frequency Ω excited by the vortex. In terms of the efficiency plots in Figures 3 and 4, this means that the dominant radiation is from the neighborhood of the peak at $\omega/\omega_c \approx M^2$. The acoustic amplitude grows exponentially with time until it is cut-off when the vortex passes over the rib at $t = 0$. The growth rate of the sound is determined by the loss factor η; a value of 0.05 is large for a homogeneous aluminum plate, but is probably representative of damped aircraft structures, and has been used to illustrate the role of the flexural wave forerunner (27) ahead of the vortex. When η is fixed the damping of the forerunner increases with frequency, so that the low

Mach number (M = 0.1) radiation shown in the figures grows much more slowly than the higher Mach number waveforms. The characteristic acoustic wavelength $\approx 2\pi c_0/\Omega \approx 2\pi d/[M^2(\omega_c h/c_0)(d/h)] \approx 285d$, 32d, 8d respectively for the three Mach numbers M = 0.1, 0.3 and 0.6 shown in the figures, i.e., the wavelength of the dominant radiation is typically large compared to the stand-off distance d of the vortex. The plots in Figures 5 and 6 are drawn to the same nominal scale. The maximum acoustic amplitude therefore increases with Mach number, and the amplitude of the sound is marginally smaller for the simply supported rib condition, which is in accord with the efficiency plots of Figures 3 and 4. The directional characteristics of the sound can be surmised from Figure 2 by noting that $\Omega/\omega_c \approx 10^{-2}$, 10^{-1}, 0.36 respectively for M = 0.1, 0.3 and 0.6. Thus, higher Mach number radiation will exhibit a monopole field shape; at very low Mach numbers a dipole directivity would be expected.

5. CONCLUSION

The sound produced by turbulent flow over the fuselage of an aircraft is a significant component of aircraft cabin interior noise. In this chapter we have examined a simple canonical problem that models an important aspect of this fluid-structure interaction, in which a hydrodynamic disturbance in the form of a line vortex convects over a parallel rib on an elastic plate.

The arrival of the vortex at the rib is preceded by a flexural wave forerunner in the plate of frequency $\Omega \approx M^2\omega_c$, whose phase velocity is equal to the vortex convection velocity, M being the convection Mach number and ω_c the coincidence frequency. The group velocity of this structural wave is twice the vortex translation velocity, and the forerunner extends a distance ahead of the vortex determined by the structural damping. There is no preferred frequency associated with the vortex motion, but the interaction radiation is dominated by sound of frequency Ω, whose amplitude increases exponentially as the vortex approaches the rib, but is subsequently rapidly annulled after passing the rib. Detailed predictions have been worked out for clamped and simply supported rib conditions for an aluminum plate in air, and in both cases indicate that the characteristics of the sound are dominated by the condition that the plate displacement is required to vanish at the rib. Conditions on the slope and curvature of the plate at the rib do not appreciably affect the radiation, although the radiation from a clamped rib is larger by a few dB. The directivity of the sound depends on the value of Ω/ω_c, i.e. on the translational Mach number of the vortex; it is effectively the same for clamped and simply supported joints.

REFERENCES

1. J. S. Mixson and J. F. Wilby 1991. *Interior noise*, Chapter 16 of *Aeroacoustics of Flight Vehicles: Theory and Practice (Vol. 2)*. NASA Ref. Pub. No. 1258.
2. J. F. Wilby, C. D. McDaniel and E. G. Wilby 1985. *In-flight acoustic measurements on a light twin-engined turboprop airplane*. NASA CR-178004.
3. W. R. Graham 1993 *Boundary layer noise and vibration*, Doctoral Thesis, Cambridge University Engineering Department.
4. W. R. Graham 1995 *J. Sound. Vib.* (in press). Boundary layer induced noise in aircraft. Part I The flat plate model.
5. W. R. Graham 1995 *J. Sound. Vib.* (in press) Boundary layer induced noise in aircraft. Part II The trimmed flat plate model.
6. M. S. Howe and P. L. Shah 1996 *J. Acoust. Soc. Am.* (in press). Influence of mean flow on boundary layer generated interior noise.
7. R. J. Silcox 1995 (editor) *Proceedings of the Interior Noise Workshop*, held at NASA Langley Research Center, 25 - 27 April.
8. G. M. Corcos 1964 *J. Fluid Mech.* **18**, 353 - 378. The structure of the turbulent pressure field in boundary layer flows.
9. D. M. Chase 1980 *J. Sound Vib.* **70**, 29 - 67. Modeling the wavevector-frequency spectrum of turbulent boundary layer wall pressure.
10. D. M. Chase 1987 *J. Sound Vib.* **112**, 125 - 147. The character of the turbulent wall pressure spectrum at subconvective wavenumbers and a suggested comprehensive model.
11. W. K. Blake 1986 *Mechanics of flow-induced sound and vibration, Vol. 2: Complex flow-structure interactions*, New York: Academic Press.
12. M. S. Howe 1991 *J. Acoust. Soc. Am.* **90**, 1041 - 1047. Surface pressures and sound produced by turbulent flow over smooth and rough walls.
13. Lord Rayleigh 1945 *Theory of Sound*, Volumes 1 and 2. New York: Dover.
14. L. L. Beranek and I. L. Vér 1992 *Noise and Vibration Control Engineering*, New York: John Wiley.
15. M. C. Junger and D. Feit 1993 *Sound, Structures and their Interactions*, New York: Acoustical Society of America.

16. M. Abramowitz and I. A. Stegun 1970 (eds.) *Handbook of Mathematical Functions* (Ninth corrected printing), US Dept. of Commerce, Nat. Bur. Stands. Appl. Math. Ser. No.55.
17. D. G. Crighton 1989 *J. Sound Vib.* **133**, 1 - 27. The 1988 Rayleigh Medal Lecture: Fluid loading - the interaction between sound and vibration.
18. M. S. Howe 1986 *IMA J. Appl. Math.* **36**, 247 - 262. Attenuation and diffraction of bending waves at gaps in fluid loaded plates.
19. M. S. Howe 1994 *Proc. Roy. Soc. Lond.* **A444**, 555 - 571. Scattering of bending waves by open and closed cracks and joints in a fluid loaded elastic plate.
20. H. Lamb 1932 *Hydrodynamics* (6th. ed.) Cambridge University Press, (reprinted 1993).
21. M. J. Lighthill 1965 *J. Ins. Maths. Applics.* 1, 1 - 28. Group velocity.
22. James Lighthill 1978 *Waves in Fluids.* Cambridge University Press.

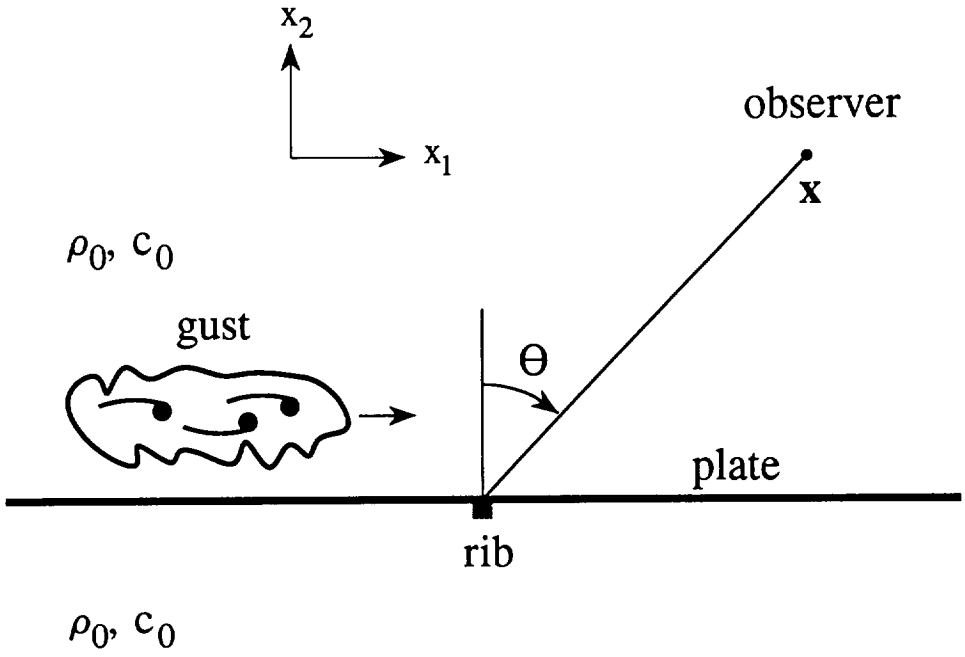

Figure 1. Aeroacoustic sources adjacent to a rib-stiffened thin elastic plate.

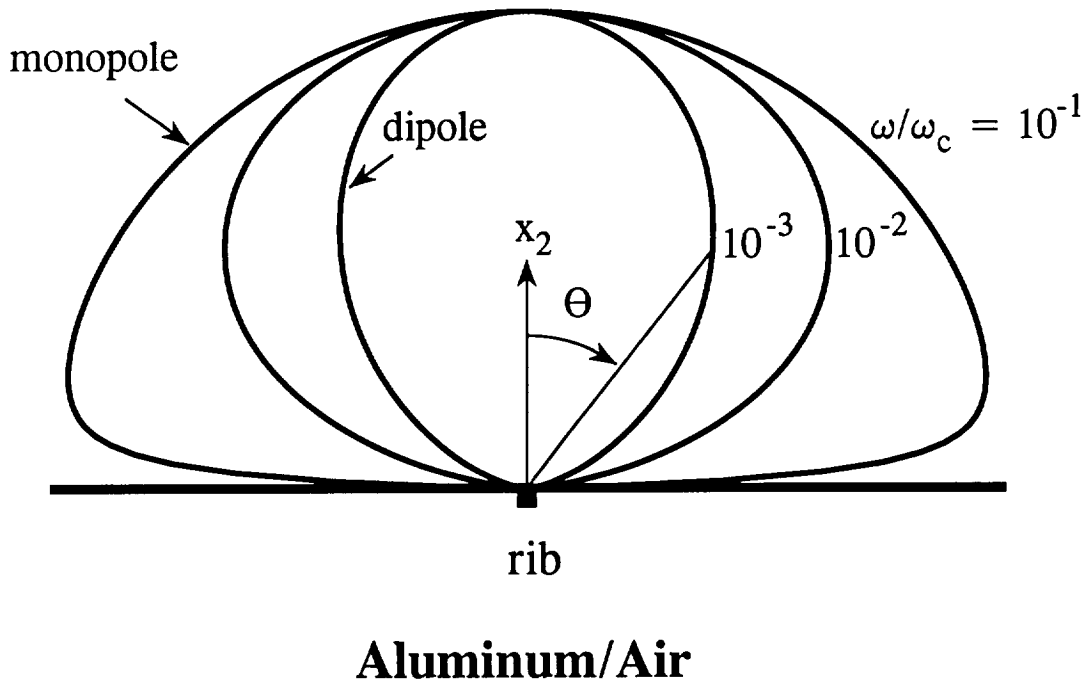

Figure 2. Directivity of the scattered sound for clamped rib conditions: aluminum/air, for a convection Mach number M = 0.5 and $\omega/\omega_c = 10^{-1}, 10^{-2}, 10^{-3}$.

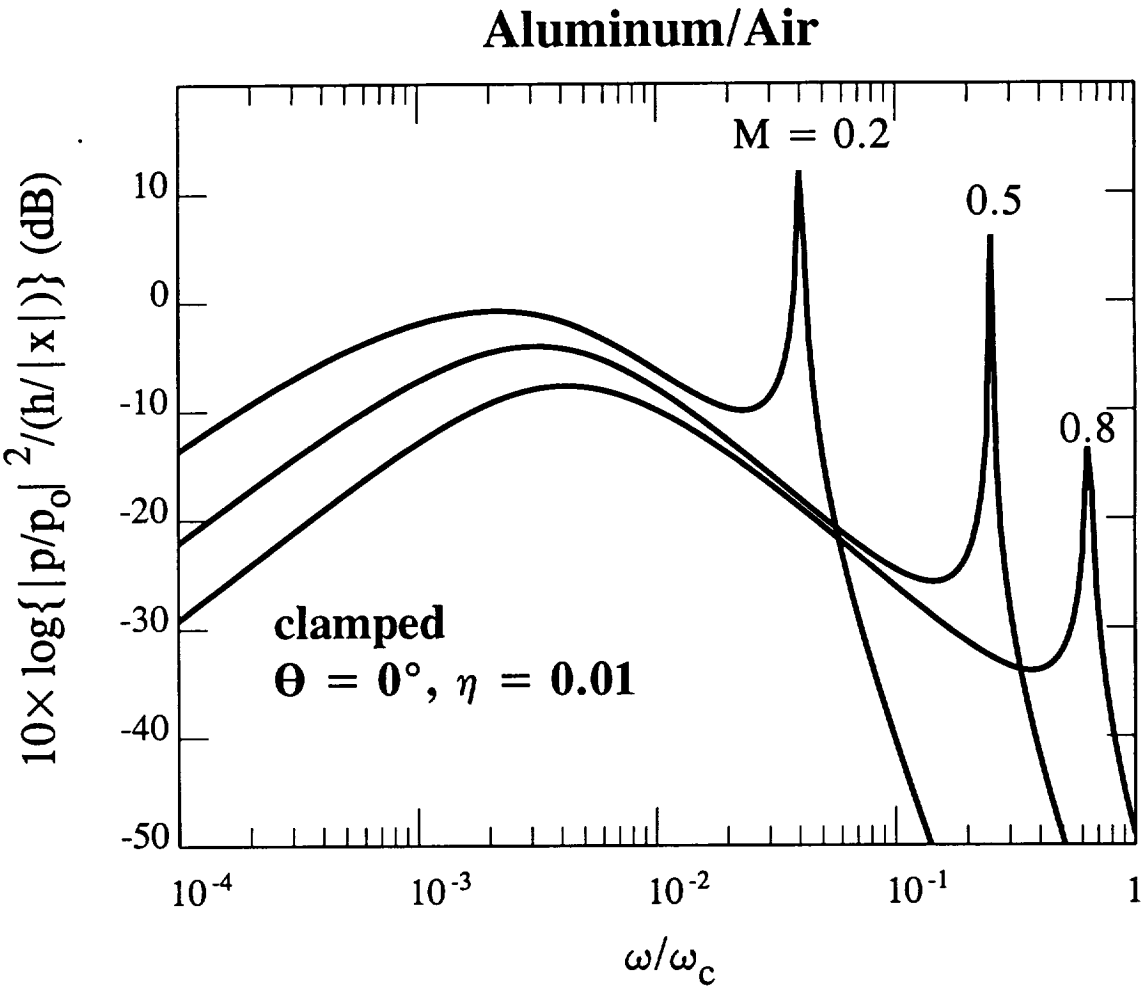

Figure 3. Efficiency of sound generation for clamped rib conditions: aluminum/air, for η = 0.01 and M = 0.2, 0.5, 0.8.

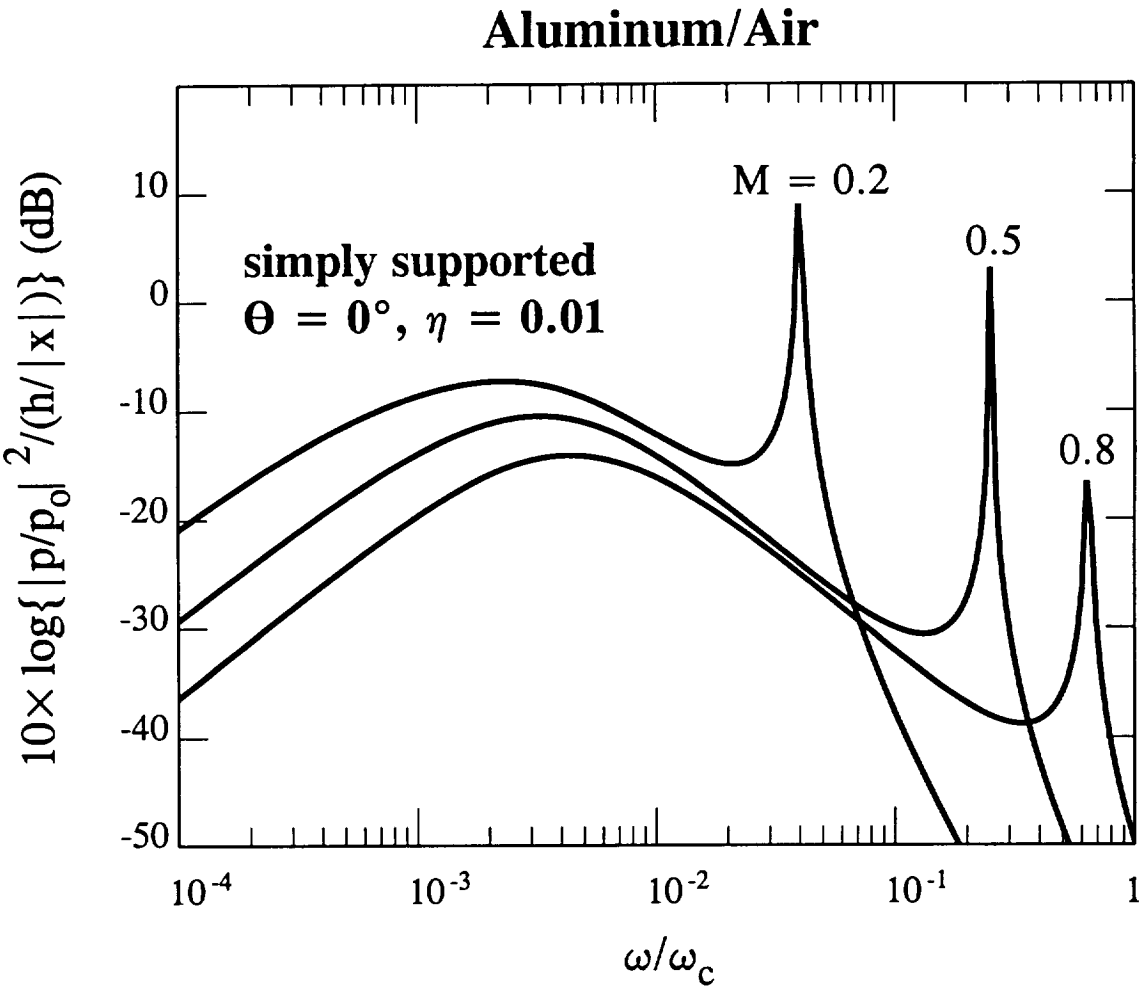

Figure 4. Efficiency of sound generation for simply supported rib conditions for $\Theta = 0°$: aluminum/air, for $\eta = 0.01$ and M = 0.2, 0.5, 0.8.

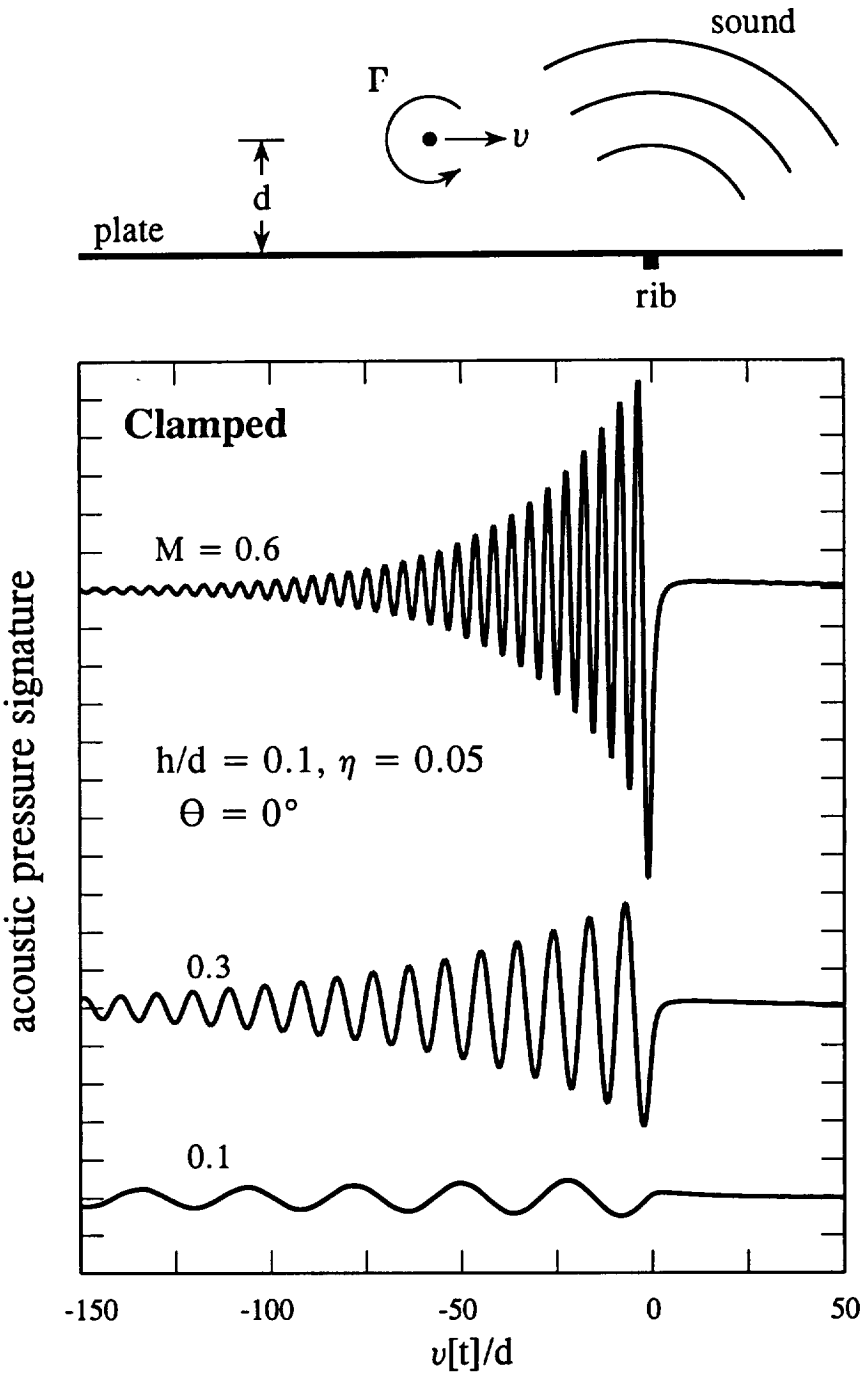

Figure 5. Acoustic pressure signatures (to the same nominal scale) of sound generated for clamped rib conditions, plotted as a function of the nondimensional retarded position $\upsilon[t]/d$ of the vortex for different translation Mach numbers $M = \upsilon/c_0$, and for $\Theta = 0°$, $h/d = 0.1$ and $\eta = 0.05$. The vortex passes over the rib at $t = 0$.

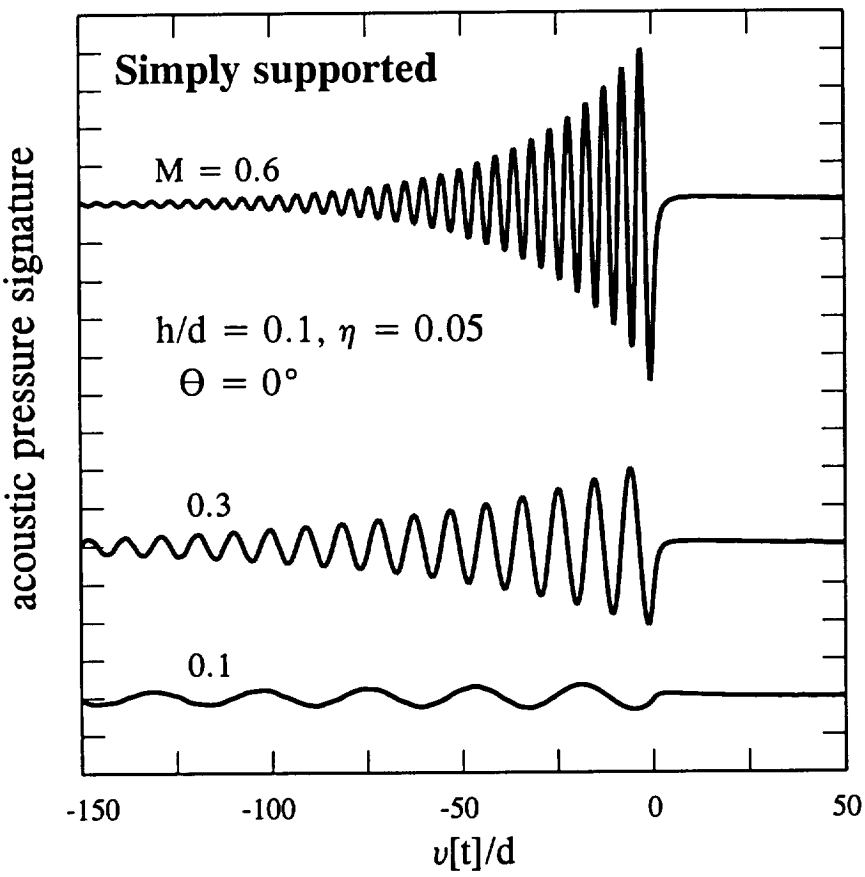

Figure 6. Acoustic pressure signatures (to the same nominal scale) of sound generated for simply supported conditions, plotted as a function of the nondimensional retarded position $\upsilon[t]/d$ of the vortex for different translation Mach numbers $M = \upsilon/c_0$, and for $\Theta = 0°$, $h/d = 0.1$ and $\eta = 0.05$.

CHAPTER 3

ON THE CONTRIBUTION FROM SKIN STEPS TO BOUNDARY LAYER GENERATED INTERIOR NOISE

SUMMARY

An estimate is made of the aircraft interior noise produced by high subsonic turbulent wall pressures interacting with a fuselage skin step formed when adjacent, elastic panels overlap. The panels are modeled as thin elastic plates bonded in the vicinity of the step, and clamped along a line transverse to the mean flow direction. Sound is produced by scattering of the turbulence induced flexural skin motions at the clamp line, and by interaction of the turbulence pressure with the step. The skin step component is found to be significant at high frequencies, *above* the convective resonance frequency of the panels (at which the turbulence convection velocity equals the flexural wave speed). At typical cruise Mach numbers, however, when boundary layer generated sound is believed to dominate interior cabin noise, the critical frequency above which skin step noise is important is of order 10 kHz, which is beyond the range of interest in practice. The critical frequency is much lower at take-off and landing approach conditions, but the turbulent boundary layer is then a relatively unimportant contributor to cabin noise.

1. INTRODUCTION

High speed turbulent flow over an aircraft fuselage is responsible for a substantial component of the interior noise [1 - 4], and is probably the most important source of cabin noise for jet powered passenger aircraft in steady cruise. The principal mechanism of sound generation in subsonic flight is the interaction of boundary layer pressures with structural inhomogeneities, such as ring-stiffeners, stringers and windows, which produce sound whose amplitude and frequency content typically vary widely with flight speed, even though the boundary layer characteristics are believed to be only weakly dependent on flow velocity, at least within the subsonic regime.

Several numerical schemes are being developed to predict the boundary layer generated interior noise [5]. Graham [6, 7] has proposed a semi-analytical model that is applicable to turbulent flow over an isolated fuselage panel, and which incorporates important structural effects of interior trim. None of these methods explicitly includes the influence of the exterior mean flow in calculating the noise. A simplified treatment that involves mean flow was proposed by Howe and Shah [8], who considered the interaction of a boundary layer with a nominally smooth elastic plate with periodically spaced rib-stiffeners. An elementary model of "coincidence scattering", i.e., of sound generation by the edge scattering of flow excited structural waves whose phase velocity exactly matches the convection velocity of a flow inhomogeneity, was discussed in [9], but no account was taken of mean flow. However, although there is currently no fully satisfactory prediction scheme, the basic principles appear to be well understood.

Most numerical prediction procedures take some account of lateral curvature of aircraft panels (e.g., see [5, 10]) and of interior panel trim, but there is no quantified understanding of the influence on sound generation of the step-like discontinuities in the outer skin that occur where adjacent fuselage panels overlap. This might be important when the step height is comparable to the boundary layer displacement thickness, so that the interaction between the turbulence and step is likely to be strong. Sound is generated by the scattering of turbulence pressures by a step, but in addition, the boundary layer wall pressures downstream of the step are also modified, and this will in turn affect the production of sound by direct panel forcing (e.g., see [11, 12]).

In this chapter an analysis is performed to estimate the relative contribution from skin steps to boundary layer interior noise. The method is a development of that used by Howe and Shah [8] for a ribbed panel, which explicitly incorporates the influence of the finite

Mach number of the boundary layer. No account is taken in this calculation of the changes in boundary layer structure caused by the step, which is therefore assumed to generate sound by interaction with a pre-existing turbulent field that is swept over the step, as in the analogous problem discussed in [13] for a step in a *rigid* wall. Such changes are associated with separation induced at the step and will be important when the step height is comparable to the boundary layer displacement thickness. From an acoustic point of view separation tends to *reduce* the radiated sound relative to that predicted when the unsteady motion is modeled according to the proposed inviscid scattering theory [14, 15], because "noisy" potential flow singularities are smoothed-out. The principal conclusion of this investigation is that, for typical aircraft structures and cruise Mach numbers, the influence of skin steps on interior noise is small except at very high frequencies, which are probably too large to be relevant in practice.

The analytical model is formulated in §2, where the sound generated by the interaction of the turbulent flow with a skin joint is expressed in terms of the unsteady, boundary layer wall pressure and a suitable acoustic Green's function that includes the combined effects of structural compliance, the skin step and a rib stiffener at the panel overlap. This is used (in §§3,4) to investigate the dependence on Mach number of skin step noise relative to the noise generated by interaction of the boundary layer with the clamp line of adjacent panels.

2. THE AERODYNAMIC SOUND PROBLEM

2.1 Formulation

Consider high subsonic mean flow over the idealized skin step depicted schematically in Figure 1(a), which consists of two skin sections, modeled as semi-infinite, thin elastic plates which overlap and are clamped together along a nominally rigid, rectilinear rib or stringer. The exterior fluid has mean density ρ_1 and sound speed c_1 with mean flow in the x_1-direction of the rectangular coordinate system (x_1, x_2, x_3), as indicated in the figure. The overlapping skin sections are in practice riveted along the clamp line, which is taken to coincide with the x_3-axis.

When the influence of the skin step on sound production is ignored, the skin thickness h, say, is taken to be sufficiently small that both plates may be assumed to lie in the plane $x_2 = 0$, where $x_2 > 0$ in the exterior mean flow. This flow is assumed to be turbulent, and the problem of calculating the sound produced by the interaction of the turbulence with the plates in the neighborhood of the clamp line was considered in [8]. The basis of this method will be briefly recalled, and the extension necessary to take account of the skin step will then be described.

The fluid in the "interior" domain $x_2 < 0$ has mean density and sound speed respectively equal to ρ_o and c_o and is in a mean state of rest. To determine the sound radiated into this region, the configuration of Figure 1(a) is first taken in the simplified form illustrated in Figure 1(b), where the skin step is ignored, and the adjacent skin sections are regarded as smoothly clamped together along the x_3-axis (at O). If U denotes the mean flow speed (in the x_1-direction) in the exterior region outside the turbulent boundary layer, where the Mach number $M = U/c_1 < 1$, the equations describing the production of aerodynamic sound can be taken in the form

$$\left[\frac{1}{c_o^2}\frac{\partial^2}{\partial t^2} - \nabla^2\right]\mathcal{B} = 0, \quad x_2 < 0, \tag{1}$$

$$\left[\frac{1}{c_1^2}\left(\frac{\partial}{\partial t} + U\frac{\partial}{\partial x_1}\right)^2 - \nabla^2\right]\mathcal{B} = Q(\mathbf{x}, t), \quad x_2 > 0, \tag{2}$$

where $\mathcal{B} = w + \frac{1}{2}v^2$ is the total enthalpy, w being the fluid specific enthalpy, $\mathbf{v}$ the velocity, and t denotes time [16]. The source term $Q(\mathbf{x}, t)$ is non-zero only within the boundary layer, and includes all effects associated with the boundary layer mean shear flow and the turbulence sources.

When the motion is isentropic, the acoustic pressure fluctuation p can be obtained from the solution of equations (1), (2) by means of the relation $\partial p/\partial t = \rho D\mathcal{B}/Dt$, where ρ is the local mean density and D/Dt is the material derivative. In those regions where the flow is irrotational, $\mathcal{B} \equiv -\partial\phi/\partial t$, where $\phi(\mathbf{x}, t)$ is the velocity potential of the unsteady motion.

Deflections of the plates are assumed to be governed by the linearized thin plate equation

$$\left[D\left(\frac{\partial^2}{\partial x_1^2} + \frac{\partial^2}{\partial x_3^2}\right)^2 + m\frac{\partial^2}{\partial t^2}\right]\zeta + [p] = 0, \tag{3}$$

where $\zeta(x_1, x_3, t)$ is the flexural displacement in the x_2-direction, D the plate bending stiffness, m the mass per unit area, and

$$[p] = p(x_1, +0, x_3, t) - p(x_1, -0, x_3, t)$$

is the pressure loading. The displacement ζ and the pressure are also related by the linearized kinematic relations

$$\frac{\partial^2\zeta}{\partial t^2} = \frac{-1}{\rho_o}\frac{\partial p}{\partial x_2}, \quad x_2 = -0; \quad \left(\frac{\partial}{\partial t} + U\frac{\partial}{\partial x_1}\right)^2\zeta = \frac{-1}{\rho_1}\frac{\partial p}{\partial x_2}, \quad x_2 = +0. \tag{4}$$

Along the clamp line the displacement satisfies the clamped edge conditions

$$\zeta = 0, \frac{\partial\zeta}{\partial x_1} = 0, \quad x_3 = 0. \tag{5}$$

2.2 Green's function in the absence of the skin step

Green's function $G_o(\mathbf{x}, \mathbf{y}, t - \tau)$ for the coupled equations (1), (2) is the solution with outgoing wave behavior, which also satisfies the appropriate conditions on the plates and on the clamp line, when Q on the right of (2) is replaced by the point source $\delta(\mathbf{x} - \mathbf{y})\delta(t - \tau)$ concentrated at $\mathbf{y}$. When G is known the acoustic pressure in the interior region (where $\mathcal{B} \approx p/\rho_o$) can be written

$$p(\mathbf{x}, t) = \rho_o \int G_o(\mathbf{x}, \mathbf{y}, t - \tau)Q(\mathbf{y}, \tau)d^3\mathbf{y}d\tau, \tag{6}$$

where the spatial integration is over the boundary layer source region and the time integration is over $-\infty < \tau < \infty$.

When the motion is isentropic, the acoustic pressure fluctuation p can be obtained from the solution of equations (1), (2) by means of the relation $\partial p/\partial t = \rho D\mathcal{B}/Dt$, where ρ is the local mean density and D/Dt is the material derivative. In those regions where the flow is irrotational, $\mathcal{B} \equiv -\partial\phi/\partial t$, where $\phi(\mathbf{x}, t)$ is the velocity potential of the unsteady motion.

Deflections of the plates are assumed to be governed by the linearized thin plate equation

$$\left[D\left(\frac{\partial^2}{\partial x_1^2} + \frac{\partial^2}{\partial x_3^2}\right)^2 + m\frac{\partial^2}{\partial t^2}\right]\zeta + [p] = 0, \tag{3}$$

where $\zeta(x_1, x_3, t)$ is the flexural displacement in the x_2-direction, D the plate bending stiffness, m the mass per unit area, and

$$[p] = p(x_1, +0, x_3, t) - p(x_1, -0, x_3, t)$$

is the pressure loading. The displacement ζ and the pressure are also related by the linearized kinematic relations

$$\frac{\partial^2\zeta}{\partial t^2} = \frac{-1}{\rho_o}\frac{\partial p}{\partial x_2}, \quad x_2 = -0; \quad \left(\frac{\partial}{\partial t} + U\frac{\partial}{\partial x_1}\right)^2\zeta = \frac{-1}{\rho_1}\frac{\partial p}{\partial x_2}, \quad x_2 = +0. \tag{4}$$

Along the clamp line the displacement satisfies the clamped edge conditions

$$\zeta = 0, \frac{\partial\zeta}{\partial x_1} = 0, \quad x_3 = 0. \tag{5}$$

2.2 Green's function in the absence of the skin step

Green's function $G_o(\mathbf{x}, \mathbf{y}, t - \tau)$ for the coupled equations (1), (2) is the solution with outgoing wave behavior, which also satisfies the appropriate conditions on the plates and on the clamp line, when Q on the right of (2) is replaced by the point source $\delta(\mathbf{x} - \mathbf{y})\delta(t - \tau)$ concentrated at $\mathbf{y}$. When G is known the acoustic pressure in the interior region (where $\mathcal{B} \approx p/\rho_o$) can be written

$$p(\mathbf{x}, t) = \rho_o \int G_o(\mathbf{x}, \mathbf{y}, t - \tau)Q(\mathbf{y}, \tau)d^3\mathbf{y}d\tau, \tag{6}$$

where the spatial integration is over the boundary layer source region and the time integration is over $-\infty < \tau < \infty$.

It will suffice for the present discussion to confine attention to the generation of sound by boundary layer disturbances $Q \equiv Q(x_1, x_2, t)$ that are independent of the spanwise coordinate x_3. This is a special case of the fully three-dimensional analysis given in [8], and is adequate for estimating the relative contribution to the sound from the skin step. For an observer at $\mathbf{x}$ in the interior domain, and at large distances from the clamp line, we then have (see [8] for details)

$$G_o(\mathbf{x},\mathbf{y},t-\tau) \approx \frac{\sqrt{i}\rho_1/\rho_o}{2\pi(8\pi|\mathbf{x}|)^{1/2}} \int_{\infty}^{\infty} \frac{T(\omega,\theta)}{\sqrt{\kappa_o}} \Bigg(e^{-i\kappa_o(n_1 y_1 - N_2 y_2)} + \frac{N_2}{c_1(c_o/c_1 - M\sin\theta)} \sum_{n=0}^{3} \int_{-\infty}^{\infty} \frac{(\omega + Uk) a_n k^n e^{i(ky_1 + \Gamma_+(k) y_2)}\, dk}{\Gamma_+(k)\mathcal{L}_+(k,\omega)} \Bigg) e^{-i\omega(t-\tau-|\mathbf{x}|/c_o)}\, d\omega, \quad |\mathbf{x}| \to \infty, \tag{7}$$

where the integration contour in the k-plane is indented to pass respectively above and below real poles and branch points of the integrand in $k \lesseqgtr 0$, $T(\omega,\theta)$ is the elastic plate, plane wave transmission coefficient

$$T(\omega,\theta) = \frac{-2i\epsilon \frac{c_1}{c_o}\left(\frac{c_o}{c_1} - M\sin\theta\right)}{N_2\left\{\left[\left(\frac{\omega}{\omega_c}\right)^2 \sin^4\theta - 1\right]\frac{\omega}{\omega_c} - i\epsilon\left[\frac{1}{\cos\theta} + \frac{\rho_1 c_1^2/\rho_o c_o^2}{N_2}\left(\frac{c_o}{c_1} - M\sin\theta\right)^2\right]\right\}}, \tag{8}$$

and the remaining new terms appearing in these formulae are defined as follows:

$$n_1 = \sin\theta,\ N_2 = \sqrt{(\tfrac{c_o}{c_1} - M\sin\theta)^2 - \sin^2\theta},\ \epsilon = \rho_o c_o/\omega_c m,\ \omega_c = c_o^2(m/D)^{1/2},$$

θ being the angle shown in Figure 1(b) defining the observer direction,

$$\gamma(k) = (\kappa_o^2 - k^2)^{1/2},\ \Gamma_\pm(k) = [(\omega/c_1 \pm Mk)^2 - k^2]^{1/2},\ \kappa_o = \omega/c_o,$$

$$\mathcal{L}_\pm(k,\omega) = Dk^4 - m\omega^2 - i\left[\rho_o\omega^2/\gamma(k) + \rho_1(\omega \pm Uk)^2/\Gamma_\pm(k)\right], \tag{9}$$

where branch cuts in the upper and lower halves of the complex k-plane are taken such that $\gamma(k)$ and $\Gamma_\pm(k)$ have positive imaginary parts on the real axis. Here, $\omega_c > 0$ is the *coincidence frequency* above which the *in vacuo* phase speed of flexural waves on the plate exceeds the interior sound speed c_o. The coefficient ϵ is a measure of the influence of fluid

loading on the motions of the plates. For an aluminum plate of thickness h in air, $\epsilon \approx 0.0022$ and $\omega_c h/c_o \approx 0.22$. The four coefficients a_n are complex functions of the frequency ω, whose values depend on conditions at the junction of two plates, and satisfy $a_n(-\omega) = a_n^*(\omega)$, where the asterisk denotes complex conjugate. For the clamped condition considered here [8]

$$a_0 = \frac{m\omega^2}{K_o} A_0,\ a_1 = \frac{m\omega^2}{K_o^2} A_1,\ a_2 = 0,\ a_3 = 0, \tag{10}$$

where $K_o = (m\omega^2/D)^{1/4} > 0$ is the *in vacuo* wavenumber of bending waves of frequency ω, and the dimensionless coefficients A_0, A_1 are given by

$$A_0 = \frac{\Psi_2 + \mu n_1 \Psi_1}{\Psi_1^2 - \Psi_0 \Psi_2}, \quad A_1 = \frac{-(\Psi_1 + \mu n_1 \Psi_0)}{\Psi_1^2 - \Psi_0 \Psi_2}, \quad \mu = \sqrt{\omega/\omega_c}, \tag{11}$$

$$\Psi_j = \int_{-\infty}^{\infty} \frac{\lambda^j \, d\lambda}{\left[\lambda^4 - 1 - \frac{i\epsilon}{\mu}\left(\frac{1}{\sqrt{\mu^2-\lambda^2}} + \frac{(\rho_o c_o^2/\rho_1 c_1^2)(c_o/c_1 + M\lambda/\mu)^2}{\sqrt{(\mu c_o/c_1 + M\lambda)^2 - \lambda^2}}\right)\right]}. \tag{12}$$

The path of integration along the real axis is indented to pass respectively above and below poles and branch points of the integrand in $\lambda \lesseqgtr 0$.

2.3 Skin step modified Green's function

In the presence of the skin step the representation (6) becomes

$$p(\mathbf{x}, t) = \rho_o \int \Big\{ G_o(\mathbf{x}, \mathbf{y}, t-\tau) + G_s(\mathbf{x}, \mathbf{y}, t-\tau) \Big\} Q(\mathbf{y}, \tau) d^3\mathbf{y} d\tau, \tag{13}$$

where G_s is the correction to Green's function (7) produced by the presence of the step. To calculate G_s we first recall that the reciprocal theorem [8, 17, 18] implies that the term in the large brackets of the integrand of (7), regarded as a function of $\mathbf{y}$, is proportional to the velocity potential in $y_2 > 0$ generated by a point source at the observer location $\mathbf{x}$ when the mean flow in the exterior region is *reversed* in direction. This potential must satisfy boundary conditions of the type (3) - (5) in the reverse flow problem. Thus, if we assume the step to be in the immediate neighborhood of the clamp line $y_3 = 0$ (as in Figure 2), the presence of the step implies that the normal surface derivative $\partial G/\partial y_n \equiv \partial(G_o + G_s)/\partial y_n$ should vanish on the step profile in the reversed flow problem. In the reciprocal problem the length scale of the unsteady fluid motion in the neighborhood of the step *when the step is ignored* is of order $1/K_o \leq 1/\kappa_o$. If $K_o h \leq 1$, i.e., if the structural wavelength is

large compared to the skin thickness, which is usually the case (and is actually necessary to justify the use of the thin plate equation (3)), the velocity potential of the unsteady motion in the neighborhood of the step *relative to that of the plates* is equal to a sum of terms proportional respectively to $n_1[y_1 + \phi^*(\mathbf{y})]$ and $k[y_1 + \phi^*(\mathbf{y})]$, where $\phi^*(\mathbf{y})$ is a solution of the homogeneous, time harmonic form of equation (2) when the mean flow is *reversed*, which satisfies

$$\frac{\partial[y_1 + \phi^*(\mathbf{y})]}{\partial y_n} = 0 \text{ on the step profile.} \tag{14}$$

This is because, near the step, the exponentials in (7) can be expanded to first order in $\mathbf{y}$; the term in y_1 must then be augmented by ϕ^* in order to satisfy (14). If the coordinate origin is taken at the foot of the step, then to first order in the step height s (which is equal to plate thickness h for simple overlapping plates), the boundary condition (14) becomes

$$\frac{\partial \phi^*}{\partial y_2} = \pm s\delta(y_1) \quad \text{on} \quad y_2 = +0,$$

and the appropriate ϕ^* is accordingly found to be given by

$$\phi^*(\mathbf{y}) = \frac{\pm s}{2\pi i}\int_{-\infty}^{\infty} \frac{e^{i(ky_1 + \Gamma_+(k)y_2)}}{\Gamma_+(k)}\, dk, \tag{15}$$

where the $\pm$ sign is taken according as the step is forward or backward facing relative to the mean flow. We then have

$$G_s(\mathbf{x},\mathbf{y},t-\tau) \approx \frac{(\rho_1/\rho_o)\phi^*(\mathbf{y})}{2\pi\sqrt{8\pi i|\mathbf{x}|}}\int_{-\infty}^{\infty} \frac{T(\omega,\theta)}{\sqrt{\kappa_o}}\Big\{\kappa_o n_1$$

$$- \frac{N_2}{c_1(c_o/c_1 - M\sin\theta)}\sum_{n=0}^{3}\int_{-\infty}^{\infty} \frac{(\omega + Uk)a_n k^{n+1}\, dk}{\Gamma_+(k)\mathcal{L}_+(k,\omega)}\Big\} e^{-i\omega(t-\tau-|\mathbf{x}|/c_o)}\, d\omega. \tag{16}$$

The integral within the brace brackets converges only for $n \leq 1$; in particular it converges for the clamped condition, for which $a_2 = a_3 \equiv 0$. This is because when $a_2 \neq 0$ there is a discontinuity in the slope of the two plates at the join, and there can then be no smooth flow over the plates in the absence of the step (see [8]), as assumed in the reciprocal problem.

3. THE INTERIOR ACOUSTIC PRESSURE

3.1 The blocked wall pressure

It is convenient to express the interior radiation in terms of the boundary layer wall pressure on the exterior skin that would be generated when the wall is regarded as rigid. This is the *blocked* pressure, and can be calculated by solving (2) subject to the boundary condition $\partial\mathcal{B}/\partial x_2 = 0$ on $x_2 = +0$, and using the relation $\partial p/\partial t \approx \rho_1(\partial/\partial t + U\partial/\partial x_1)\mathcal{B}$. If $p_b(k_1,\omega)e^{i(k_1x_1-\omega t)}$ is the component of the blocked pressure of frequency ω and wavenumber k_1 in the streamwise direction, then it is readily shown that

$$p_b(k_1,\omega) = \frac{2\pi i\rho_1(\omega - Uk_1)}{\omega\Gamma_-(k_1)}\hat{Q}(k_1,-\Gamma_-(k_1),\omega)\ , \tag{17}$$

where

$$\hat{Q}(k_1,k_2,\omega) = \frac{1}{(2\pi)^3}\int\int_{-\infty}^{\infty} dx_1dt\int_0^{\infty} Q(x_1,x_2,t)e^{-i(k_1x_1+k_2x_2-\omega t)}\,dx_2. \tag{18}$$

The dominant components of the blocked wall pressure occur in the vicinity of $k_1 = \omega/U_c$ where U_c is a convection velocity approximately equal to $0.7U$ [19 - 22].

3.2 Sound radiated from the clamp line

The acoustic pressure $p_o(\mathbf{x},t)$, say, produced by the interaction of the boundary layer pressure field with the clamp line is given by (6). The contribution from the first, exponential term in the round brackets in the representation (7) of G_o can be ignored, since it does not correspond to the generation of sound at the clamp line, but to the transmission through the wall of boundary layer pressure fluctuations that are *already* sound, exactly as if the clamp were absent. Relations (17) and (18) can be used to express the contribution from the second term in the round brackets of (7) in the form

$$p_o(\mathbf{x},t) \approx \sqrt{\frac{\pi}{2i|\mathbf{x}|}}\frac{N_2}{\frac{c_1}{c_0}\left(\frac{c_o}{c_1} - M\sin\theta\right)}\sum_{n=0}^{3}\int_{-\infty}^{\infty}\frac{T(\omega,\theta)\sqrt{\kappa_o}a_n(-k_1)^n}{\mathcal{L}_-(k_1,\omega)}\,p_b(k_1,\omega)e^{-i\omega(t-|\mathbf{x}|/c_o)}\,dk_1d\omega. \tag{19}$$

3.3 Sound radiated from the skin step

Similarly, the contribution $p_s(\mathbf{x},t)$ to the acoustic pressure from the step, given by the term in G_s in (13) becomes

$$p_s(\mathbf{x},t) \approx \frac{\mp s}{2\pi}\sqrt{\frac{\pi}{2i|\mathbf{x}|}}\int\int_{-\infty}^{\infty}\frac{\sqrt{\kappa_o}\omega T(\omega,\theta)}{(\omega-Uk_1)}\Bigg\{\sin\theta$$

$$-\frac{N_2}{\kappa_o c_1\left(\frac{c_o}{c_1}-M\sin\theta\right)}\sum_{n=0}^{3}\int_{-\infty}^{\infty}\frac{(\omega+Uk)a_n k^{n+1}\,dk}{\Gamma_+(k)\mathcal{L}_+(k,\omega)}\Bigg\}p_b(k_1,\omega)e^{-i\omega(t-|\mathbf{x}|/c_o)}\,dk_1 d\omega, \tag{20}$$

the upper/lower sign being taken respectively for forward and backward facing steps.

3.4 Acoustic efficiencies

Consider the sound generated by the interaction of the component $p_I \equiv p_b(k_1,\omega)dk_1 d\omega$ of the blocked wall pressure with the clamp line and skin step. The relative efficiencies of sound generation by these two mechanisms is determined by the relative magnitudes of the ratios $p_o(\mathbf{x},t)/p_I$ and $p_s(\mathbf{x},t)/p_I$. Let us suppose that p_I is characteristic of the dominant wall pressure fluctuations, for which $\omega/k_1 = U_c$. It then follows from (19) and (20), using also results given in §2, that

$$\frac{p_o}{p_I} \approx \sqrt{\frac{\pi h}{2i|\mathbf{x}|}}\frac{N_2 T(\omega,\theta)\mu^2\bar{M}_c^4[A_0-\mu A_1/\bar{M}_c]e^{-i\omega(t-|\mathbf{x}|/c_o)}}{\sqrt{\frac{\omega_c h}{c_o}}\frac{c_1}{c_o}\left(\frac{c_o}{c_1}-M\sin\theta\right)\left\{(\mu^4-\bar{M}_c^4)\mu^2-\epsilon\bar{M}_c^5\left[\frac{1}{\sqrt{1-\bar{M}_c^2}}+\frac{(\rho_1/\rho_o)(1-M/M_c)^2}{\sqrt{1-(M-M_c)^2}}\right]\right\}}, \tag{21}$$

$$\frac{p_s}{p_I} \approx \pm\sqrt{\frac{\pi h}{2i|\mathbf{x}|}}\frac{(s/h)\sqrt{\frac{\omega_c h}{c_o}}\mu T(\omega,\theta)}{2\pi(M/M_c-1)}\left[\sin\theta-\frac{N_2[A_0\Phi_0+A_1\Phi_1]}{\frac{c_o}{c_1}-M\sin\theta}\right]e^{-i\omega(t-|\mathbf{x}|/c_o}\,, \tag{22}$$

where

$$M_c = U_c/c_1, \quad \bar{M}_c = U_c/c_o,$$

and

$$\Phi_n = \int_{-\infty}^{\infty}\frac{\left(\frac{c_o}{c_1}+M\frac{\lambda}{\mu}\right)\lambda^{n+1}\,d\lambda}{\sqrt{\left(\frac{\mu c_o}{c_1}+M\lambda\right)^2-\lambda^2}\left\{\lambda^4-1-\frac{i\epsilon}{\mu}\left[\frac{1}{\sqrt{\mu^2-\lambda^2}}+\frac{(\rho_1 c_1^2/\rho_o c_o^2)\left(\frac{c_o}{c_1}\mu+M\lambda\right)^2}{\mu^2\sqrt{\left(\frac{\mu c_o}{c_1}+M\lambda\right)^2-\lambda^2}}\right]\right\}}\,. \tag{23}$$

4. NUMERICAL RESULTS

The curves in figures 3 - 5 are plots of the calculated efficiency $20*\log\left(|p(\mathbf{x},t)/p_I|/\sqrt{h/|\mathbf{x}|}\right)$ (dB) of interior sound production by the clamp line and by the skin step at three different mean flow Mach numbers M, and for the nominal radiation direction $\theta = 45°$ (see Figure 1(b)). The calculations have been performed for aluminum plates in air; for simplicity it is assumed that $\rho_o = \rho_1$, $c_o = c_1$, for which the remaining non-dimensional parameters describing the fluid-structure interaction have been assigned the values $\epsilon = 0.0022$, $\omega_c h/c_o = 0.22$, $M_c = 0.7M$.

The peaks labeled "convective resonance" occur where the convection velocity $\omega/k_1 = U_c$ of the blocked wall pressure component $p_b(k_1,\omega)$ is the same as the phase speed of bending waves in the plates of the same frequency and wavenumber, and occurs approximately at $\omega = M_c^2\omega_c$. At frequencies exceeding the convective resonance frequency the efficiency of sound generation by scattering at the clamp line decreases very rapidly. At frequencies below resonance the overall level of the skin step generated sound is always negligible. At higher frequencies, however, it becomes dominant because of the precipitous decrease in the efficiency of sound generation by clamp line scattering. The peaks in the skin step sound evident in Figures 4 and 5 occur at sufficiently large frequencies that $\omega/\omega_c = 1/\sin^2\theta > 1$. This condition is satisfied by those structural waves generated at the step whose phase velocity is just equal to the trace velocity of sound waves launched in the observer direction θ, and corresponds to the vanishing of the first term in the brace brackets of the denominator of the definition (8) of the plane wave transmission coefficient $T(\omega,\theta)$.

The figures indicate that the skin step sound will be dominant at sufficiently high frequency. To illustrate the orders of magnitude involved, Table 1 lists approximate values of the critical frequency $\omega_s/2\pi \equiv f_s$ Hz, say, above which skin step noise is dominant for the three Mach numbers considered in Figures 3 - 5 when $\theta = 45°$, and when the skin thickness $h = 0.1$ cm.

Mach Number	ω_s/ω_c	f_s Hz
0.01	0.0008	10
0.4	0.17	2000
0.8	1	12000

Table 1. Critical frequency when $\theta = 45°$.

Thus, at $M \approx 0.8$, which is appropriate for cruise conditions at which boundary layer generated interior noise is believed to be significant, it appears that the contribution from skin steps will be unimportant at frequencies less than, say, 10 kHz. According to Table 1, the critical frequency decreases rapidly with decreasing flight speed, being as small as 2 kHz when $M = 0.4$. However, such flight speeds are characteristic of takeoff and landing, when boundary layer generated noise within the cabin is negligible compared to that generated by other sources. The critical frequency varies relatively little with radiation direction θ. This is evident from Figure 6, which depicts the variation of $20 \times \log |p_o/p_s|$ (dB) with frequency for $\theta = -45°$, $0°$, $45°$.

5. CONCLUSION

Turbulent boundary layer generated noise is one of the dominant components of passenger aircraft interior noise at high subsonic cruise conditions. This noise is produced by the interaction of turbulent pressures with fuselage inhomogeneities, in particular with skin panel junctions. In this chapter an analysis has been made to estimate the likely contribution from interaction of the turbulent flow with skin steps, where adjacent panels overlap. Sound and structural vibrations are excited by the interaction. In addition, the step causes a localized, temporary change in the boundary layer turbulence characteristics. This has been ignored, and the turbulence has been regarded as *frozen* during its interaction with the step. Skin step noise is found to be significant only at high frequencies, *beyond* the structural convective resonance frequency (at which the boundary layer eddy convection velocity coincides with the phase speed of flexural waves in the skin); above this frequency the efficiency of sound production by the scattering of turbulence pressures at a clamped panel edge decreases precipitously. However, at cruise Mach numbers, where boundary layer generated noise is important, the skin step noise is dominant only at frequencies typically in excess of about 10 kHz, which is beyond the range of interest in practice. At lower flight speeds, appropriate to take-off and landing approach conditions, the skin step contribution is significant at lower frequencies, but in these circumstances cabin interior noise is no longer controlled by the fuselage boundary layer.

REFERENCES

1. J. F. Wilby, C. D. McDaniel and E. G. Wilby 1985 NASA CR-178004. In-flight acoustic measurements on a light twin-engined turboprop airplane.
2. J. S. Mixson and J. F. Wilby 1991 in *Aeroacoustics of Flight Vehicles: Theory and Practice*, Vol. 2. NASA Ref. Pub. No. 1258, Chapter 16: Interior noise.
3. W. R. Graham 1993 Boundary layer noise and vibration. *Doctoral Thesis*, Cambridge University Engineering Department.
4. Wilby, J.F. 1996 *Journal of Sound and Vibration* **190**, 545 - 564. Aircraft interior noise.
5. R. J. Silcox 1995 (editor) *Proceedings of the Interior Noise Workshop*, held at NASA Langley Research Center, 25 - 27 April.
6. W. R. Graham 1996 *Journal of Sound and Vibration* **192**, 101 - 120. Boundary layer induced noise in aircraft, Part I: the flat plate model.
7. W. R. Graham 1996 *Journal of Sound and Vibration* **192**, 121 - 138. Boundary layer induced noise in aircraft, Part II: the trimmed flat plate model.
8. M. S. Howe and P. L. Shah 1996 *Journal of the Acoustical Society of America* **99**, 3401 - 3411. Influence of mean flow on boundary layer generated interior noise.
9. P. L. Shah and M. S. Howe 1996 *Journal of Sound and Vibration* **197**, 103 - 115. Sound generated by a vortex interacting with a rib-stiffened elastic plate.
10. W. R. Graham 1995 *Journal of the Acoustical Society of America* **98**, 1581 - 1595. The influence of curvature on the sound radiated by vibrating panels.
11. T. M. Farabee and M. J. Casarella 1988 ASME paper entitled: Wall pressure fluctuations beneath a disturbed turbulent boundary layer, pp 121 - 135 of *Acoustic Phenomena and Interaction in Shear Flows Over Compliant and Vibrating Surfaces–Volume 6* (Editors: W. L. Keith, E. M. Uram and A. J. Kalinowski.)
12. J. Sulc, J. Hofr and L. Benda 1982 *Journal of Sound and Vibration* **84**, 105 - 120. Exterior noise on the fuselage of light propeller driven aircraft in flight.
13. M. S. Howe 1989 *Journal of Fluids and Structures* **83**, 83 - 96. Sound produced by turbulent boundary layer flow over a finite region of wall roughness, and over a forward facing step.

14. M. S. Howe 1976 *Journal of Fluid Mechanics* **76**, 711 - 740. The influence of vortex shedding on the generation of sound by convected turbulence.

15. M. S. Howe 1988 *Proceedings of the Royal Society* **A420**, 157 -182. Contributions to the theory of sound production by vortex-airfoil interaction, with application to vortices with finite axial velocity defect.

16. M. S. Howe 1975 *Journal of Fluid Mechanics* **71**, 625 - 673. Contributions to the theory of aerodynamic sound, with application to excess jet noise and the theory of the flute.

17. M. S. Howe 1975 *Journal of Fluid Mechanics* **67**, 579 - 610. The generation of sound by aerodynamic sources in an inhomogeneous steady flow.

18. W. Möhring 1979 Modelling low Mach number noise, pp 85 - 96, *Proceedings of the Symposium on Mechanics of Sound Generation in Flows*, Göttingen, August 28 - 31 (editor E.-A. Müller: Springer, Berlin).

19. B. M. Efimtsov 1982 *Soviet Physics Acoustics* **28**, 289 - 292. Characteristics of the field of turbulent wall pressure fluctuations at large Reynolds numbers.

20. D. M. Chase 1987 *Journal of Sound and Vibration* **112**, 125 - 147. The character of the turbulent wall pressure spectrum at subconvective wavenumbers and a suggested comprehensive model.

21. A. E. Landmann 1995. *Spatial-Temporal boundary layer models for aircraft interior noise.* Paper presented at the *NASA Langley Workshop on Interior Noise*, Hampton VA, 25 - 27 April.

22. W. R. Graham 1995 *AIAA Paper* 95-097. A comparison of models for the wavenumber-frequency spectrum of turbulent boundary layer pressures.

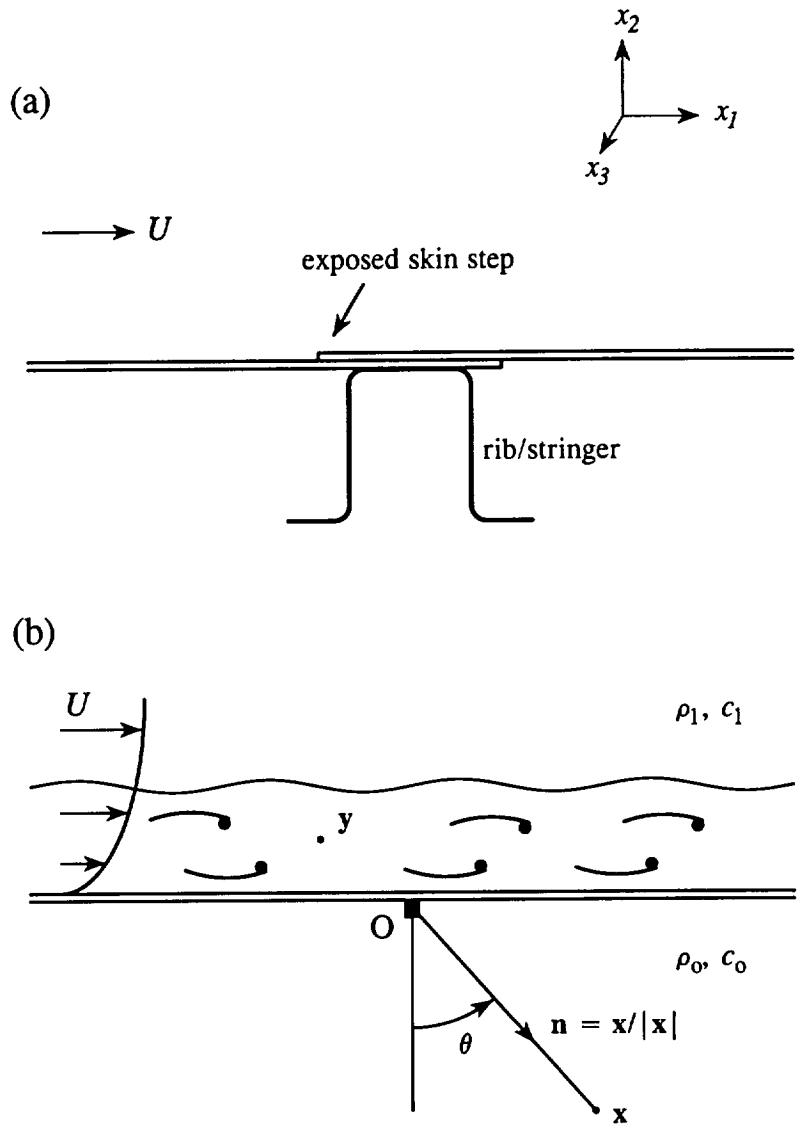

Figure 1. (a) Schematic skin-step configuration.
(b) Simplified model in absence of skin step.

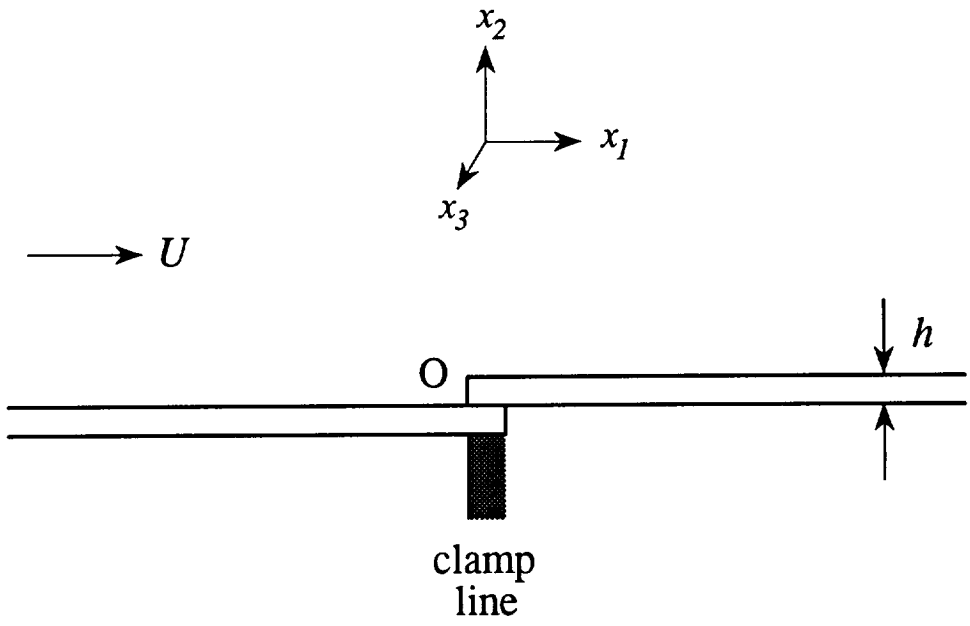

Figure 2. Idealization of skin step and clamp line.

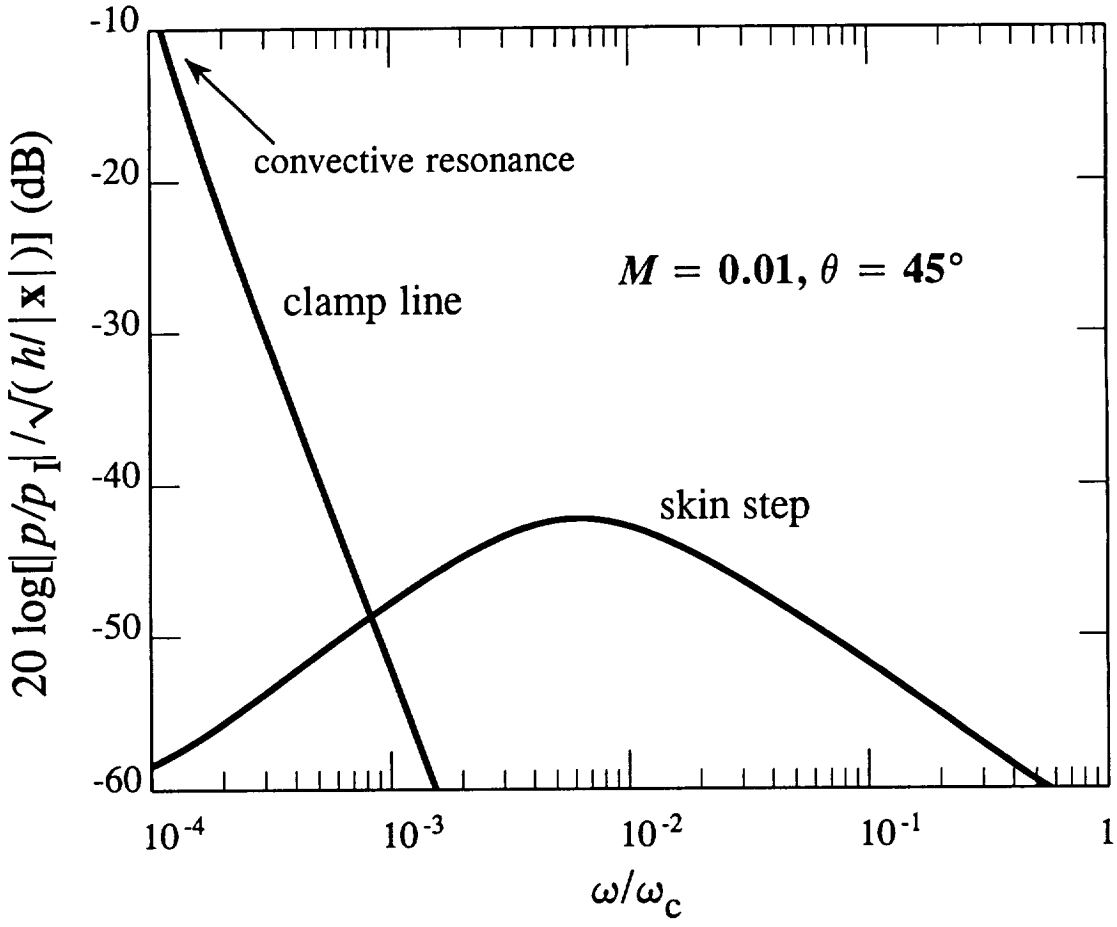

Figure 3. Efficiencies of sound generation by scattering from the clamp line and from the skin step; aluminum skin, $M = 0.01$, $\theta = 45°$.

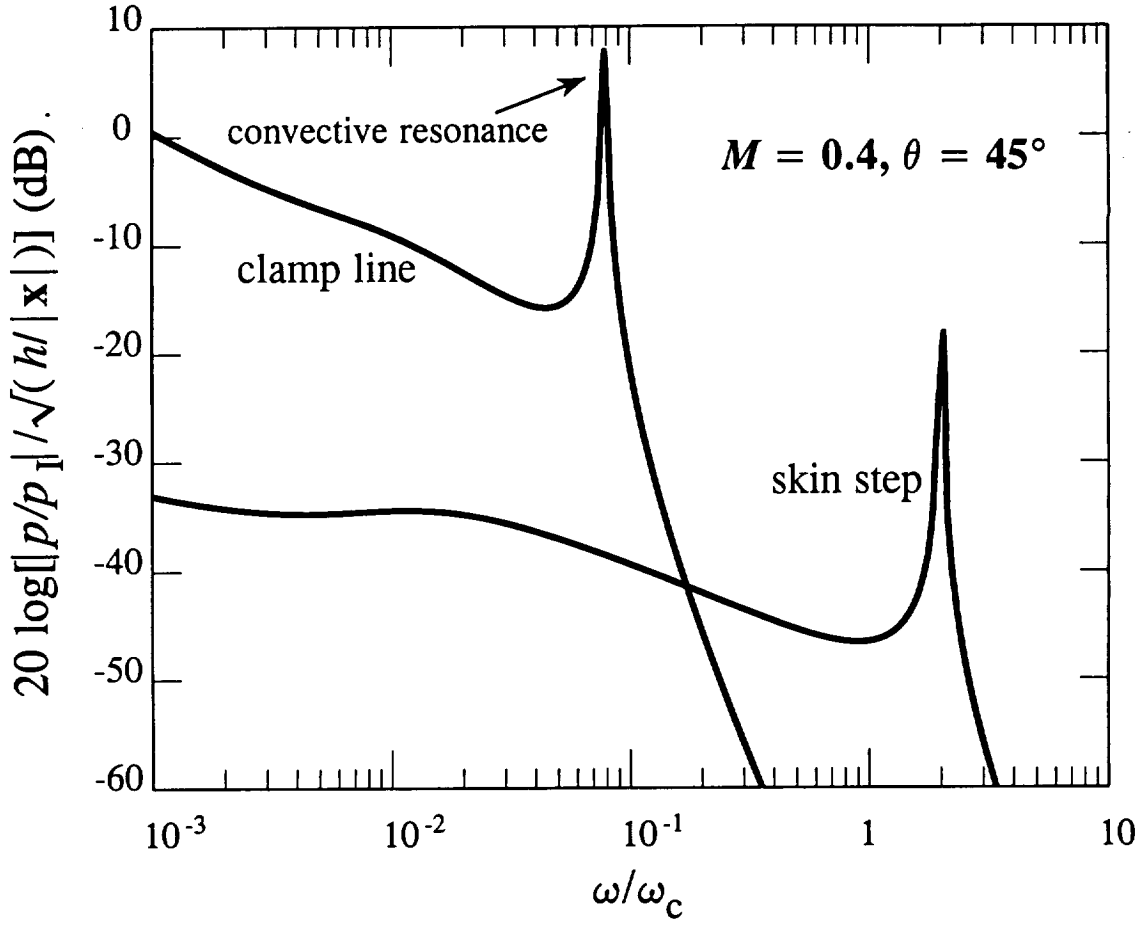

Figure 4. Efficiencies of sound generation by scattering from the clamp line and from the skin step; aluminum skin, $M = 0.4$, $\theta = 45°$.

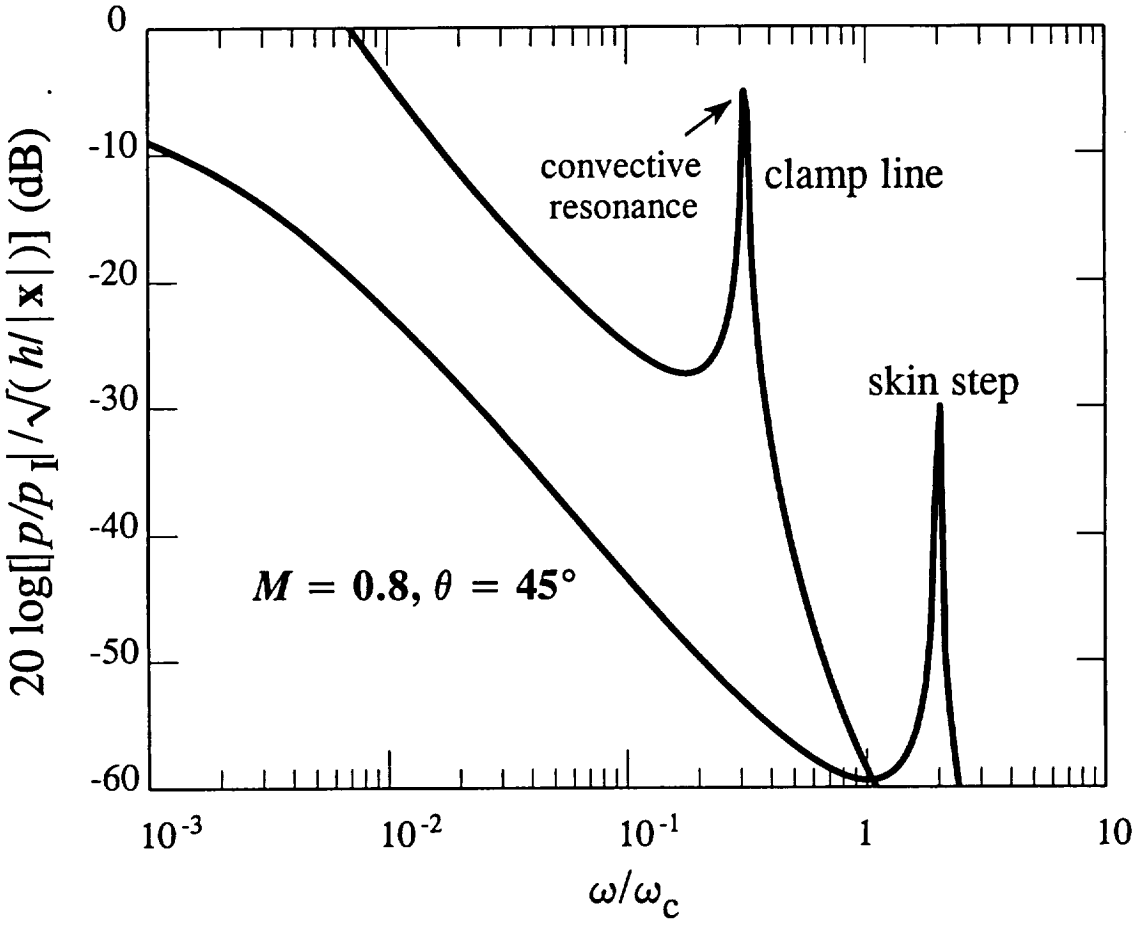

Figure 5. Efficiencies of sound generation by scattering from the clamp line and from the skin step; aluminum skin, $M = 0.8$, $\theta = 45°$.

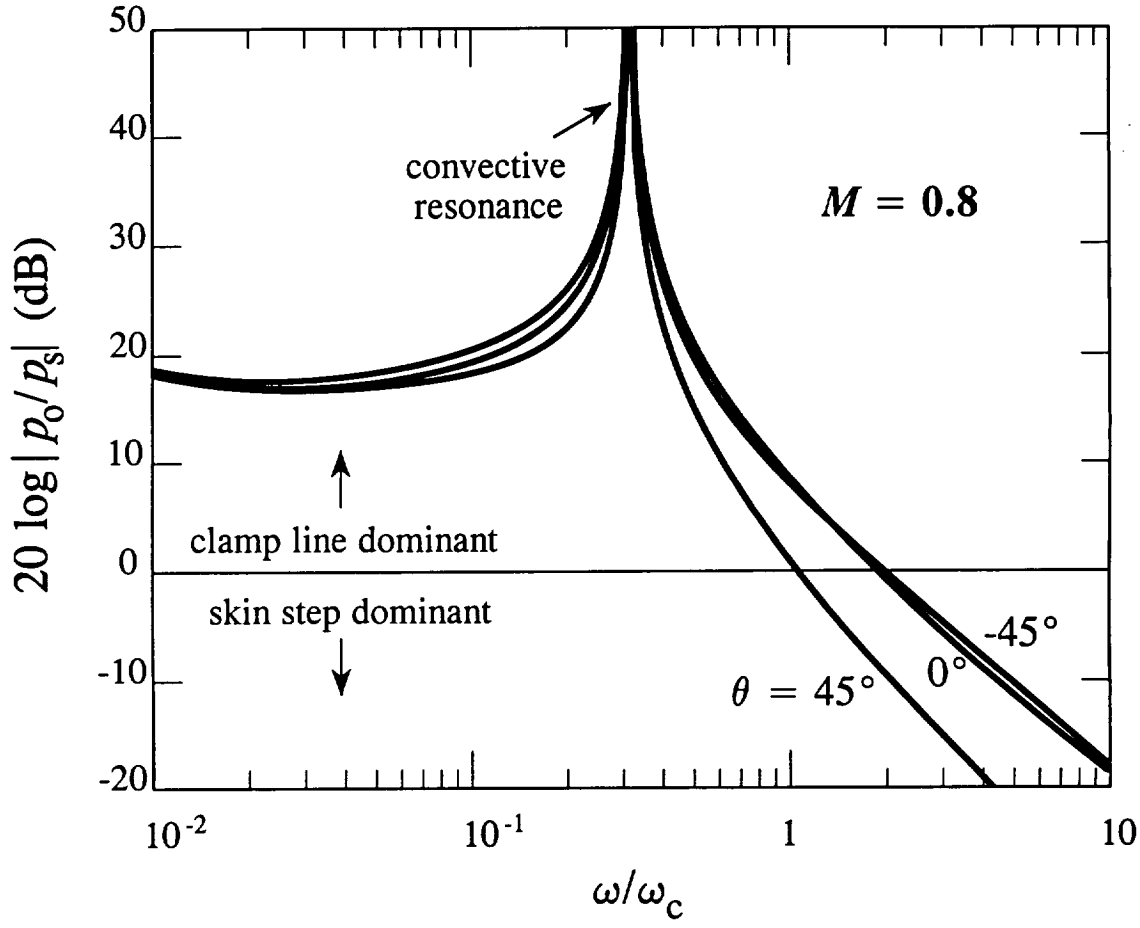

Figure 6. Ratio $|p_o/p_s|^2$ (in dB) of the sound generated respectively by scattering at the clamp line and skin step for different radiation angles θ; aluminum skin, $M = 0.8$.

CHAPTER 4

INFLUENCE OF SEPARATION ON SOUND GENERATED BY VORTEX-STEP INTERACTION

SUMMARY

An analysis is made of the sound produced when a line vortex interacts at low Mach number with forward or backward facing steps. The radiation is dominated by an aeroacoustic dipole whose strength is equal to the unsteady drag on the step. The drag is determined by the vorticity distribution, and a correct estimate of the sound must therefore include contributions from vorticity in the separated flow induced by the vortex. Separation is modelled by assuming that shed vorticity rolls up into a concentrated core, fed by a connecting sheet from the edge of the step of negligible circulation. The motion everywhere is irrotational except at the impinging vortex and the separation core, and the trajectory of the core is governed by an emended Brown and Michael equation. For large steps it is found that estimates of the generated sound that neglect separation are typically an order of magnitude too large. The sound levels predicted for small steps with and without separation are of comparable magnitudes, although the respective *phases* are different. *Turbulent* flow over a step frequently involves separation and large surface pressure fluctuations at reattachment zones. The results of this chapter suggest that numerical schemes for determining the noise generated by turbulent flow over a step must take proper account of "forcing" of the separation region by the impinging turbulence and of vorticity production via the no-slip condition.

1. INTRODUCTION

Boundary layer turbulence and other flow inhomogeneities can induce unsteady separation from structural irregularities, such as rivet heads, lap-joints, cutouts, etc. The unsteady drag exerted on the irregularity is equivalent to a localized aeroacoustic dipole, and is responsible for the production of both sound and structural vibration. Lap-joints (or "skin steps") occur at junctions of neighboring panels on an aircraft fuselage, and are a possible source of boundary layer generated interior cabin noise, either because they enhance downstream wall pressure fluctuations that drive vibrations of the cabin walls, or because the drag dipole is a direct source of sound and vibration (Efimtsov 1996; Howe 1997).

Irregularities in the form of forward or backward facing steps have been studied extensively (Bradshaw and Wong 1972; Chandrsuda and Bradshaw 1981; Eaton and Johnston 1981; Farabee and Casarella 1984, 1986, 1988; Moss and Baker 1980) because their free shear layers possess well defined separation and reattachment zones. More generally, reattachment occurs downstream of a stagnation point, and is a region of high fluctuating wall pressure, where free shear layer eddies bifurcate into upstream and downstream travelling components (Bradshaw and Wong 1972). According to Farabee and Casarella (1984, 1986), low Mach number turbulent wall pressures at reattachment for backward and forward facing steps (with step heights comparable to the boundary layer thickness) are respectively about 5 and 10 times larger than the smooth wall boundary layer pressures. The wall pressure must ultimately revert to that of a smooth wall boundary layer, but differences have been observed at distances as large as 72 step heights downstream of the step.

The large changes in the boundary layer structure at a step must be carefully modeled to obtain accurate estimates of the sound produced by the boundary layer-step interaction. For example, in low to moderate Mach number flows, the unsteady drag (which is the dipole source strength) is determined by the vorticity distribution near the step (Howe 1989a, 1995), which includes vorticity in the impinging flow together with any produced by the interaction and "trapped" in the recirculating separation bubble. Hitherto, theoretical predictions of the generated sound (e.g., Conlisk and Veley 1985; Dhanak and Gundlapalli 1992; Howe 1989b, 1997) have tended to ignore separation and vorticity production. Conlisk & Veley (1985) and Dhanak & Gunlapalli (1992) represented the impinging inhomogeneous flow by an assembly of line (or *point*) vortices, whose motions over a large step (comparable in size to the boundary layer thickness) were determined from inviscid equations of motion. Howe (1989b, 1997) considered "small" steps, and calculated the sound as a by-product of

the scattering of the boundary layer pressure field, which was assumed to be *frozen* during convection over the step.

In this chapter we assess the accuracy of these inviscid approximations from an analysis of the interaction of a single line vortex with a forward or backward facing step. Separation is modeled by assuming that vorticity shed during the interaction rolls up into a concentrated core, which grows in strength by the passage of continuously shed vorticity along a connecting sheet from the edge of the step. The motion is irrotational everywhere except at the impinging vortex and the core of the shed vorticity, and the trajectory of the core is determined by the emended Brown and Michael equation (Brown and Michael 1954, 1955; Howe 1996). For large steps, it is concluded that estimates of the sound that neglect separation are typically an order of magnitude too large. This is because the calculated drag on the step is greatly overestimated when the potential theory singularity at the edge of the step is not suppressed by vortex shedding. For small steps, predicted sound levels with and without separation are of comparable magnitudes, but exhibit large differences in *phase*.

The aerodynamic sound problem is formulated in §2 for low Mach, self-induced vortex motion over forward or backward facing steps on a plane wall. Numerical predictions of the sound are presented in §3.

2. THE AERODYNAMIC SOUND PROBLEM

2.1 Formulation

A line vortex of circulation $\Gamma_o > 0$ is in translational motion adjacent to a rigid wall. The vortex is parallel to the z-axis of the rectangular coordinate system (x, y, z), and the wall is parallel to the plane $y = 0$, except for a "vertical" step of height h, whose foot coincides with the z-axis. To fix ideas, consider the forward facing step illustrated schematically in Figure 1, where the coordinate origin is at O, and the fluid and vortex lie in the region $y \geq 0$ "above" the wall.

In the undisturbed state the fluid is at rest, and is inviscid except that vortex shedding is permitted from the right-angled edge S of the step to remove the singular velocity and pressure that would otherwise occur. Vortex shedding is uniform along the step, and is modeled by a line vortex of variable strength $\Gamma(t)$ (t denoting time) whose axis intersects the plane $z = 0$ at $(x, y) = \mathbf{x}_\Gamma(t)$, and translates at velocity $d\mathbf{x}_\Gamma/dt \equiv \mathbf{V}$. The vortex strength increases as shed vorticity is continuously "fed" along a connecting sheet from S. The circulation of the connecting sheet is assumed to be negligible compared to Γ. This model of vortex shedding, involving a time-dependent core Γ containing all of the shed vorticity, includes a pressure jump across the connecting sheet, and requires the translational velocity $\mathbf{V}$ to be different from the fluid velocity $\mathbf{v}$ at the core (Brown & Michael 1954, 1955). $\Gamma(t)$ is assumed to vary monotonically until the vortex is finally "released" from S when $d\Gamma/dt$ changes sign. The "free" vortex (with no connecting sheet) then proceeds to convect with the fluid at velocity $\mathbf{v}$, and a new vortex is released from S. In the present discussion $d\Gamma/dt$ turns out to be one-signed during the dominant interaction of the incident vortex Γ_o with the step.

Let (x_o, y_o) be the position of the incident vortex in the plane $z = 0$ at time t. The vorticity $\boldsymbol{\omega}$ can then be written

$$\begin{aligned} \boldsymbol{\omega} &= \boldsymbol{\Omega}_o + \boldsymbol{\Omega}, \\ \boldsymbol{\Omega}_o &= \Gamma_o \mathbf{k}\delta(x - x_o(t))\delta(y - y_o(t)), \\ \boldsymbol{\Omega} &= \Gamma(t)\mathbf{k}\delta(x - x_\Gamma(t))\delta(y - y_\Gamma(t)), \end{aligned} \tag{2.1}$$

where $\mathbf{k} = (0, 0, 1)$ is a unit vector in the z-direction (out of the plane of the paper in Figure 1). For an ideal fluid the momentum equation is

$$\frac{\partial \mathbf{v}}{\partial t} + \nabla\left(\int \frac{dp}{\rho} + \frac{1}{2}\mathrm{v}^2\right) = -\boldsymbol{\omega} \wedge \mathbf{v} + \frac{\mathbf{F}}{\rho} \tag{2.2}$$

where p and ρ are respectively the pressure and density, and for two-dimensional motion $\mathbf{v} = (u, v, 0)$. $\mathbf{F}$ is the distributed force

$$\mathbf{F} = \rho\boldsymbol{\Omega} \wedge (\mathbf{v} - \mathbf{V}) - \rho\frac{d\Gamma}{dt}\mathbf{n}\delta(x_\perp)H(s_\Gamma - s), \quad s > 0, \tag{2.3}$$

where $x_\perp$ is distance from the connecting sheet measured in the direction of the local normal $\mathbf{n}$ of Figure 1, s_Γ is the length of the sheet (between S and Γ), and s is distance measured along the sheet from S. The first term on the right is concentrated at the core of the shed vortex, and is equal and opposite to the Joukowski lift on Γ which arises when $\mathbf{V} \neq \mathbf{v}$; the second term represents the pressure force across the connecting sheet (Howe 1996).

2.2 Equations of motion of the vortices

The incident vortex is "free" and translates at the fluid velocity $\mathbf{v}(x, y, t)$ evaluated at its core

$$\frac{d\mathbf{x}_\mathrm{o}}{dt} = \mathbf{v}(x_\mathrm{o}, y_\mathrm{o}, t). \tag{2.4}$$

This velocity is calculated according to potential flow theory, and consists of a contribution from the *images* of Γ_o in the rigid wall and from the shed vortex Γ and its images.

Brown and Michael (1954, 1955) obtain the equation of motion of the shed vortex by requiring the net force exerted on the fluid by the distribution $\mathbf{F}$ to vanish. In general, it is not sufficient to require $\int \mathbf{F}\, dxdy = \mathbf{0}$, since the surface reaction to the remaining unbalanced couple ($\int \mathbf{x} \wedge \mathbf{F}\, dxdy$) is usually equivalent to a surface force on the fluid. However, for an infinitely large rigid wall, the aggregate normal reaction is equal and opposite to the normal (i.e., the y-) component of $\int \mathbf{F}\, dxdy$, and it is therefore sufficient to require that this should vanish. Performing the integration for the y-component of (2.3), we find

$$\frac{dx_\Gamma}{dt} + \frac{x_\Gamma}{\Gamma}\frac{d\Gamma}{dt} = u(x_\Gamma, y_\Gamma, t). \tag{2.5}$$

The net horizontal component of the force on the fluid (in the x-direction) induced by $\mathbf{F}$ and its interaction with the step is eliminated by requiring the shed vortex path to satisfy

the equation (Howe 1996)

$$\int \mathbf{F} \cdot \nabla X \, dxdy = 0, \tag{2.6}$$

where $X \equiv X(x, y)$ is a harmonic function that depends only on the shape of the step, and is equal to the velocity potential of ideal, incompressible flow past the step that has unit speed in the x-direction at large distances from the step. Equation (2.6) is expressed in differential form by making use of the Cauchy-Riemann relations

$$\partial X/\partial x = \partial \Psi/\partial y, \quad \partial X/\partial y = -\partial \Psi/\partial x, \tag{2.7}$$

where Ψ is the stream function conjugate to X. When $\Psi \equiv 0$ on the wall, equation (2.6) is equivalent to

$$\frac{d\mathbf{x_\Gamma}}{dt} \cdot \nabla \Psi + \frac{\Psi}{\Gamma}\frac{d\Gamma}{dt} = \mathbf{v} \cdot \nabla \Psi, \quad (x, y) = (x_\Gamma, y_\Gamma). \tag{2.8}$$

This equation is reduced to the following simplified form by subtracting equation (2.5) multiplied by $\partial \Psi/\partial x$

$$\frac{dy_\Gamma}{dt} + \frac{(\Psi - x_\Gamma \Psi_x)}{\Psi_y}\frac{1}{\Gamma}\frac{d\Gamma}{dt} = v(x_\Gamma, y_\Gamma, t), \tag{2.9}$$

where $(\Psi_x, \Psi_y) = (\partial \Psi/\partial x, \partial \Psi/\partial y)$.

2.3 The aerodynamic sound

At low Mach numbers the production of aerodynamic sound by the vorticity and force distribution on the right of (2.2) is governed by the inhomogeneous wave equation (Howe 1975, 1996)

$$(\partial^2/c_o^2 \partial t^2 - \nabla^2)\mathcal{B} = div(\boldsymbol{\omega} \wedge \mathbf{v}) - div(\mathbf{F}/\rho_o) \tag{2.10}$$

where $\mathcal{B} \equiv p/\rho_o + \frac{1}{2}\mathrm{v}^2$ (the total *enthalpy* in isentropic flow) and ρ_o, c_o are respectively the mean density and sound speed. In irrotational regions the motion can be described by a velocity potential $\phi(\mathbf{x}, t)$, and $\mathcal{B} \equiv -\partial \phi/\partial t$. Thus, at large distances from the step, where the perturbed motion is small, the pressure $p \approx \rho_o \mathcal{B}$, and the solution of (2.10) can be expressed in the form

$$p(\mathbf{x}, t) \approx -\int \Big(\rho_o \boldsymbol{\omega} \wedge \mathbf{v} - \mathbf{F}\Big)(\mathbf{y}, \tau) \cdot \frac{\partial G}{\partial \mathbf{y}}(\mathbf{x}, \mathbf{y}, t - \tau) \, d^3\mathbf{y} d\tau, \quad \mathbf{y} = (x', y', z'), \tag{2.11}$$

where the integration is over the fluid and all times τ. In this formula $G(\mathbf{x},\mathbf{y},t-\tau)$ is the Green's function with outgoing wave behavior that has vanishing normal derivative on the wall, i.e., the solution of (2.10) when the right hand side is replaced by $\delta(\mathbf{x}-\mathbf{y})\delta(t-\tau)$.

The characteristic wavelength of the generated sound is much larger than the step height h when the Mach number is small, and G is then well represented by the *compact* approximation (Howe 1989b)

$$G(\mathbf{x},\mathbf{y},t-\tau) \approx \frac{\delta\big(t-\tau-|\mathbf{x}-\mathbf{Y}|/c_o\big)}{4\pi|\mathbf{x}-\mathbf{Y}|}+\frac{\delta\big(t-\tau-|\mathbf{x}-\bar{\mathbf{Y}}|/c_o\big)}{4\pi|\mathbf{x}-\bar{\mathbf{Y}}|}, \quad |\mathbf{x}|\to\infty,$$

$$\mathbf{Y} = (X(x',y'),y',z'), \quad \bar{\mathbf{Y}} = (X(x',y'),-y',z'). \tag{2.12}$$

To use this formula in the general solution (2.11), it will be assumed that the effective source region lies within the finite span $-\frac{1}{2}\ell < z < \frac{1}{2}\ell$, where ℓ is small compared to the dominant acoustic wavelengths. This approximation is not essential to the following discussion, but corresponds more closely to conditions in practical problems, where the radiation spreads three-dimensionally rather than cylindrically. When end effects (from $z=\pm\frac{1}{2}\ell$) of the source distributions are ignored, the only non-trivial contributions to the radiation are supplied by the following approximation to G, obtained by taking the first term in the expansion of (2.12) in powers of the retarded source position,

$$G(\mathbf{x},\mathbf{y},t-\tau) \approx \frac{X(x',y')\cos\theta}{2\pi c_o|\mathbf{x}|}\delta'(t-\tau-|\mathbf{x}|/c_o) \tag{2.13}$$

where the prime denotes differentiation with respect to time, and $\theta=\cos^{-1}(x/|\mathbf{x}|)$ is the angle between the observer direction in the acoustic far field and the $x-$axis.

When this expression is substituted into the general solution (2.11) it follows from (2.6) and the Cauchy-Riemann equations (2.7), that the contribution from $\mathbf{F}$ vanishes identically, and that the acoustic pressure can be written

$$p(\mathbf{x},t) \approx \frac{\rho_o \ell\cos\theta}{2\pi c_o|\mathbf{x}|}\frac{d}{dt}\Big[\big(\Gamma_o\mathbf{v}\cdot\nabla\Psi\big)_{\mathbf{x}_o(t)}+\big(\Gamma(t)\mathbf{v}\cdot\nabla\Psi\big)_{\mathbf{x}_\Gamma(t)}\Big]_{t-|\mathbf{x}|/c_o}, \quad |\mathbf{x}|\to\infty, \tag{2.14}$$

where the notation implies that the terms in the square braces are evaluated at the retarded time $t-|\mathbf{x}|/c_o$.

3. NUMERICAL RESULTS

3.1 Vortex trajectories

The vortex paths are determined by equation (2.4) for the incident vortex Γ_o and equations (2.5), (2.9) for the shed vortex Γ. The irrotational velocity $\mathbf{v}$ is computed in the usual way, by introducing the dimensionless complex variable

$$Z = \frac{x}{h} + i\frac{y}{h},$$

and transforming the fluid region above the step onto the upper half of the complex ζ-plane. This is accomplished by the mapping

$$Z = \frac{1}{\pi}\left\{\sqrt{\zeta^2-1} \mp \ln\left(\zeta + \sqrt{\zeta^2-1}\right)\right\} + \frac{i}{2}(1 \pm 1), \qquad \mathrm{Im}\,\zeta \geq 0, \tag{3.1}$$

where here and henceforth, upper/lower signs are to be taken respectively for the forward/backward facing step. The foot of the step O maps into the point $\zeta = \mp 1$, and the top S maps into $\zeta = \pm 1$.

Let ζ_o, ζ_Γ denote the respective images in the ζ-plane of the incident and shed vortices. At low Mach numbers, when the step is acoustically compact, the motion near the step may be regarded as incompressible, with complex potential

$$w = \frac{-i\Gamma_o}{2\pi}\Big(\ln(\zeta-\zeta_o) - \ln(\zeta-\zeta_o^*)\Big) + \frac{-i\Gamma}{2\pi}\Big(\ln(\zeta-\zeta_\Gamma) - \ln(\zeta-\zeta_\Gamma^*)\Big)\,, \tag{3.2}$$

where the asterisk denotes complex conjugate. The instantaneous value of $\Gamma(t)$ is determined from the Kutta condition that dw/dz should be finite at S, which is satisfied provided $dw/d\zeta \to 0$ as $\zeta \to \pm 1$ respectively for forward and backward facing steps. This yields

$$\frac{\Gamma(t)}{\Gamma_o} = -\left|\frac{1 \mp \zeta_\Gamma}{1 \mp \zeta_o}\right|^2 \left(\frac{\zeta_o - \zeta_o^*}{\zeta_\Gamma - \zeta_\Gamma^*}\right)\,, \tag{3.3}$$

which implies that Γ and Γ_o always have opposite signs.

The velocity $\mathbf{v}(x_o, y_o, t)$ of the incident vortex, on the right of equation (2.4), is calculated from the velocity potential (3.2) by first excluding the free field self-potential $\frac{-i\Gamma_o}{2\pi}\ln(Z - Z_o)$, where $Z_o = x_o/h + iy_o/h$. In the ζ-plane equation (2.4) is equivalent to

$$\frac{d\zeta_o}{dT} = -i|\mathcal{F}(\zeta_o)|\left[\left(\frac{1}{\zeta_o^* - \zeta_o} + \frac{1}{2(\zeta_o^2-1)^*}\right) - \frac{\Gamma}{\Gamma_o}\left(\frac{1}{\zeta_o^* - \zeta_\Gamma^*} - \frac{1}{\zeta_o^* - \zeta_\Gamma}\right)\right], \tag{3.4}$$

where

$$T = \frac{\pi\Gamma_o t}{2h^2}, \quad \mathcal{F}(\zeta) = \sqrt{\frac{\zeta \pm 1}{\zeta \mp 1}}. \tag{3.5}$$

Similarly, the velocity components $u(x_\Gamma, y_\Gamma, t)$ and $v(x_\Gamma, y_\Gamma, t)$ in the equations of motion (2.5) and (2.9) of Γ are evaluated from (3.2) by excluding $\frac{-i\Gamma}{2\pi}\ln(Z - Z_\Gamma)$, $Z_\Gamma = x_\Gamma/h + iy_\Gamma/h$. The stream function $\Psi = \mathrm{Im}(h\zeta/\pi)$, so that, in the ζ-plane, ζ_Γ satisfies

$$\frac{d\zeta_\Gamma}{dT} + \frac{\mathcal{F}(\zeta_\Gamma)}{\mathrm{Re}[\mathcal{F}(\zeta_\Gamma)]}\Big(i\mathrm{Im}(\zeta_\Gamma) + \pi\mathrm{Re}(Z_\Gamma)\mathcal{F}^*(\zeta_\Gamma)\Big)\frac{1}{\Gamma}\frac{d\Gamma}{dT}$$

$$= -i|\mathcal{F}(\zeta_\Gamma)|\left[\frac{\Gamma}{\Gamma_o}\left(\frac{1}{\zeta_\Gamma^* - \zeta_\Gamma} + \frac{1}{2(\zeta_\Gamma^2-1)^*}\right) - \left(\frac{1}{\zeta_\Gamma^* - \zeta_o^*} - \frac{1}{\zeta_\Gamma^* - \zeta_o}\right)\right], \tag{3.6}$$

where $\mathrm{Re}(Z_\Gamma)$ on the left hand side is given in terms of ζ_Γ by (3.1).

Equations (3.3) - (3.6) are solved numerically by assigning a large and negative initial value to $\mathrm{Re}\,\zeta_o$ and adjusting the corresponding value of $\mathrm{Im}\,\zeta_o$ to make the stand-off distance d, say, of the vortex Γ_o from the wall equal to some prescribed initial value. The starting value of ζ_Γ is taken at some point close to the image $\zeta = \pm 1$ of the step top S; the precise location depends on the integration step length, but does not critically affect the solution, since Γ is very small when the shed vortex is close to S, and any starting errors rapidly become negligible as the solution builds up with the approach of Γ_o to the step. A fourth-order Runge-Kutta procedure was used; the equations form a robust system and no difficulty was experienced in achieving convergence.

3.2 Acoustic pressure

The acoustic pressure (2.14) may now be expressed in the form

$$p(\mathbf{x}, t) \approx 8\pi^3\rho_o U^2 M\left(\frac{d}{h}\right)^3 \frac{\ell\cos\theta}{|\mathbf{x}|}\frac{d}{dT}\left[\mathrm{Im}\Big(\frac{d\zeta_o}{dT}\Big) + \frac{\Gamma(T)}{\Gamma_o}\mathrm{Im}\Big(\frac{d\bar{\zeta}_\Gamma}{dT}\Big)\right]_{t-|\mathbf{x}|/c_o}, \quad M = \frac{U}{c_o}, \tag{3.7}$$

where $d\bar{\zeta}_\Gamma/dT$ is proportional to the fluid velocity at the core of the shed vortex Γ (which is the same as the vortex translation velocity $\mathbf{V}$ only when $d\Gamma/dt = 0$) and is equal to the

right hand side of (3.6) evaluated at the retarded position of Γ. The velocity $U \equiv \Gamma_o/4\pi d$ is the initial translational velocity (which is parallel to the wall) of the incident vortex before its motion is affected by the step. The acoustic pressure is proportional to $\rho_o U^2 M$, which is typical of an aeroacoustic source of *dipole* type; the dipole strength is just the unsteady drag exerted on the step during the interaction.

3.3 The forward facing step

Consider first the hypothetical case of vortex motion and acoustic radiation in the *absence* of vortex shedding (Conlisk & Veley 1985; Dhanak & Gundlapalli 1992). Only the incident vortex Γ_o is present; its trajectory is governed by equation (3.4) with $\Gamma \equiv 0$. The trajectory is depicted in Figure 2a for $d/h = \frac{1}{2}$, i.e., when the initial distance of the vortex from the wall is half the step height. The points labeled along the path indicate the vortex position at various non-dimensional times Ut/h, where time is reckoned from the instant at which the vortex passes the step (at $x = 0$).

When $Ut/h \to -\infty$ (far from the step) the kinetic energy of the (incompressible) motion per unit length of the vortex is equal to $(\rho_o \Gamma_o^2/4\pi)\ln(d/r_o)$, where r_o is a length of the order of the radius of the vortex core (Lamb 1932). In the absence of shedding this energy is conserved during interaction with the step, so that the distance of the vortex from the wall ultimately returns to d after the interaction when Ut/h becomes large. Because of this, the ratio Ut/h is approximately equal to the horizontal distance of the vortex from the step measured in step heights.

The non-dimensional acoustic pressure

$$\frac{p(\mathbf{x},t)}{\rho_o U^2 M (d/h)^3 (\ell/|\mathbf{x}|)\cos\theta}\,, \tag{3.8}$$

is plotted in Figure 2b as a function of the nondimensional retarded time $U[t]/h$, $[t] = t - |\mathbf{x}|/c_o$. Most of the sound is generated just prior to the arrival of the vortex at the step, within a distance equal approximately to the step height h.

Figure 3 illustrates how this picture is dramatically changed when account is taken of separation at the step. The incident vortex path is deflected sideways by the shed vortex (Figure 3a), and the two vortices proceed away from the wall in a direction initially inclined towards negative x. The times indicated on the trajectories correspond to those in Figure 2, i.e., $t = 0$ defines the instant at which the vortex Γ_o would pass over the step in the absence

of shedding. The strength of the shed vortex increases as Γ_o approaches the step until its value at $Ut/h = 1$ is about $-1.2\Gamma_o$. More details of the variation of $\Gamma(t)$ are given below. It should be noted, however, that, because $|\Gamma| > \Gamma_o$ when $Ut/h \geq 1$, the vortex pair traverses a circular path which ultimately causes the vortices to return to the wall and subsequently to separate at a "reattachment" point far to the right of the step. In more realistic flows, in particular in the presence of mean flow over the step in the x-direction, both the deflection distance away from the wall and the reattachment length would be much smaller.

The sound pressure produced by this interaction is represented by the solid curve in Figure 3b. Also shown (dashed) are the acoustic pressures generated by the incident and shed vortices, which correspond respectively to the first and second terms in the square braces of equation (3.7). These separate contributions are both large, but of opposite sign, and interfere to produce a net radiated sound pressure that is much weaker than in the absence of shedding (shown dotted).

When the initial stand-off distance of Γ_o increases to $d = h$, Figure 4 shows that the trajectories and the pressure signatures are qualitatively similar to those of Figure 3; the acoustic amplitudes with and without vortex shedding are weaker, and the amplitude difference is smaller. If the vortex is assumed to be a crude model of a discrete eddy in a turbulent boundary layer, a larger value of d/h would be representative of turbulent flow over a small skin step, when the boundary layer thickness tends to be large compared to h. The case in which $d/h = 4$ is illustrated in Figure 5. Here the deflection of the incident vortex is relatively small (about three step heights), and the circular path of the vortex pair terminates just to the right of the step (near $Ut/h \approx 3$), the trajectory being reminiscent of reattachment profiles observed in experiments (Farabee & Casarella 1984, 1986, 1988): the "eddy" formed by the vortex pair is torn apart, Γ_o proceeding to the right along the wall and away from the step, while Γ is captured within a "separation bubble". Actually $d\Gamma/dt$ changes sign at $Ut/h \approx 5.2$, at which time it is "released" from the edge S with a final circulation $\Gamma = -1.27\Gamma_o$. The vortex then proceeds back towards the step and proper continuation of the calculation requires that a new vortex be released from S. However, this latter phase of the motion will not be pursued (being similar to the interactions discussed below for the backward facing step), since the interaction of the incident vortex Γ_o with the step is now complete. The acoustic pressures with and without vortex shedding are seen in Figure 5b to be of very similar amplitude, but practically opposite in phase.

The variation of $\Gamma(t)/\Gamma_o$ when $d/h = 4$ is shown in Figure 6. The vortex is released at

$Ut/h \approx 5.2$ as indicated. In all of these cases the sound is generated principally over an interval of time $\sim h/U$, with characteristic wavelength $\sim h/M \gg h$ at the small Mach numbers for which the present theory is applicable.

3.4 The backward facing step

Typical interactions for a backward facing step are illustrated in Figures 7 and 8, respectively for $d/h = 0.5$ and 2. In the absence of shedding, the vortex paths and the acoustic pressure signatures are identical with their respective counterparts for the forward facing step when the time direction is reversed. This is because of our assumption that the span ℓ of the wall "wetted" by the unsteady flow is small compared to the acoustic wavelength. As $\ell \to \infty$, an observer at a given far field point $\mathbf{x}$ first receives sound from the interaction of the vortex and step occurring at the closest point of the step (corresponding essentially to the pressures calculated in this chapter), but this is subsequently augmented at progressively increasing values of the retarded time with sound generated by interactions at increasing spanwise distances on the step from the observer.

When vortex shedding occurs at a backward facing step, the incident vortex is displaced temporarily away from the wall (cf. Figures 7a, 7b and 8a), thereby reducing the intensity of the generated sound. The incident and shed vortex form a vortex pair (with $\Gamma \approx -\Gamma_o$ when $Ut/h \approx 1$) whose circular trajectory approaches the wall "downstream" of the step, where the pair split up as the flow "reattaches". The incident vortex continues along a path parallel to the wall and the shed vortex translates back towards the step within the separation "bubble". This vortex is "released" before reaching the step (respectively at $Ut/h \approx 2.8$ and 2.2 in Figures 7 and 8), whereupon a new vortex must be regarded as shed from S in order to continue the calculation. This secondary shedding has not been modeled because it occurs long after the interaction of Γ_o with the step, and is probably not important in practice, since at these times surface interactions would be dominated by other dissipative mechanisms within the separation zone.

When $d/h = 0.5$ the acoustic pressure (Figure 7) is much smaller than in the absence of shedding, and is "phase advanced" with respect to the no-shedding pressure signature. The separate contributions to the radiation from the incident and shed vortices are again both large, but of opposite sign, and their interference determines the amplitude of the sound. Figure 8 shows that (in contrast to the forward facing step) an increase in the initial stand-off distance to $d = 2h$ leaves the relative amplitudes of the acoustic pressures

with and without shedding effectively unchanged until the shed vortex is released. The subsequent sharp increase in the radiation after the release of the shed vortex at $Ut/h \approx 2.2$ is of no practical significance, because it represents the sound generated when Γ returns to the step after being released.

4. CONCLUSION

The unsteady drag exerted on a stationary body in incompressible flow can be expressed entirely in terms of the vorticity distribution. To calculate drag fluctuations produced by impinging turbulence it is important to include contributions from vorticity generated at the surface of the body. At low Mach numbers the drag is equal to the strength of the aeroacoustic dipole that dominates the acoustic radiation. The numerical results given in this chapter for an idealized vortex-step interaction suggest that vorticity in the separation zone significantly modifies the radiation compared to predictions based on a potential flow "edge scattering" modeling of the surface generated sound. This may be representative of the kind of interaction that occurs when a large scale, turbulent structure convects over forward or backward steps.

	Attenuation (dB)	
d/h	forward step	backward step
0.5	11.8	10.1
1	6.3	9.7
2	3.5	9.0
4	1.4	4.8

Table 1. Attenuation of vortex-step interaction noise by vorticity production

The influence of shedding from a step of height h depends on the stand-off distance d of the vortex from the wall prior to the interaction. Predictions for large or small values of d/h might be expected to be relevant to sound production by turbulent flow over a step when the corresponding ratio δ/h of the boundary layer thickness δ to the step height is large or small. Vorticity production affects both the amplitude and the phase of the sound. An overall estimate of the *attenuation* of the step noise by the surface-generated vorticity can be made by comparing the respective net radiated acoustic energies $\mathcal{E}_s$ and $\mathcal{E}_o$, say, with and without vortex shedding. This is done by comparing corresponding values of $\int_{-\infty}^{t_{max}} p^2(\mathbf{x}, t)\, dt$, where the interaction of the step with the incident vortex is regarded as being negligible beyond a "cut-off" time t_{max}, which is introduced to eliminate spurious, large amplitude contributions from secondary interactions of the shed vorticity with the step

(that are suppressed in practice by viscous dissipation and additional vorticity production at the wall). This comparison is made in Table 1, where the attenuation $-10 \times \log_{10}(\mathcal{E}_s/\mathcal{E}_o)$ (dB) is given for several values of d/h. The attenuation decreases with increasing d/h ("boundary layer thickness"), but less so for the backward facing step, indicating that "reattachment" on top of a forward facing step is noisier for a given value of d/h.

For a forward facing step, when d/h is large, Figure 5 and Table 1 indicate that the amplitudes of the sound with and without shedding are roughly equal, but the phases are reversed; phase reversal is also evident in Figure 8 for the backward facing step. These results suggest that predictions of the frequency spectrum of rough wall boundary layer noise based on the *potential flow scattering* of the turbulence blocked pressure by very small roughness elements (see, e.g., Howe 1989b) are probably satisfactory for practical purposes, and justifies in addition recent estimates of the noise generated by turbulent flow over small fuselage *skin steps* (Howe 1997).

REFERENCES

Bradshaw, P. and Wong, F. Y. F. 1972 *J. Fluid Mech.* **52**, 113 - 135. The reattachment and relaxation of a turbulent shear layer.

Brown, C. E. and Michael, W. H. 1954 *J. Aero. Sci.* **21**, 690 - 706. Effect of leading edge separation on the lift of a delta wing.

Brown, C. E. and Michael, W. H. 1955 *NACA Tech Note* 3430. On slender delta wings with leading-edge separation.

Chandrsuda, C. and Bradshaw, P. 1981 *J. Fluid Mech.* **110**, 171 - 179. Turbulent structure of a reattaching mixing layer.

Conlisk, A. T. and Veley, D. 1985 *Phys. Fluids* **28**, 3004 - 3012. The generation of noise in impinging vortex motion past a step.

Dhanak, M. R. and Gundlapalli, R. 1992 Paper presented at the 1992 *ASME Winter Annual Meeting.* Flow noise due to interaction between an eddy and a forward facing step.

Eaton, J. K. and Johnston, J. P. 1981 *AIAA J.* **19**, 1093 - 1100. A review of research on subsonic turbulent flow reattachment.

Efimtsov, B. M. 1996 *Non-homogeneous boundary layer noise prediction.* Paper presented at the *NASA Langley Interior Noise Workshop*, Hampton VA, 10 - 12 September.

Farabee, T. M. and Casarella, M. J. 1984 *ASME J. Vib., Stress and Rel. in Design* **106**, 343 - 350. Effects of surface irregularity on turbulent boundary layer wall pressure fluctuations.

Farabee, T. M. and Casarella, M. J. 1986 *ASME J. Vib., Stress and Rel. in Design* **108**, 301 - 307. Measurements of fluctuating wall pressure for separated/reattached boundary layer flows.

Farabee, T. M. and Casarella, M. J. 1988 pp 121 - 135 of *Acoustic phenomena and interaction in shear flows over compliant and vibrating surfaces*, ASME Book G00446 (Editors: W. L. Keith, E. M. Uram and A. J. Kalinowski). Wall pressure fluctuations beneath a disturbed turbulent boundary layer.

Howe, M. S. 1975 *J. Fluid Mech.* **71**, 625 - 673. Contributions to the theory of aerodynamic sound, with application to excess jet noise and the theory of the flute.

Howe, M. S. 1989a *J. Fluid Mech.* **206**, 131 - 153. On unsteady surface forces, and sound produced by the normal chopping of a rectilinear vortex.

Howe, M. S. 1989b *J. Fluids and Structures* **3**, 83 - 96. Sound produced by turbulent boundary layer flow over a finite region of wall roughness, and over a forward facing step.

Howe, M. S. 1995 *Quart. J. Mech. and Appl. Math.* **48**, 401 - 426. On the force and moment exerted on a body in an incompressible fluid, with application to rigid bodies and bubbles at high and low Reynolds numbers.

Howe, M. S. 1996 *J. Fluid Mech.* **329**, 89 - 101. Emendation of the Brown and Michael equation, with application to sound generation by vortex motion near a half plane.

Howe, M. S. 1997 *J. Sound Vib.* (submitted). On the contribution from skin steps to boundary-layer generated interior noise.

Lamb, Horace 1932 *Hydrodynamics* (6th. edition; reprinted 1994). Cambridge University Press.

Moss, W. D. and Baker, S. 1980 *Aeronautical Quarterly* 1980 (August edition), 151 - 172. Re-circulation flows associated with two-dimensional steps.

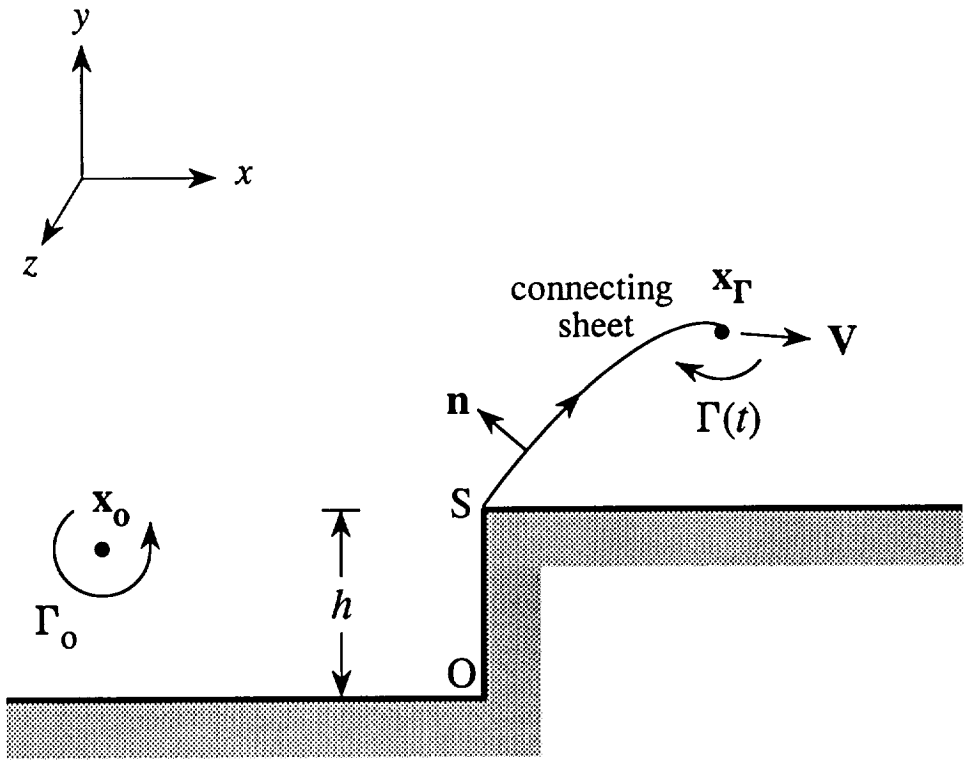

Figure 1. Configuration of the incident and shed vortices for a forward facing step.

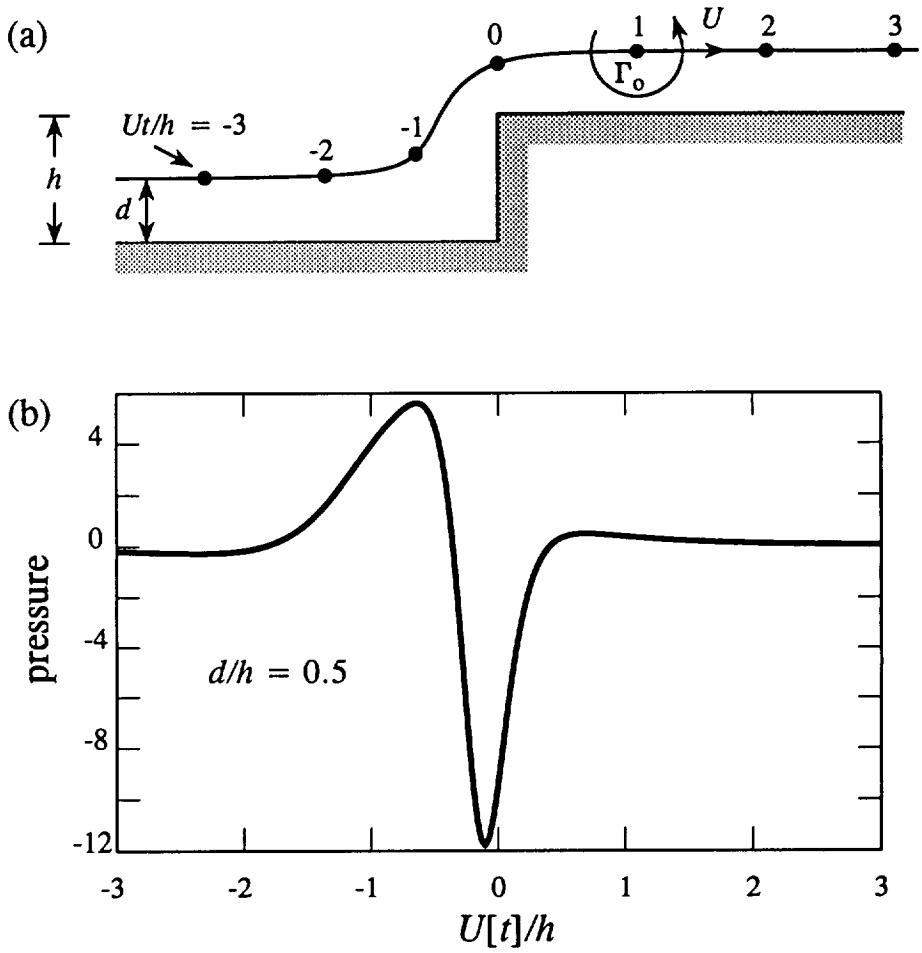

Figure 2. (a) Trajectory of incident vortex in the absence of shedding for $d/h = 0.5$. (b) Non-dimensional acoustic pressure $p(\mathbf{x}, t)/[\rho_o U^2 M (d/h)^3 (\ell/|\mathbf{x}|) \cos\theta]$.

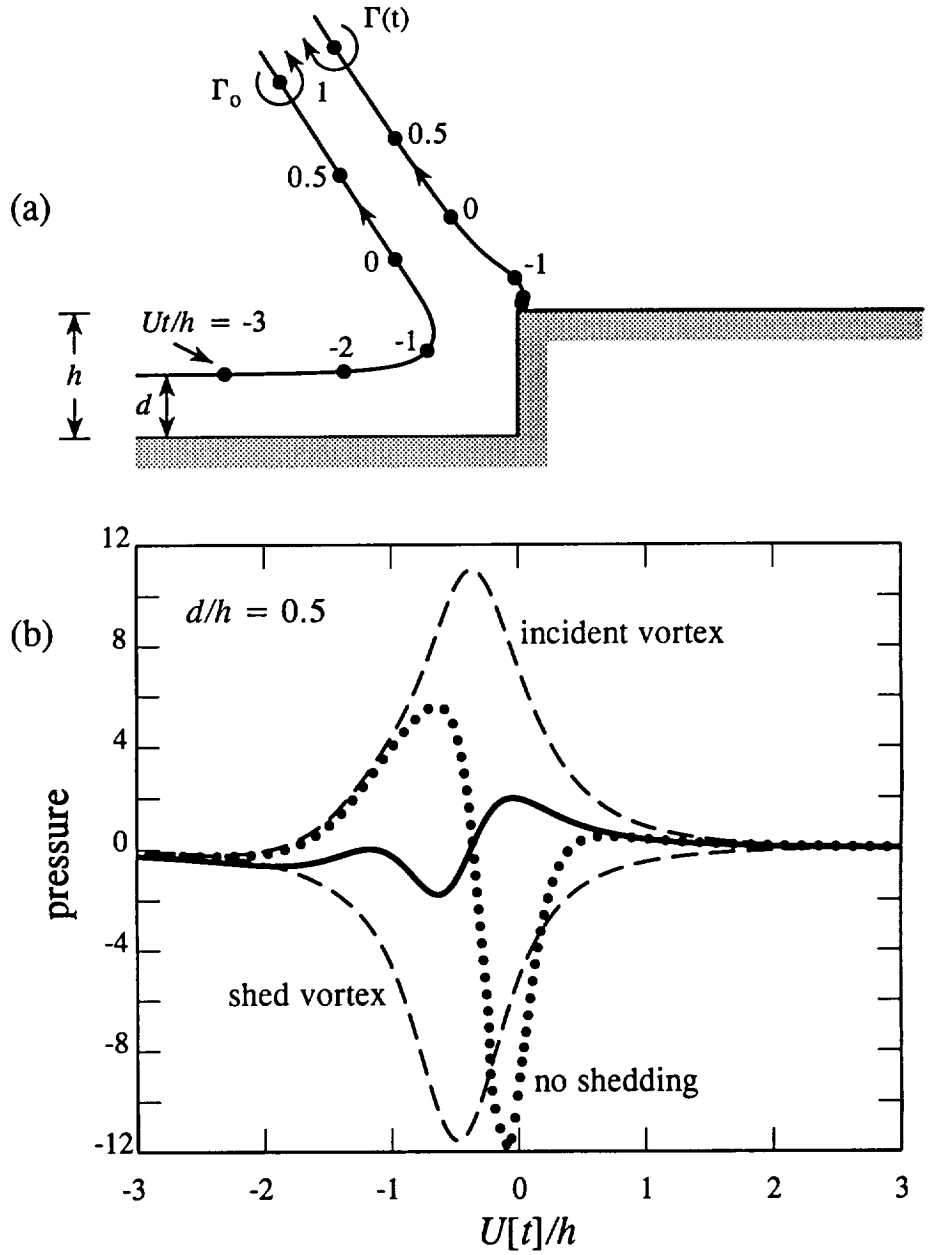

Figure 3. (a) Vortex trajectories when $d/h = 0.5$. (b) ———, non-dimensional acoustic pressure $p(\mathbf{x},t)/[\rho_o U^2 M (d/h)^3 (\ell/|\mathbf{x}|)\cos\theta]$; • • • • •, acoustic pressure in the absence of shedding. The broken curves are the separate contributions from the incident and shed vortices.

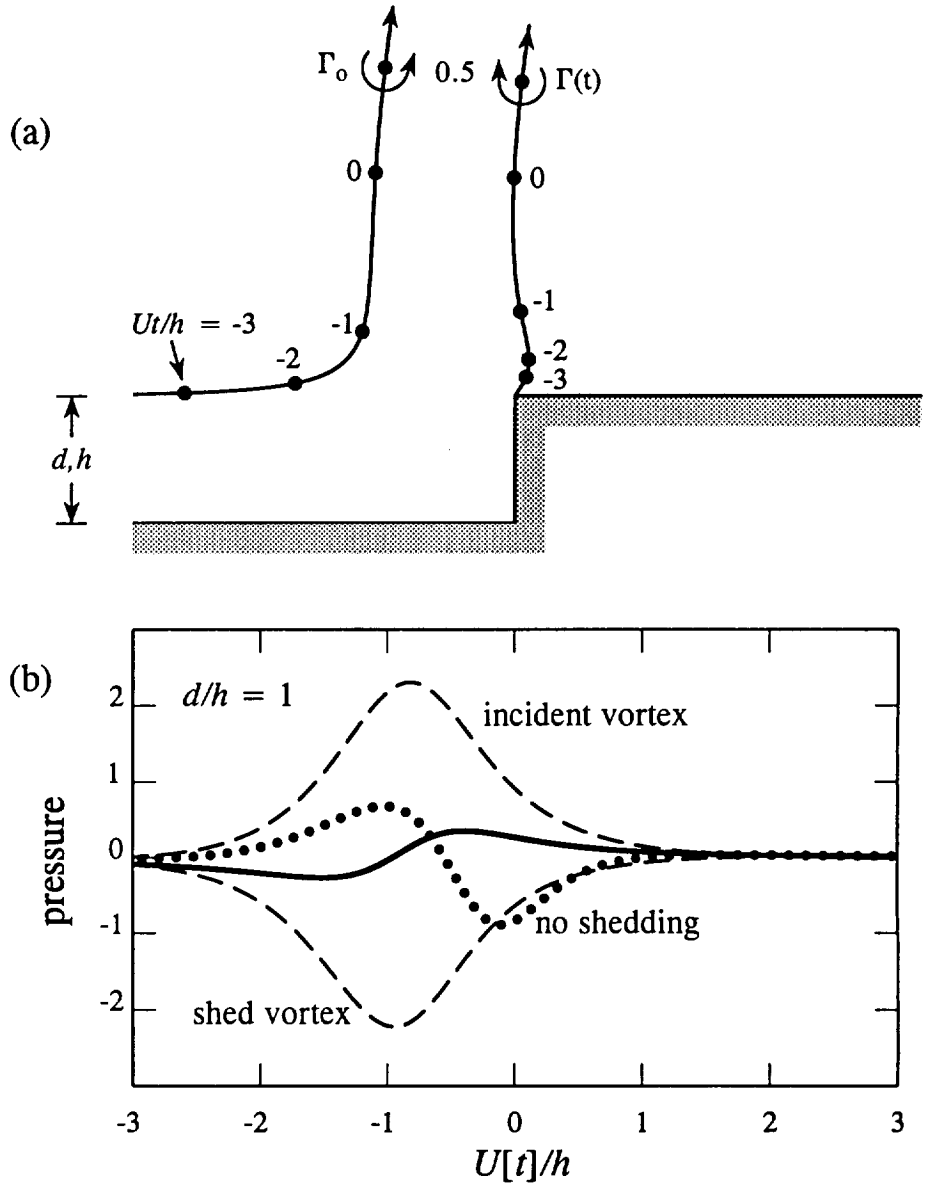

Figure 4. (a) Vortex trajectories when $d/h = 1$. (b) ———, non-dimensional acoustic pressure $p(\mathbf{x},t)/[\rho_o U^2 M(d/h)^3(\ell/|\mathbf{x}|)\cos\theta]$; • • • • •, acoustic pressure in the absence of shedding. The broken curves are the separate contributions from the incident and shed vortices.

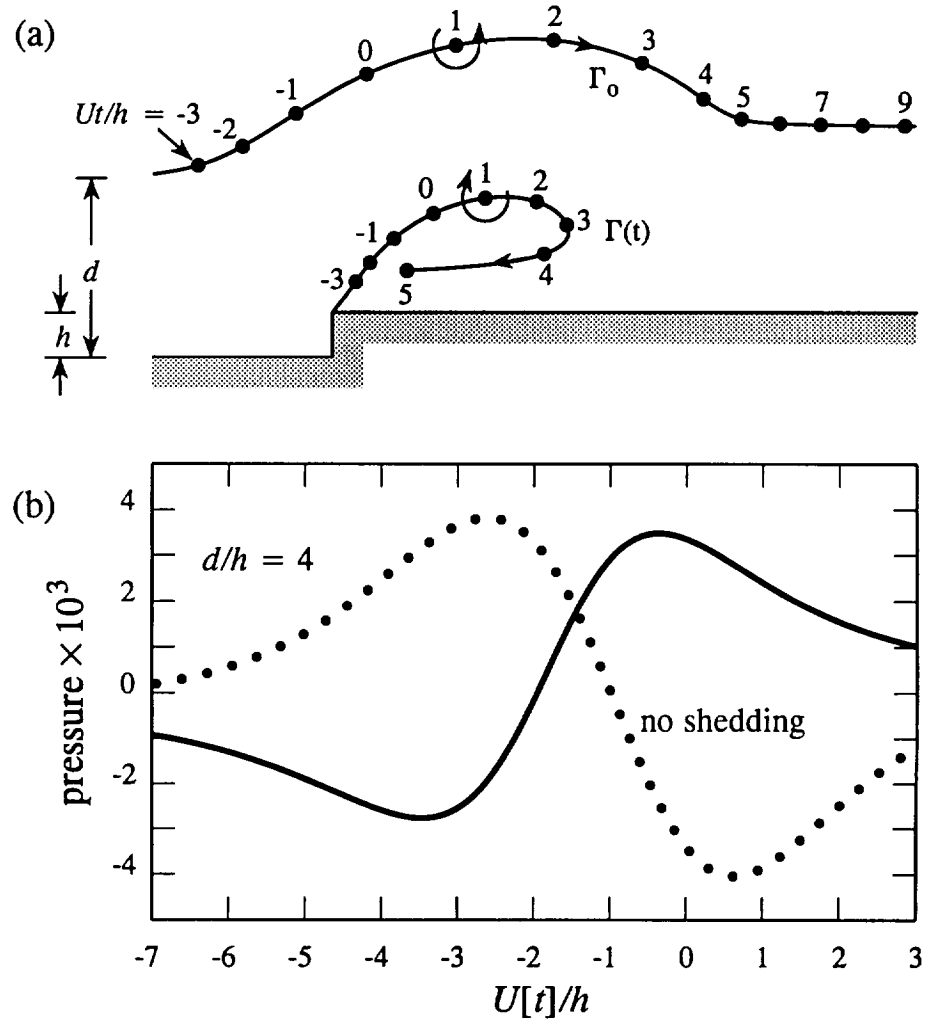

Figure 5. (a) Vortex trajectories when $d/h = 4$. (b) ———, non-dimensional acoustic pressure $p(\mathbf{x}, t)/[\rho_o U^2 M (d/h)^3 (\ell/|\mathbf{x}|) \cos\theta]$; •••••, acoustic pressure in the absence of shedding.

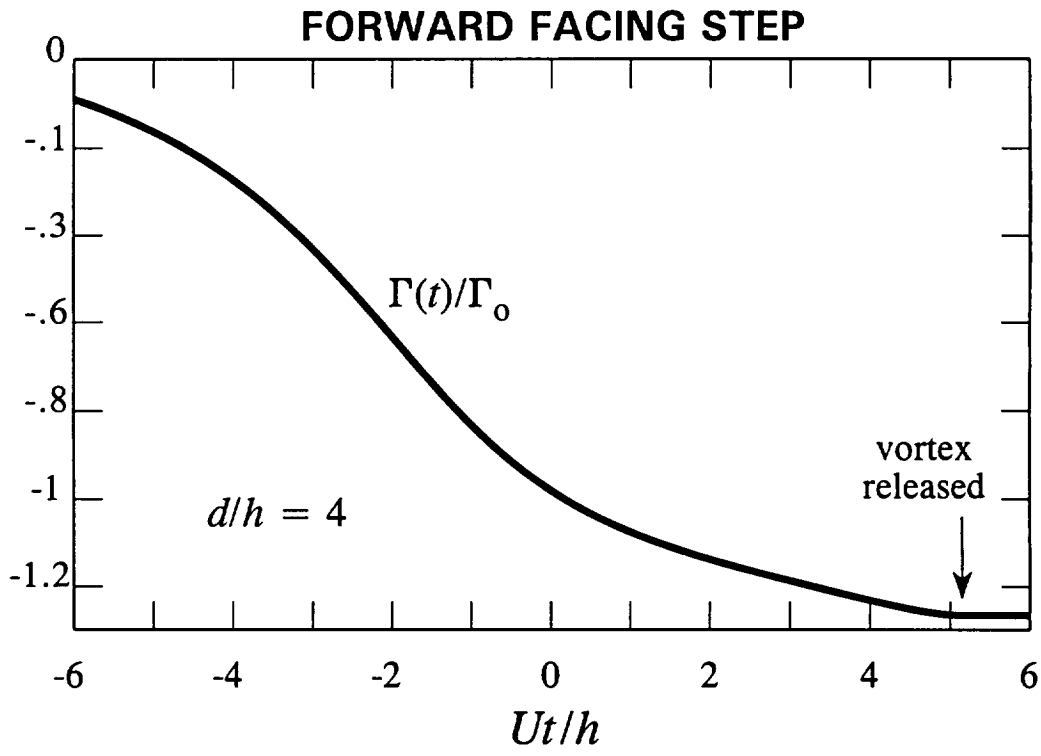

Figure 6. Shed vortex strength $\Gamma(t)/\Gamma_o$ for a forward facing step when $d/h = 4$. The vortex is "released" from the edge S of the step at $Ut/h \approx 5.2$.

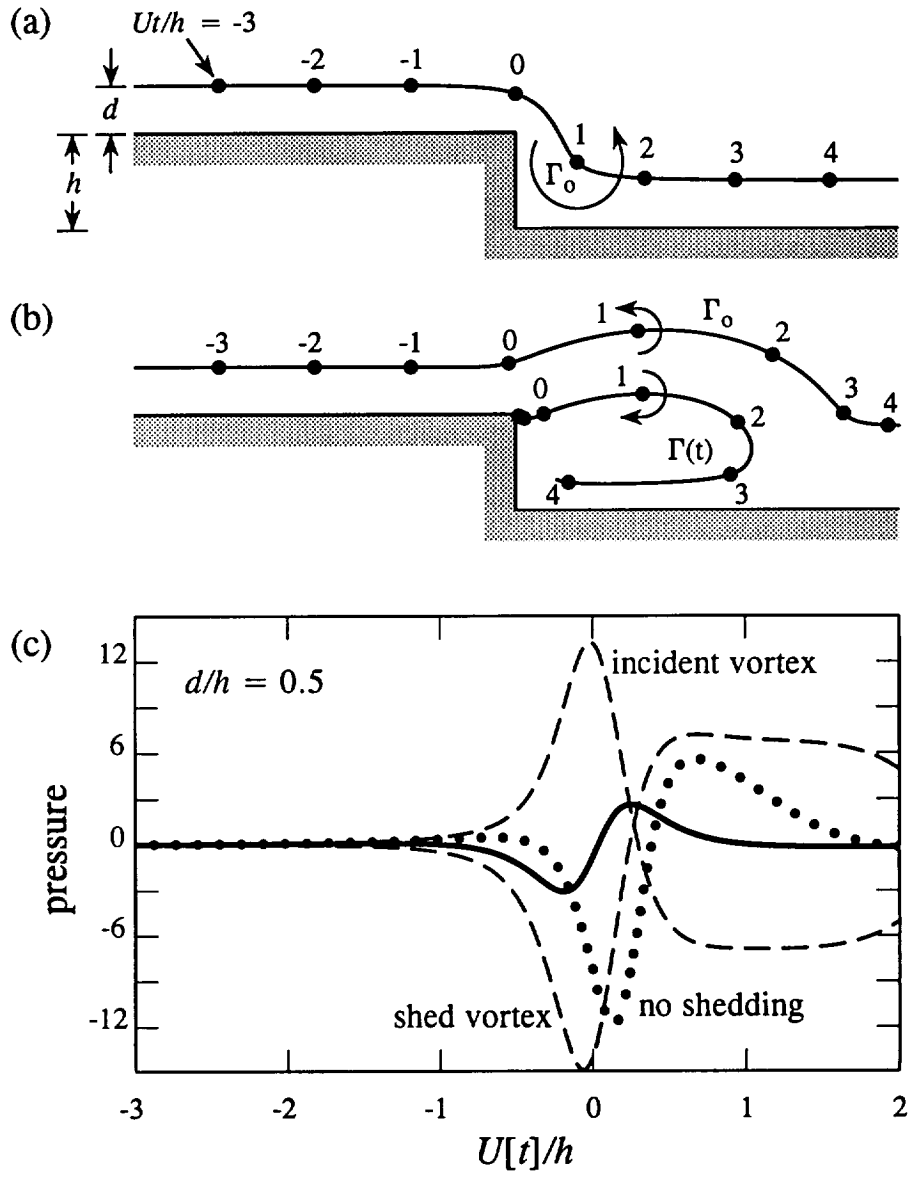

Figure 7. (a) Vortex trajectory for $d/h = 0.5$ with no shedding.

(b) Trajectories with shedding.

(c) ———, non-dimensional acoustic pressure $p(\mathbf{x}, t)/[\rho_o U^2 M (d/h)^3 (\ell/|\mathbf{x}|) \cos\theta]$;

• • • • •, acoustic pressure in the absence of shedding.

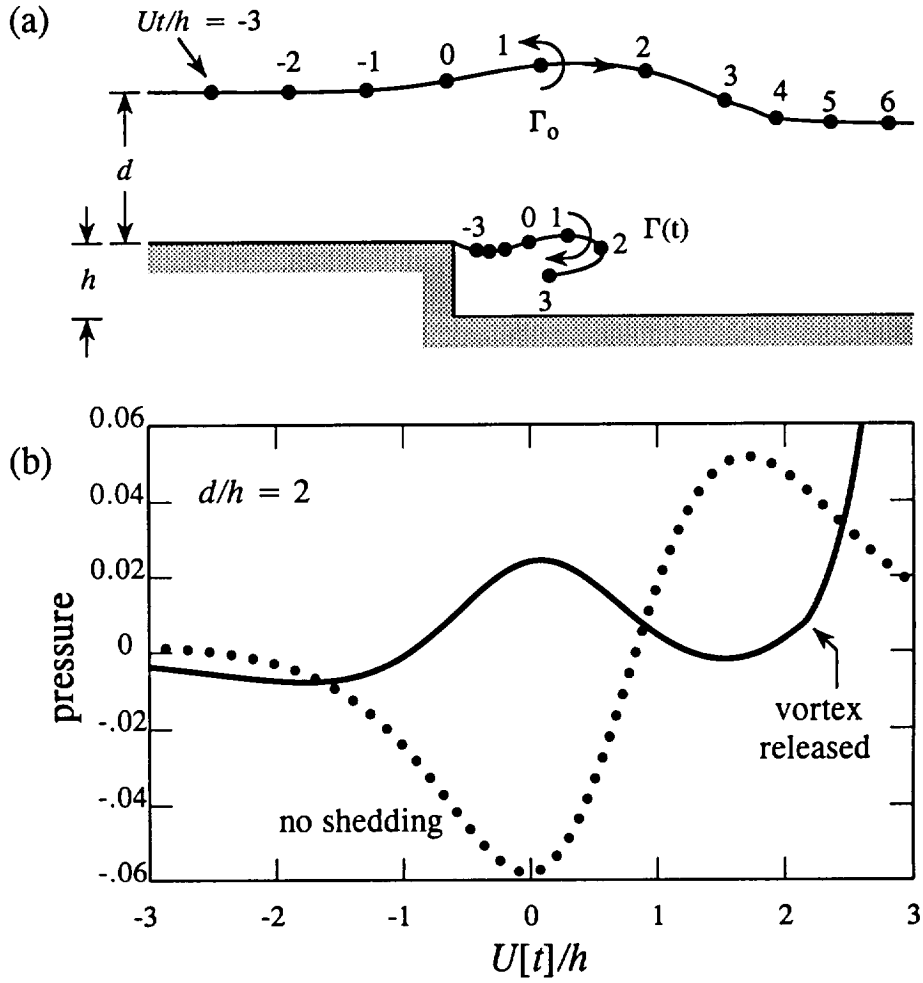

Figure 8. (a) Vortex trajectories when $d/h = 2$. (b) ———, non-dimensional acoustic pressure $p(\mathbf{x}, t)/[\rho_o U^2 M (d/h)^3 (\ell/|\mathbf{x}|) \cos\theta]$; •••••, acoustic pressure in the absence of shedding.

REPORT DOCUMENTATION PAGE

Form Approved
OMB No. 0704-0188

1. AGENCY USE ONLY (Leave blank)	2. REPORT DATE	3. REPORT TYPE AND DATES COVERED
	6 October, 1997	Final:15 March 1995 - 30 September, 1997

4. TITLE AND SUBTITLE

Analytical Studies of Boundary Layer Generated Aircraft Interior Noise.

5. FUNDING NUMBERS

NAG1-1688

6. AUTHOR(S)

Michael S. Howe and Patricia L. Shah.

7. PERFORMING ORGANIZATION NAME(S) AND ADDRESS(ES)

Boston University, College of Engineering,
110 Cummington Street, Boston MA 02115

8. PERFORMING ORGANIZATION REPORT NUMBER

AM-97-027

9. SPONSORING / MONITORING AGENCY NAME(S) AND ADDRESS(ES)

Dr. Richard J. Silcox
Structural Acoustic Branch,
MS 463, NASA Langley Research Center,
Hampton VA 23681-0001.

10. SPONSORING / MONITORING AGENCY REPORT NUMBER

11. SUPPLEMENTARY NOTES

12a. DISTRIBUTION / AVAILABILITY STATEMENT

12b. DISTRIBUTION CODE

13. ABSTRACT *(Maximum 200 words)*

Analytical investigations are made of the generation of aircraft interior noise by turbulent flow over the fuselage. Theoretical models are constructed to determine the influence on sound generation of

(i) the exterior mean flow;
(ii) vortex structures interacting with rib-stiffeners;
(iii) fuselage skin steps;
(iv) flow separation.

14. SUBJECT TERMS

aircraft interior noise, skin steps, forward and backward facing steps, turbulent boundary layer, vortices, rib-stiffened elastic plate, fluid-structure interaction

15. NUMBER OF PAGES
109 + iii

16. PRICE CODE

17. SECURITY CLASSIFICATION OF REPORT	18. SECURITY CLASSIFICATION OF THIS PAGE	19. SECURITY CLASSIFICATION OF ABSTRACT	20. LIMITATION OF ABSTRACT